Kinetic analysis of karyopherin-mediated transport through the nuclear pore complex

LOLODI, Ogheneochukome

Abstract

The nuclear envelope spatiotemporally separates the nucleoplasm from the cytoplasm such that molecular communication between both compartments is mainly through the nuclear pore complexes (NPCs). Karyopherin family proteins, importins and exportins, mediate the transport of a specific cargo protein in one direction. However, the overall cycle of karyopherins across the NPC has not been well examined. In this study, the concentration distributions and kinetic flux details of karyopherin-facilitated diffusion in living cells were examined. Continuous photobleaching of the cytoplasm of live cells, which were expressing nuclear localization signal (NLS) cargoes, led to a progressive Crm1-independent decrease in the nuclear fluorescence intensity compared with unbleached control cells. This strongly suggests that importins facilitate reversible translocation of importin-cargo complex *in vivo*. The kinetic details of these *in vivo* observations further revealed that karyopherin availability and affinity for cargo in the cytoplasm are the most likely rate-limiting factors in the nuclear import transport cycle. Indeed, the rate of karyopherin-cargo complex formation in the cytoplasm was the slowest compared with karyopherin-nucleoporin interactions, RanGTP-dependent or spontaneous cargo dissociation in the nucleus. In addition to these bulk kinetic measurements, single molecule fluorescence microscopy was used to evaluate the actual dynamics in individual NPCs. This revealed that the NPCs differed from one another in terms of the number of transport events as well as the cargo residence time. Taken together, the results presented in this thesis strongly indicate that steady state conditions and kinetics are maintained in living cells by constant back-and-forth shuttling of karyopherin-cargo complexes through apparently functionally-diverse and heterogeneous NPCs.

Dedication

I dedicate this doctoral thesis to:

—My grandmother, mother, son and wife.

Martina Ughewo,

Elizabeth Chioma Ogwezzy,

Ebenezer Ochukome Lolodi, and

Mercy Enimienosen Lolodi (nee Avbadevboro).

Acknowledgement I

This doctoral thesis is based on material contained in the following scholarly paper:

Lolodi O, Yamazaki H, Otsuka S, Kumeta M and Yoshimura SH. Dissecting *in vivo* steady-state dynamics of karyopherin-dependent nuclear transport. *Mol Biol Cell* **27:** 167-176 (2016)

Acknowledgement II

This thesis is the culmination of a journey that started about 30 years ago. I am completely overwhelmed by emotions, and would like to profusely say 'THANK YOU' to everyone on whose shoulders I've stood to get to this point. I haven't achieved anything in life all by myself; I've always had tremendous help EVERY step of the way. Therefore, it's only natural that I appreciate those who ensured I got to the foot of the mountain as well those who propped me up until I breasted the peak.

My supervisors:

Without them, this thesis would not have been possible. Of all the applications (yes, there were literally more than 100) that I made in 2011, Professor Kunio Takeyasu's was one of the few positive replies that I got. He specified the most beneficial study route for me. Without his accepting me into his lab, I could have forfeited my scholarship. I'll be eternally grateful to him.

Dr. Shigehiro Yoshimura—the head of my lab and my co-supervisor. I remember the countless times I popped into his office with requests for 5-, 10-minute consultations that always turned out to last for 1-, 2- and sometimes several hours! He always obliged me and gave me fresh insights that sharpened my clumsy graduate student-grade narratives. His comments were, and still are, always constructive. It was a great privilege for me to have been groomed by him. Yoshimura-Sensei: I'm grateful, THANK YOU!

I could write an entire thesis on my de facto supervisor—Dr. Masahiro Kumeta. **EVERY** practical skill I know, he taught me. He is the reason I can use a confocal microscope, efficiently do several routine biochemistry/molecular biology experiments. He'd stop at nothing to ensure his students understand every aspect of their projects: design, techniques, analysis, interpretation, presentation and communication. I remember when my experiments hit a dead-end and Despair had me in her choking clutches, the solace I got was his soothing and reassuring counsel. He's always available at the shortest notice. His guidance and support extended beyond science; he was always willingly to translate and

interpret the tonnes of documents that were sent to me. I owe him a gratitude that I could never repay; the closest I'd ever come to scratching the surface of the debt is to be a scientist that cares about all humanity and to also ensure that my future students enjoy these privileges and more. Kumeta-sensei: THANK YOU VERY MUCH!

I'm also indebted to my sub-supervisors, Professors Nagao and Nakaseko, for the fruitful suggestions that they proffered whenever I sought their input on the tenor of my research.

Members of Yoshimura Lab:

Fukuda-san, our efficient and amiable secretary. Having her around meant I had no worries whatsoever about dealing with administrative matters. I can't thank members of my lab enough for the several discussion sessions and useful comments during our lab meetings that also contributed to sharpening my various research goals. The exquisitely cordial relations and fun times (especially the few karaoke outings) that we all had will fondly be etched in my memories. I'll miss all of you: Hiroya, Jamie, Deguchi, Abeer, Aiko, Asai, Diyana, Yashu, Sayuri and of course Konishi (you increased my lifespan by introducing Mendeley to me!)

Graduate School of Biostudies

I want to specially thank Nishimoto-san. You could call her the Guardian Angel of EVERY international student in the Graduate School of Biostudies, and you wouldn't be wrong! She was always ready to give vital administrative information/advice.

I’m also grateful to **ALL** the professors and staff of the Graduate School of Biostudies who ensured that I had a very fulfilling graduate student life in Kyoto University. I particularly liked the study tours that were graciously organized for us. The pleasant memories from the visits to Lake Biwa and Awaji Island will stay with me for the rest of my life.

International Centre, Kyoto University

The reason I know a tad about Japanese culture and a smattering of Japanese that helped me on several occasions is the four-month intensive language program that I took at the beginning of my journey in 2012. I am grateful to all my senseis at the International Centre—Hashimoto-sensei, Shiratori-sensei, Sawanishi-sensei, Kawakami-sensei, Furukawa-sensei, Nagayama-sensei, Uraki-sensei and Ieamoto-sensei. みんなありがとうございます

Secondary School Teachers

For want of space, I'd not be able to mention all the other numerous teachers who diligently performed their duties to ensure that I got to this point in life. I am eternally grateful to **ALL** my teachers who taught me in Etiti Primary School, Emu-Obodeti; Asoro Primary School, Benin City; Etiti Grammar School; and Saint Patrick's College, Asaba. Their lessons and lashes helped to build the solid foundation upon which most of us stand today.

Dr. Igbojiwonku (I feel I've spelt his name wrongly; maybe because we called him Gbojis). He was my favourite teacher. He made me love Biology and Chemistry. No doubt, he's the reason I had the best grade (A1) in the two subjects which eventually made me choose to study Biochemistry in the university. Dr Igbojinwoku also played a great role, albeit indirectly, in improving my understanding of the English language. The few months, in early 1997, that I attended his extramural classes at Asagba Primary School Asaba, brought me in contact with the English teacher who sharpened my comprehension and general grammar skills, which my regular English teacher (Mr Okoro) had hitherto exposed us to. It's a shame that the only detail I can recall about him is that he used to come from Onitsha to teach us in Asaba.

Mr Okoro, our English teacher. How would I have passed all my exams in life if he had not exposed us to the different rules of English grammar? He was a thorough no-nonsense teacher who made sure that his students took his classes seriously. If our brains became too impervious to assimilate his lessons, he dutifully and lovingly administered several lashes of the cane to make us understand how important his lessons were because he would be the last English teacher we'd ever encounter in our lives. He was right. I thank you sir.

Lecturers at the Department of Biochemistry, UNIBEN.

There are no words to describe the debt of gratitude that I have for all my lecturers who exposed me to the beauty and mysteries of Biochemistry and Molecular Biology. I am grateful to Professors I.O Onoagbe, E.S. Omoregie, E.C. Onyeneke, N.P Okolie, E.A.C. Nwanze, P.O. Uadia, P.I Campbell, F.O Obi and A.U. Osagie (of blessed memories). I am equally indebted to Drs S.O Uanseoje, S. Ojeaburu, R. Nimenibo-Uadia, N.J Orhue, M. Adaikpoh, K. Imafidon and B.O Agoreyo.

I am particularly grateful to Professors George E. Eriyamremu and Chris C. Osubor for the privilege of mentorship that they have given me to this very point in my life and career. I can never ever forget the fact that Professor Osubor, the very embodiment of humility, personally brought the MEXT scholarship application form to me at the point when I had already lost every hope of studying in a world class university as Kyoto University.

Sponsorship:

My very special appreciation goes to the Japanese government and all the 127 million Japanese people who, through the very generous MEXT scholarship, paid for the immeasurable knowledge that I have gained in these past four years. I am also grateful to all the wonderful people of Japan for their genuine warmth and hospitality that made my living environment conducive to focus on my research. I know I will miss Japan when I eventually leave to further my career. I am also grateful to Mr John Nwankwo and the entire staff of the Embassy of Japan in Nigeria for the great role they played in ensuring that I had a seamless journey from Nigeria to Japan.

Similarly, I am also grateful to the British government for sponsoring my master's degree at the University of Nottingham in 2008/09. Words cannot express my gratitude to the entire staff (Professor Steve Harding et al.) of the Applied Biomolecular Technology (ABT) master's program for exposing me to several aspects of cell and molecular biology. The experience I got there contributed enormously to building my career.

Others:

I thank Mr John Odigie who works at Labour Relations in UNIBEN for meticulously and selflessly doing his job at the point I submitted my MEXT scholarship application form. He ensured that my form did not maliciously gather dust in his office by quickly dispatching it to the Japanese Embassy before the deadline for submission. I thank you sir. I thank everyone, too numerous to mention, who played any role whatsoever to ensure that my academic journey got this far.

Finally…

Family and Friends:

i My grandmother:

I'm forever grateful that I have a grandmother whose prayers and blessings have never had any taint of prejudice. You catered for me, groomed me in my formative years and have never ceased to love me. I thank you for all your love and prayers that immensely helped me throughout my PhD program.

ii. My mother:

I could write an entire book, and it still would not be enough, to tell my mother 'THANK YOU' for sustaining 99.5% of my first 25 years on earth as well as supporting me as best as she could thereafter.

iii. My wife:

My greatest fan. My most loyal supporter. My nonjudgmental intercessor. The one who stayed up late for me whenever my experiments had me in a chokehold. This thesis would never ever have been possible without your unflinching and unconditional support, love and care. If degrees were divisible, I certainly would have split my PhD in three parts and given you two parts for all the sacrifice you made to see me succeed.

iv. My son:

You make me complete and fulfilled in life. Anytime (there were **countless times)** I felt I was going to flunk my PhD, the reset button that I needed to hit was the frightful thought of setting a bad precedence for you. In the future, when you're a grown man, I'd be able to look back and say to you: 'Son, it is not in **us** to give up—every cloud has a silver lining: **look for it!**'

v. My in-laws:

I also thank all my in-laws for the support they gave me during the course of my doctoral studies. I'm particularly grateful to my mother-in-law for all her prayers and unwavering love throughout the turbulent period of my studies. I equally appreciate my brothers-in-law, Ehimen and Clement Avbadevboro, as well as my sisters-in-law, Lilian Napoleon and Dora Enoghaman. You all gave me the peace of mind that I needed to successfully finish my doctoral program.

vi. Friends:

I'd also like to acknowledge the support of my numerous great friends, whose various contributions helped me in the course of my doctoral studies. For want of space, I can only say 'THANK YOU' to the following: Hilda Iyobosa Avwenagha, Vincent Eze, Elvis 'Desage' Osung, Ehigbai Oikeh, Nekky Jemima Erhunse, Olutoyosi Omotoso, Tubodenyefa Zibima, Reuben Temerigha, Abbot Oghenekaro, Oghenemise Abirhire, Amonia Rita, Jesse Ojobor and of course my very own brother Ena Ofugara.

Table of Contents

Abbreviations

DTT	Dithiothreitol
EGFP	Enhanced Green Fluorescent Protein
FLIP	Fluorescence loss in photobleaching
FRAP	Fluorescence recovery after photobleaching
Kap	Karyopherin(s)
NPC	Nuclear Pore Complex
NE	Nuclear Envelope
Nup	Nucleoporin
NLS	Nuclear Localization Signal
NES	Nuclear Export Signal
FG	Phenylalanine-Glycine

List of Figures

List of Tables

Chapter 1

General Introduction

1.1 Signal Transmission across the Nuclear Envelope

A distinguishing feature of eukaryotes and prokaryotes is the encasement of eukaryotic genome within the nucleus. Eukaryotic nucleus is bounded by a double-membrane nuclear envelope (NE) that comprises an outer nuclear membrane (ONM) and inner nuclear membrane (INM; Figure 1.1). The enclosed space between the ONM and INM is called the perinuclear space (PNS), which is essentially an extension of the lumen of the endoplasmic reticulum that is continuous with the ONM (Liu et al., 2007). Embedded within the nuclear envelope—perforating both the ONM and INM—are several copies of nuclear pore complexes (NPCs). The NE is also characterized by the nuclear lamina, which is composed of A- and B-type lamins that interact with the NPCs, INM and nuclear components. It is essential for eukaryotic cells to physically and functionally link the two compartments across the NE to achieve proper regulations of a variety of cellular events.

One means of molecular communication between the nucleus and cytoplasm is mediated by Sad1 and UNC-84 (SUN) domain proteins in the inner nuclear membrane and Klarsicht, ANC-1, and Syne homology (KASH) domain proteins in the outer nuclear membrane (Starr, 2011; Tapley and Starr, 2013 Chang et al., 2015). A set of SUN domain-containing proteins reside in the INM and extend their SUN domains into the PNS (Tran *et al.*, 2001; Bupp *et al.*, 2007). Cytoplasmic Nesprin1 and 2 are transmembrane proteins that reside in the ONM and extend their KASH domains into the PNS, where they directly interact with SUN domain (Starr and Fridolfsson, 2010). Along with their interactions with nuclear lamina and actin cytoskeleton, the entire SUN-KASH assembly bridges the cytoskeleton with the nucleoskeleton, and is reported to be the primary medium by which

forces generated in the cytoplasm are communicated to the nuclear matrix (Figure 1.1; Starr, 2009).

The other means of molecular communication between the nucleus and the cytoplasm is through the nuclear pore complexes (NPCs) which account for the vast majority of molecules that shuttle between both compartments (Wente and Rout 2010). The constant crosstalk between the spatiotemporally segregated compartments is characterized by the entry, into the nucleus, of transcription factors and many DNA-binding proteins that are synthesized in the cytoplasm as well as the concomitant exit, from the nucleus, of mRNA, rRNA, tRNA and ribosomal subunits which are needed for protein synthesis and/or ribosomal assembly (Weis, 2002).

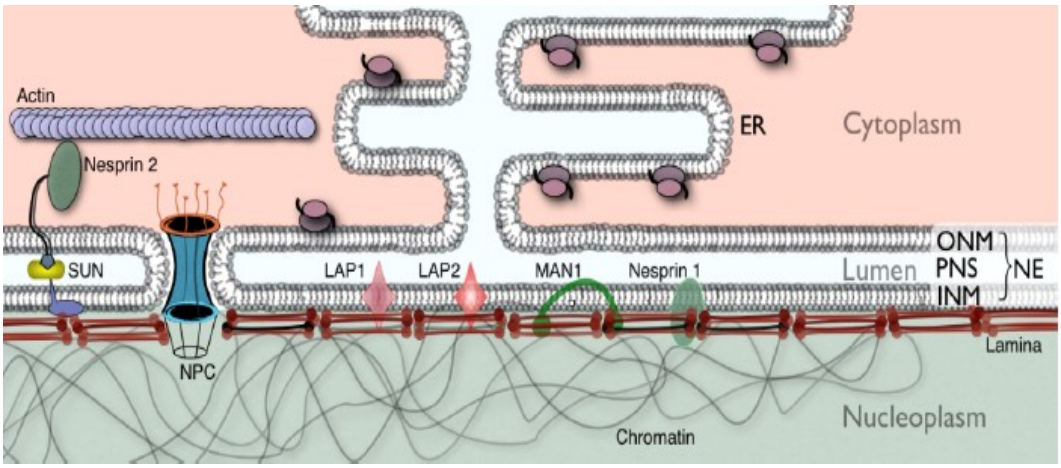

Figure 1.1 The structure of the nuclear envelope (adapted from Mckenna et al., 2013 with permission from InTech, http://www.intechopen.com/books/genetic-disorders/laminopathies). The nuclear envelope (NE) encases the eukaryotic genome within the nucleus. It is characterized by a double membrane: the outer nuclear membrane (ONM) and inner nuclear membrane (INM). The lumen between the ONM and INM is called the perinuclear space (PNS), which is an extension of the lumen of the endoplasmic reticulum (ER). Signal communication between the cytoplasm and the nucleoplasm is mainly by two means: the nuclear pore complex (NPC), and the SUN-KASH interactions.

1.2 Nuclear Pore Complexes (NPCs)

1.2.1 Structure of NPCs

The first methodical identification of the NPC was in the 1950s by two independent groups (Callan and Tomlin, 1950; Watson, 1959). The NPCs were described as cylindrical structures with diameters of about 100 nm. Subsequent studies showed that they have a predominantly octagonal symmetry along their nucleocytoplasmic axis, with a few nine- and ten-fold symmetry observed too (Gall, 1967; Hinshaw and Milligan, 2003). Each NPC traverses both the outer and inner membranes of the NE and opens, on both sides, to the nucleoplasm and cytoplasm.

Essentially, the NPC comprises three inter-linked ring-like structures: a cytoplasmic ring, a central spoke ring and a nuclear ring (Figure 1.2; Frenkiel-Krispin *et al.*, 2010; Grossman *et al.*, 2012). Present within the NPC is a deformable central channel with a functional diameter of ~30 nm that is believed to be the transport link between the cytoplasm and the nucleoplasm (Hinshaw et al., 1992; Akey and Radermacher, 1993; Görlich et al., 1996; Pante and Kann, 2002; Stoffler et al., 2003; Wente and Rout, 2010; Solmaz et al., 2013). The molecular mass of the NPC in yeast and higher eukaryotes is estimated to be ~66 MDa and ~112 MDa respectively (Reichelt *et al.*, 1990; Rout and Blobel, 1993). The number and density of NPCs vary among organisms, tissues and cell cycle, and may be indicative of the physiological demands of the cells: vertebrates, yeasts and *Xenopus laevis* oocytes have 2-5 x 10^3 NPCs/nucleus (10-20 NPCs/μm^2), 200

NPCs/nucleus (~12 NPCs/μm^2) and ~5 x 10^7 NPCs/nucleus (~60 NPCs/μm^2) respectively (Fabre and Hurt, 1997; Winey *et al.*, 1997; Gorlich and Kutay, 1999).

The NPC is not an empty channel, but is formed by and filled with several copies of ~30 different subunits called nucleoporins (Nups) which can be classified into transmembrane Nups, scaffold Nups and barrier Nups on the grounds of structure, sequence motifs and location (Grossman et al., 2012). The transmembrane Nups (Gp210, Pom 121 and Ndc1) anchor the entire NPC in the nuclear envelope; the barrier Nups (Nups 98, 62, 54, e.t.c) occupy the central pore while the scaffold Nups (Nups 160, 93, 205, e.t.c.) function as a bridge between the transmembrane layer and the barrier Nups. A unique feature of the barrier Nups is their high content of unstructured, disordered regions and domains replete with phenylalanine-glycine (FG) repeats (Bayliss *et al.*, 2000; Rout *et al.*, 2000; Denning et al., 2003; Strawn et al., 2004; Patel et al., 2007). Vertebrate FG repeats present as FXFG (X is any amino acid), proline-XFG (PXFG) or glycine-leucine-FG (GLFG). These FG repeats are also present on the cytoplasmic filaments as well as the nuclear basket, and are reported to be the sites of interaction with transport receptors (Rout *et al.,* 2000; Xu and Powers, 2013).

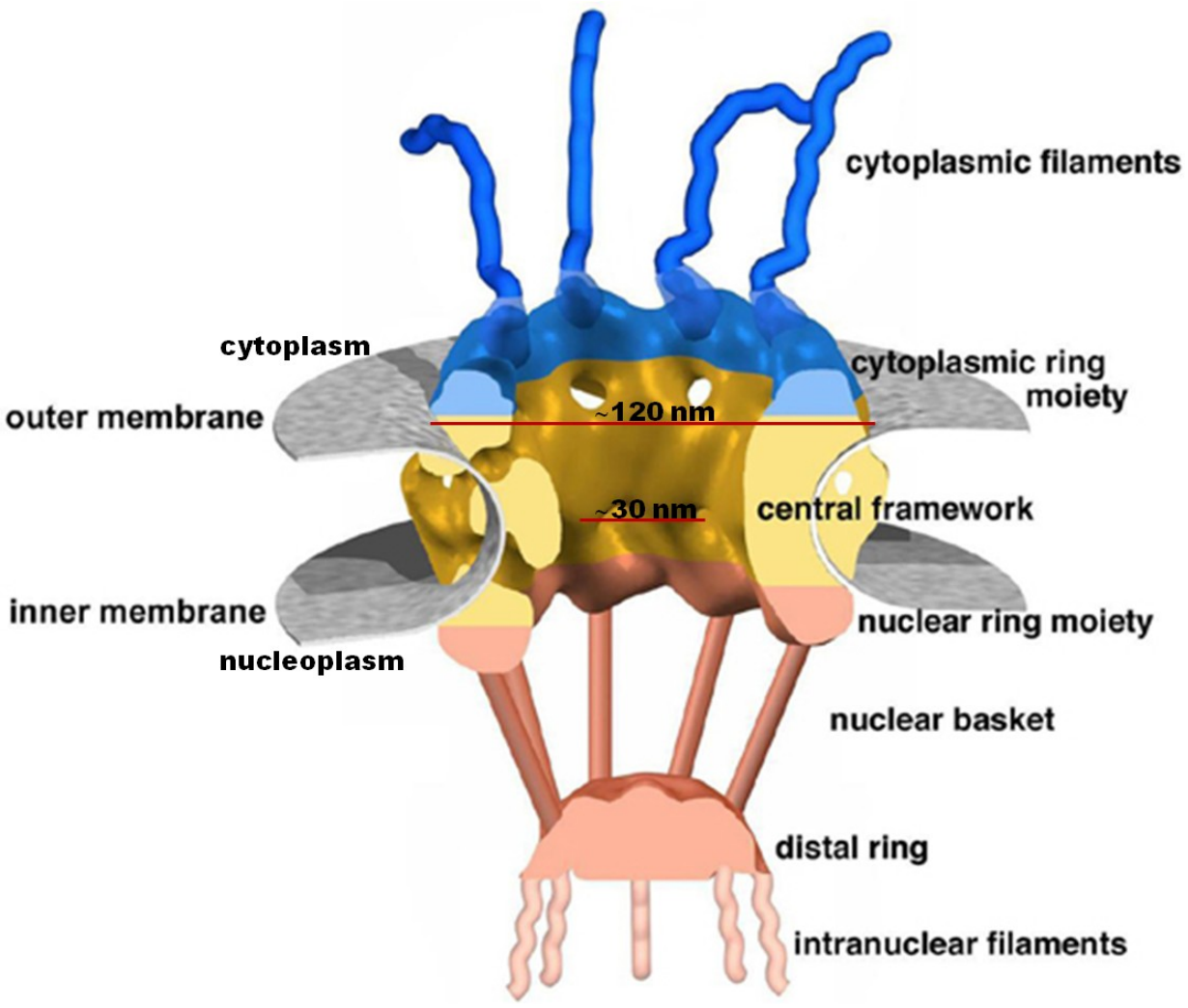

Figure 1.2 Structure of the NPC (adapted from Fahrenkrog and Aebi (2003) with permission from Nature Publishing Group). The outer diameter of the NPC is estimated to be ~120 nm while the functional diameter of the central channel (or plug) is ~30 nm. FG-Nups fill the central channel and are involved in interactions with cargo receptors.

1.2.2 Structural models of transport selectivity

Molecular transport through the NPC is either by passive diffusion or active transport. Protein molecules with molecular weights (M.W) ≤ 40 kDa (or < 9nm in diameter) can freely diffuse through the central channel of the NPCs, in both directions (Pante and Kann, 2002; Panté, 2007). Molecules larger than this cut-off limit have two options: spontaneous shuttling (β-spectrin, β-catenin and actinin, with M.Ws > 100 kDa, can adapt their structural motifs to the hydrophobic interior of the pores), or facilitated transport that primarily involves proteins called karyopherins (Wente, 2000; Macara, 2001; Rout and Aitchison, 2001; Weis, 2002; Suntharalingam and Wente, 2003; Kumeta et al., 2012; Sharma et al., 2012). However, the precise mechanism of transport through the NPCs is still elusive, and several models have been propounded in an attempt to make sense of this quandary: the Brownian affinity gating, affinity gradient, selective phase, polymer brush, forest, reduction of dimensionality (ROD), and many other models.

The Brownian affinity gating model was the first to be proposed Rout et al. (2000) following their experimental observation that the NPCs lack molecular motors that could drive translocation. They subsequently described the model in more details and renamed it the 'virtual gating model' (Figure 1.3A; Rout et al., 2003). Essentially, on the basis of their experimental observations, they proposed that vigorous thermal motion of the FG repeats could create an entropic barrier that would prevent molecules that do not bind to the FG domains from gaining access to the NPC interior. Conversely, molecules that could transiently bind and thus overcome the entropic barrier would have a much higher

probability of rapid translocation through the NPC which, they argued, is decorated with numerous binding sites that have low affinities (high dissociation rate). However, this diffusion-based model does not seem to explain the translocation of large molecules like ribosomal subunits that have diameters greater than the ~9 nm threshold for diffusion (Pante and Kann, 2002; Paschal, 2002).

The Affinity gradient model was propounded by Ben-efraim and Gerace (2001). This model holds that the central barrier Nups do not have the same affinity for transport receptors; rather, it argues that the NPC has binding sites with increasing affinity from one side to the other. So, cargoes are envisaged to be handed from sites of lower affinity to sites of progressively higher affinity until they exit the NPC in an irreversible translocation process. However, several lines of investigations have strongly pointed to the reversibility of the nuclear transport process (Englmeier et al., 1998; Ribbeck et al., 1998; Nachury and Weis, 1999; Ribbeck et al., 1999).

The selective phase model assumes that the central channel of the NPC is large, filled with FG repeats that form a sieve-like hydrophobic meshwork that excludes inert molecules that lack a localization signal (Figure 1.3B; Ribbeck and Görlich, 2001). The meshwork permits the passage of molecules that can compete, via hydrophobic interactions, with the FG repeat clusters so that translocation is achieved by selective partitioning of the receptor-cargo complex in the hydrophobic NPC permeability barrier (Ribbeck and Görlich, 2002). Additional experimental evidence for the ability of FG repeat

motifs to form hydrogel-like structures by inter-repeat bonding was provided in a study by Frey et al. (2006).

Another related model is the oily-spaghetti model which speculates that the NPC is an open channel that is filled with FG repeats which are extended like loose, oily spaghetti (Macara, 2001). This model predicts that the FG repeats spaghetti forms a 7 nm-thick layer in the ~10 nm central channel of NPC (Keminer and Peters, 1999). It also assumes that the Gibbs Free Energy for conformational transitions in the FG repeat chains is low enough for them to move freely in the central pore, and consequently easier for cargo-receptor complexes to push them apart during translocation.

The reduction of dimensionality model was also proposed in an attempt to understand the mystery of nucleocytoplasmic transport (Figure 1.3C; Peters, 2005). The author suggested that the central channel of the NPC as well as the cytoplasmic filaments is lined by a cohesive FG surface that has various sections. The model proposes that a transport receptor binds to the filament or channel sections of the FG surface and then proceeds to search it (the FG surface), in a random two-dimensional walk, until it encounters the channel exit.

The polymer brush model, on its part, makes important improvements to the virtual gating and selective phase models (Lim et al., 2006). It predicts that the selectivity of hydrophobic meshwork is as a result of the entropic fluctuations of the highly disordered

FG repeat domains at the peripheral portions of the NPC. It proposes that the periphery of the NPC is gated by extended, flexible brush-like FG-repeats that are in constant thermal motion. When a molecule that can overcome the entropic barrier comes in contact with the brush-like gate, it collapses to allow inward or outward passage through the NPC.

There is also the 'two-gate' or forest model (Figure 1.3D; Patel et al., 2007; Yang, 2011). This model predicts that two channels (gates) are formed by the intrinsically disordered regions of the barrier FG Nups: one gate (the 'shrubs') is formed by the collapsed-coil FG domains of Nups tethered at the NPC centre, and the other gate (the 'trees') is formed by clusters of extended- or collapsed-coiled FG domains of peripherally-anchored Nups. The model envisages that the gate of choice for molecular transport is dependent on size, charge and hydrophobicity: small molecules will preferentially access the shrubs while large molecules are selectively translocated through the 'trees' region.

The common denominator of all these transport models is the interaction of cargo carrier machinery with the barrier Nups during translocation. The direction of transport is still widely believed to be dictated by the RanGTP gradient that exists across the nuclear envelope.

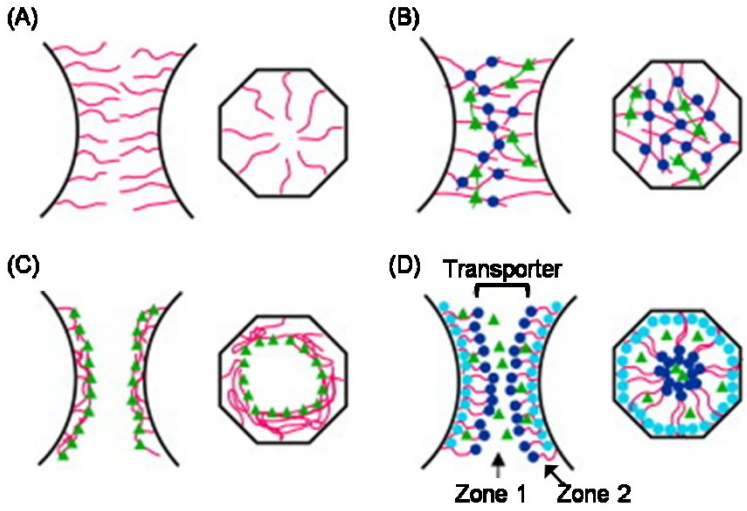

Figure 1.3 Models of nucleocytoplasmic transport (adapted from Wälde and Kehlenbach (2010) with permission from Elsevier). **(A). Virtual gating model:** FG-Nups (pink) form an entropic barrier that prevents the entry of molecules that cannot transiently bind to lower the barrier. **(B). Selective phase model:** FG-Nups transiently form FG-FG contacts (blue) to form a sieve-like meshwork. Amphiphilic molecules (green triangles) can disrupt the FG-FG contacts and partition into the sieve. Molecules that cannot bind are excluded. **(C). Reduction of dimensionality model:** FG-Nups coat the walls of the central channel such that small molecules (≤40 kDa) are permitted to passively diffuse through the central channel. However, molecules (green triangles) larger than the cut-off limit 'walk' on the FG-Nup wall from one interaction site to another until they exit the NPC. **(D). Forest model:** Domains of FG-Nups that are in a globular, collapsed conformation form the shrubs (light blue), whereas domains that take on an extended-coil conformation form the trees (dark blue), forming two transport zones as shown. Small molecules readily access the shrubs, whereas larger molecules are translocated through the trees (Zone 1). [A-D, side views (left) and top views (right) of the NPC].

1.3 Receptor-mediated Nucleocytoplamic Transport

1.3.1 Karyopherins

Most cases of facilitated nucleocytoplasmic transport are mediated by members of the karyopherin β (Kapβ) superfamily, also known as importins and exportins (Chook and Blobel, 2001; Conti and Izaurralde, 2001; Gorlich and Kutay, 1999; Weis, 2003). While the importins are dedicated to importing numerous diverse cargoes into the nucleus, the latter ferry cargoes out of the nucleus.

There are about 14 different types of kapβ in *Saccharomyces cerevisiae*, and 20 different types in mammalian cells. They are classified, on the basis of evolutionary analyses, into 15 sub-families whose nomenclature derive from their UniProt gene names (Quan et al., 2008; Chook and Süel, 2011). All Kapβ proteins share similar molecular mass (90-150 kDa), isoelectric points (4.0-5.0), low sequence identity, and most importantly, have several tandem superhelical repeats that are called HEAT motifs (Chook and Blobel, 2001; Conti et al., 2006; Chook and Süel, 2011). The HEAT repeat, a helix-loop-helix structure, derives its name from its first discovery in four proteins: **H**untingtin, **E**longation factor 3, '**A**' subunit of protein phosphatase A (PR65/A) and **T**OR1 lipid kinase (Andrade and Bork, 1995; Chook and Blobel, 2001).

Importin β, the best-studied Kap, has 19 tandem superhelical HEAT repeats, each of which comprises two helices designated A and B (Figure 1.4; Harel and Forbes 2004). In the crystal structure of importin β bound to the IBB domain of importin α, the A-helices are

on the convex face while the B-helices line the concave face of the entire structure (Cingolani et al., 1999; Marfori et al., 2011). Several crystal structures of importin β bound to different cargoes have revealed diverse karyopherin-cargo interactions (Chook and Blobel, 1999; Bayliss et al., 2000; Lee et al., 2003). Similarly, over 20 crystal structures of Crm1 (also known as exportin1) and its complex with various cargoes have been solved (Monecke *et al.*, 2014). In general, the abundance and flexibility of HEAT motifs in karyopherins has been confirmed to be basis the multiple cargo recognition as well as interaction with nucleoporins.

1.3.2 Import and export signals

In practically all cases of karyopherin-cargo interaction, possession of a specific signal for import or export is a sine qua non. For karyopherin-dependent nuclear transport of molecules above the size-limit barrier of the NPC, the cargo must have a recognition site/sequence for karyopherins, typically described as a nuclear localization signal (NLS) for nuclear import, or a nuclear export signal (NES) for export (la Cour et al., 2003; Nair et al., 2003). There are many types of NLSs which may broadly be classified into two: the classical NLS (cNLS) and the non-classical NLS.

The cNLS, the first discovered NLS, is characteristically rich in basic amino acids and comprises either a single domain SV40 large T-antigen (monopartite cNLS; PKKKRKV) or two interdependent domains of nucleoplasmin NLS (bipartite cNLS; $KRX_{(10-12)}KRRK$; Kalderon et al., 1984; Robbins et al., 1991). Depending on the cargo, the

cNLS binds specifically to the C-terminus of the intermediary adaptor molecule (importin α or Snurportin-1; Conti et al., 1998; Herold et al., 1998; Stewart, 2007). Karyopherin β1 (Kapβ1; also known as importin β) recognizes the complex by binding to the N-terminal importin β-binding (IBB) domain of the adaptor, and then translocates the entire Kapβ-adaptor-cNLS cargo complex through the NPC (Görlich et al., 1995; Huber et al., 1998; Pemberton et al., 1998).

There are also cases where some cargoes interact directly with importin β (Marfori et al., 2011). The human T-cell leukemia virus type 1 (HTLV-1), sterol regulatory element binding protein (SREBP)-2, cyclin B1, human immunodeficiency virus (HIV) Rev and Tat, parathyroid hormone related protein (PTHrP) and ribosomal proteins are some examples of import cargoes that do not require an adaptor molecule to bind to importin β (Jakel and Gorlich, 1998; Lam et al., 1999; Nagoshi et al., 1999; Moore et al., 1999; Palmeri and Malim, 1999; Truant and Cullen, 1999; Forwood et al., 2001a; Forwood et al., 2001b; Kurisaki et al., 2001; Forwood and Jans, 2002; Harley et al., 2003).

The NLSs of the cargoes that bind directly to importin β vary in sequence length and basicity: whereas SREBP-2 has an NLS with 120 amino acids, HIV Tat has only 9 (Marfori et al., 2011). In addition, the mode of binding to importin β differs from how the IBB domains of importin α and snurportin-1 are bound. The large network of electrostatic bonds that mediate the importin β-IBB interactions are distinctly different from the

electrostatic bonds involved in the importin β-PTHrP and the hydrophobic interactions that govern importin β-SREBP-2 interactions (Lam et al., 1999; Cingolani et al., 2002).

Further versatility in importin β-cargo interactions is guaranteed by the use of different sets of HEAT repeats for binding the different cargoes. The well-documented flexibility of importin β enables it to bind a vast array of cargo proteins that are involved in nuclear transport (Stewart, 2006; Riddick and Macara, 2007). The use of importin α, as well as snurportin, as adaptor molecules for cargo recognition is peculiar to importin β among the Kapβs, most of which involve direct Kap-cargo interactions. It is speculated that this adaptor pathway confers evolutionary advantages on importin β on account of its higher sensitivity to environmental signals (Riddick and Macara, 2007).

On the other hand, non classical NLSs have completely different primary sequences that enable them bind directly and specifically to the different importin β homologues that make up the karyopherin β family (Cingolani et al., 2002). A prominent example is the proline-tyrosine (PY)-NLS that is recognized by Kapβ2 (also known as transportin; Chook and Süel, 2011). Unlike the cNLSs, the PY-NLSs cannot be defined by a traditional sequence motif. Rather, three defining mutually-inclusive characteristics are holistically considered: high predisposition to intrinsic disorderliness, overall basic content, and presence of a consensus C-terminal R/H/KX(2-5)PY motif preceded by a central hydrophobic or basic motif (Lee et al., 2006). A typical example is the glycine-rich M9 sequence—a 38-amino acid domain at the carboxyl terminus of heteronuclear

ribonucleoprotein A1 (hnRNP A1) that is recognized by Kapβ2 (Michael et al., 1995; Siomi and Dreyfuss, 1995).

In the case of nuclear export, the best-studied NES is the leucine-rich sequence that is directly recognized by Crm1 (Fornerod et al., 1997; Fukuda et al., 1997; Neville et al., 1997; Stade et al., 1997). It was first discovered in HIV-1 Rev (LPPLERLTL) and cAMP-dependent protein kinase inhibitor (PKIα; LALKLAGLDL; Fischer et al., 1995; Wen et al., 1995; Xu et al., 2012). In the past two decades, the NES of several Crm1-dependent export cargoes have been identified, and found to not necessarily be rich in leucine, but generally posses a hydrophobic character that has been approximated to the traditional consensus sequence: Φ1-X2,3-Φ2-X2,3-Φ3-X-Φ4 where Φn stands for L, I, V, F or M and X is any amino acid (Bogerd et al., 1996; la Cour et al., 2003; Engelsma et al., 2004; Kutay and Güttinger, 2005; Xu et al., 2012). In addition to sequence hydrophobicity, export capabilities of NESs have been reported to be complementarily determined by a number of other factors such as: the preferential adoption of an α-helical conformation that readily changes to loops at their C-termini; greater surface accessibility and localization within intrinsically disordered regions of the protein (Xu et al., 2012).

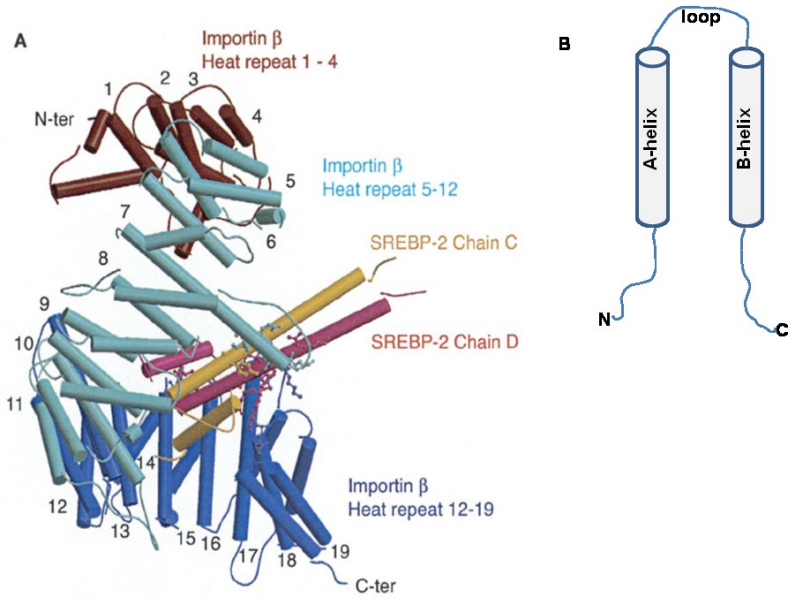

Figure 1.4 Interaction of importin β with sterol element binding protein 2 (SREBP2). **A.** (culled from Lee et al., 2003 with permission from The American Association for the Advancement of Science). The 19 HEAT (H 1 -19) repeats of importin β are colour-coded brown, light blue and blue. It directly binds to the dimeric SREBP2 using H7-17. The flexibility of these HEAT repeats accounts for the ability of importin β to bind a wide array of cargoes. **B.** Schematic representation of a typical HEAT repeat. It consists of two helices linked by a loop.

1.3.3 Nuclear import cycle

In the classical importin β cycle, the NLS of the import cargo is recognized either directly by importin β, or indirectly by prior binding to the importin β-binding (IBB) domain of importin α in the cytoplasm (Figure 1.5; Lee et al., 2003; Riddick and Macara, 2007). Then, the importin β-cargo (or importin β-α-cargo) complex translocates through the NPC by interacting with the FG-Nups (Stewart, 2006). On encountering a high concentration of RanGTP on the nucleoplasmic face, the cargo and importin α are displaced from importin β. The adaptor protein, importin α exits the nucleus in a complex with the protein, Cellular Apoptosis Susceptibility (CAS) while the resultant importin β-RanGTP is recycled back to the cytoplasm unassisted (Sun et al., 2013). Here, RanGAP, aided by RanBP1, facilitates the hydrolysis of RanGTP to RanGDP which leads to the dissociation of importin β, in readiness for another round of cargo import (Kuhlmann et al., 1997; Görlich et al., 2003). RanGDP, in a complex with NTF2, is imported back into the nucleus to be converted back to RanGTP so as to maintain the RanGTP gradient (Ribbeck et al., 1998).

Ran is a small ~25 kDa GTPase that freely diffuses into and out of the nucleus, and alternates between a GDP-bound state and a GTP-bound form (Nemergut and Macara, 2000). The latter (RanGTP) predominates in the nucleus while the former is the main form of the protein in the cytoplasm, thus a RanGTP gradient exists across the nuclear envelope with a high concentration in the nucleus and low concentration in the cytoplasm. This gradient is maintained by the compartmentalization of two key proteins: a chromosome-tethered RCC1 (also known as guanyl nucleotide exchange factor, Ran GEF), and the

cytoplasmic Ran GTPase-activating protein, RanGAP (Görlich et al., 1996; Görlich et al., 2003).

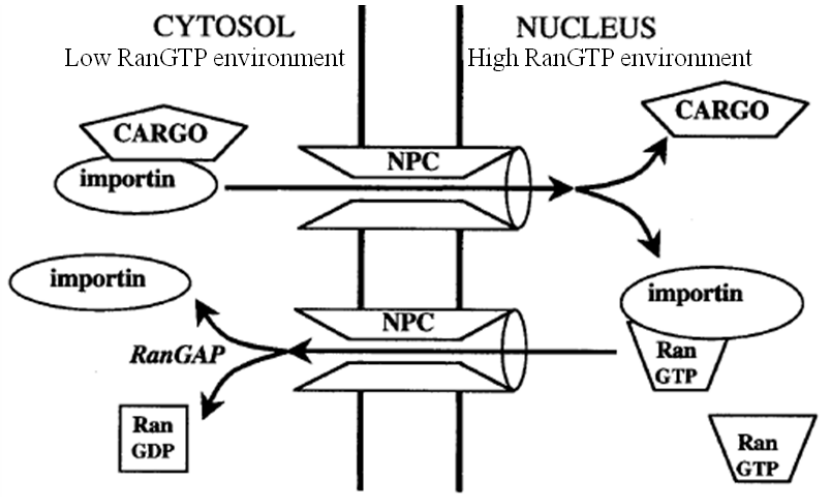

Figure 1.5 Karyopherin-facilitated nuclear import (adapted from Macara, 2001 with permission from American Society for Microbiology). Importin binds its NLS cargo, directly or via an adaptor, in the cytosol, which has a low RanGTP concentration. The complex then translocates through the NPC, into the nucleus, where dissociation is prompted by the high RanGTP environment. The resultant importin-RanGTP complex then returns to the cytoplasm, where RanBP1 and RanGAP facilitate RanGTP hydrolysis to free importin for another round of transport.

1.3.4 Nuclear export cycle

Chromosome region maintenance 1 (Crm1)-mediated export of cargoes is the best studied export route from the nucleus (Fukuda *et al.*, 1997; Monecke *et al.*, 2014). Although the export cycle is not as robustly studied as the import pathway because of the paucity of appropriate experimental systems, available evidence suggest that it is almost the opposite of the import process (Figure 1.6). In the presence of the high RanGTP concentration in the nucleoplasm, an export cargo possessing a requisite NES is recognised by a cognate exportin (Dong et al., 2009). The resultant ternary complex of RanGTP-exportin-cargo then translocates through the NPC to the cytoplasm. GTP hydrolysis, mediated by RanGAP and RanBP1 leads to cargo displacement and the exportin-RanGDP migrates back to the nucleus where GDP is exchanged for GTP leading to the dissociation of exportin in preparation for another round of export (Floer and Blobel, 1999; Koyama and Matsuura 2010).

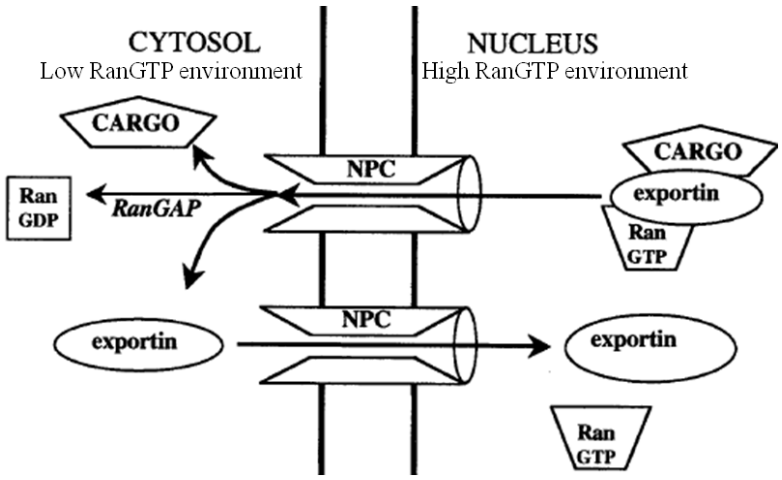

Figure 1.6 Karyopherin-facilitated nuclear export (adapted with permission from Macara, 2001 with permission from American Society for Microbiology). Exportin binds cargo in nucleus, translocates through the NPCs. RanGTP hydrolysis leads to cargo release in the cytosol. Exportin is then free to return to the nucleus for another round of export.

1.4 Objective

In the field of nucleocytoplasmic transport, the bidirectionality of karyopherin-mediated transport often describes the importin-dependent import of cargoes into the nucleus and the exportin-dependent export of cargoes out of the nucleus. This description seems to confer irreversibility on the separate import and export pathways. Moreover, a lot of studies have investigated the translocation of diverse cargoes through the NPCs, but not much is known about the detailed kinetics and interactions that precede/succeed the translocation steps. In addition, the rate-limiting step/reaction for nuclear transport is still not clear. Therefore, the goal of this thesis was to unravel the *in vivo* dynamic molecular events that characterize nucleocytoplasmic transport at steady state in bulk experiments as well as in single NPCs.

Chapter 1 is a broad literature context within which the results that form the basis of this thesis are situated.

Chapter 2 dwells on the use of fluorescence loss in photobleaching (FLIP) and fluorescence recovery after photobleaching (FRAP) to examine live HeLa cells transfected with EGFP-labelled, NLS-containing cargoes. The *in vivo* data was then confirmed by the set of *in vitro* experiments done by my supervisor, Dr. Shige H. Yoshimura.

In Chapter 3, the data obtained from the *in vivo* experiments were probed further by kinetic simulations to fully dissect the various interactions that signpost the nuclear import cycle facilitated by importin β. Of all the 13 figures reported in this chapter and Chapter 2,

two were done by my co-authors. Specifically, Dr Shige H. Yoshimura performed the *in vitro* experiments reported in Figure 2.4, as well as the surface plasmon resonance (SPR) experiments for the kinetic parameters (k_{on} and k_{off}) that are shown in Table 3.1 and used to design the kinetic model; Dr Shotaro Otsuka did the FRAP experiment for EGFP- importin β shown at the top of Figure 2.6A; I did all the other experiments and simulations.

In Chapter 4, the kinetic details of visualizing the molecular dynamics in single NPCs using single molecule imaging are presented. Quasi-TIRF microscope was used to image single NPCs in digitonin-permeabilized HeLa cells bathed in a buffer containing fluorescently labelled importin β. The results described here were obtained in close collaboration with Dr Takahiro Fujiwara of the Center for Meso-Bio Single Molecule Imaging/Institute for Integrated Cell-Material Science (CeMI/iCeMS), Kyoto University.

The last chapter of this thesis (Chapter 5) provides a holistic discussion of the results presented in the preceding chapters, and ends with probable future perspectives.

Chapter 2

Intracellular dynamics of karyopherins and their cargos in a living cell

2.1 Introduction.

In the simplest terms, a system is said to be at steady-state if the concentration and kinetic flux of its components are constant in spite of dynamic factors that tend to change them. The unique features of the NPCs, which have already been discussed in Chapter 1, in addition to the crowded environment of the nuclear pores, check the free exchange of macromolecules between the nucleoplasm and the cytoplasm (Timney et al., 2006; Zilman et al., 2007; Tetenbaum-Novatt et al., 2012). Molecules that are smaller than 40 kDa are capable of passively diffusing through the NPC. On the other hand, large and hydrophilic molecules usually require transport mediators for translocation to occur (Paine et al., 1975; Gorlich and Kutay, 1999; Pante and Kann, 2002; Peters, 2009)

Proteins that belong to the karyopherin β family are the most extensively studied nuclear transport receptors. They facilitate the translocation of a wide range of cellular proteins/molecules (Cingolani et al., 1999; Ström and Weis, 2001; Cingolani et al., 2002; Lee et al., 2003; Cansizoglu et al., 2007). As already discussed in Chapter 1, the high content of HEAT repeats in karyopherins confer on them the ability to pass through the NPCs by themselves regardless of their large molecular weights (about 100 kDa). Transport cargoes exploit this feature to piggyback on karyopherins to access their destinations. Karyopherins and other HEAT-motif proteins undergo flexible and extensive conformational changes, which enable them to spontaneously pass through the hydrophobic environment of the nuclear pores (Kumeta et al., 2012; Yoshimura et al., 2014).

In spite of the compelling body of evidence that confirms that the HEAT repeats enable karyopherins to overcome the hydrophobic barrier in NPCs, there is still the question regarding the intrinsic directionality of karyopherins through the nuclear pores (Chook and Blobel, 1999). Transient hydrophobic bonds are the primary modes of interaction between karyopherins and nucleoporins during transit in the NPCs (Rout et al., 2000; Frey et al., 2006; Lim et al., 2006; Hutten et al., 2008). *In vitro* measurement of the interaction between importin β and Nups show that the degree of affinity for importin β is different (Ben-Efraim and Gerace, 2001), suggesting that the movement of importin β towards the nucleoplasm might depend on increasing affinity with Nups (affinity gradient; Shah and Forbes, 1998; Ribbeck and Görlich, 2001). Consequently, it was reasonably proposed that directional nuclear import of cargo by importin β is attributable to its intrinsic directionality. However, the additional requirement of other protein(s) or mechanism(s) to effect the release of importin β from the NPC, and ferry it back to the cytoplasm severely limits this model (Zilman et al., 2007). Moreover, there are no reports yet of any structural differences between exportins and importins that might explain the opposite directionality.

Conversely, non-directional models do not have the limitation of requiring other proteins to effect successful shuttling of karyopherins across the NPCs. They can also account for the active/facilitated transport of cargo when combined with RanGTP-dependent cargo loading and dissociation in the nucleus and cytoplasm respectively (Görlich et al., 1996; Görlich et al., 2003). Indeed, Gorlich and Kutay (1999) used an *in*

vitro transport assay system to provide one of the earliest proofs of the bidirectionality of importin β through the NPC. One prerequisite for this bidirectional model to establish a cargo gradient across the nuclear envelope *in vivo* is that the entire transport system must involve certain interaction kinetics that incorporate the cargo, karyopherins and RanGTP, in addition to a balanced concentration of each component in the appropriate compartments. Although *in vitro* transport assays can be used to demonstrate that this model is capable of establishing a cargo gradient, it is remains to be known if this is also the case in living cells.

In this study, karyopherin-dependent cargo transport *in vivo* was quantitatively investigated with a view to elucidating the shuttling of karyopherin-cargo complex across the nuclear pores, and what role it plays in the maintenance of the cargo gradient. Flux rate constants and association-dissociation rate constants of the interactions between karyopherins and cargoes were obtained from *in vitro* assays. These rate constants were then integrated with the data obtained from FRAP and FLIP measurements of fluorescently-tagged cargoes and karyopherins in live cells. These analyses provided insights into the intracellular dynamics of the transport components, as well as information on how they are integrated into the entire nuclear transport system to reach steady-state in cells.

2.2 Materials and Methods

2.2.1 DNA constructs

cDNA encoding human rpL23A and eIF1A were purchased from Kazusa DNA Research Institute, Japan. They were then inserted in-frame into pEGFP-C1 vector to form EGFP-rpL23A DNA and EGFP-eIF1A constructs, which were used for transfection of HeLa cells. pEGFP-C1 was digested with *Sal*I, purified with invitrogen™ PureLink® PCR Purification Kit, dephosphorylated with Shrimp Alkaline Phosphatase (Takara, Japan), purified again before digestion with Klenow Fragment to generate blunt ends for ligation. The cDNAs for eIF1A and rpL23A were double-digested with *Kpn*I and *Pvu*I, and the specific DNA sequence extracted from agarose gel before digestion with Klenow Fragment for ligation with vector. Expression vectors for importin β and Snail were kind gifts from Dr. Yoneda (Osaka University, Japan). cNLS-EGFP-eIF4A1 was constructed and purified by Hiroya Yamazaki. EGFPx3-cNLS was constructed by Dr S.H. Yoshimura.

2.2.2 FRAP and FLIP analyses

A fusion of three tandem EGFP with the cNLS of the large T-antigen of SV40 (EGFPx3-cNLS), EGFP-Snail, EGFP-eIF1A, EGFP-rpL23A or EGFP-eIF4A1 fused with SV40 NLS were expressed in HeLa cells. All microscopic analyses (photobleaching, observation and image acquisition) were done by confocal laser scanning microscope (Olympus FV 1200 IX83). The sample chamber of the microscope was maintained at 37 ^{o}C with a steady stream of 5% CO_2 during the live cell imaging protocols. For the FRAP and FLIP

experiments, three images were acquired at 10 s per frame prior to bleaching. All post-bleaching images were captured with laser intensity set at 1% so as to minimize the loss of fluorescence intensity.

For the FLIP experiments, a clearly defined area of the cytoplasm was irradiated alternately at maximum output for 2 s and images were acquired for 15 s between rounds of laser irradiation. The duration of the FLIP experiment was 30 min. Analysis of captured images was done by subtracting background signals and expressing fluorescence intensity in the nucleus relative to the pre-bleach intensity. A simple sketch of the FLIP protocol is shown below:

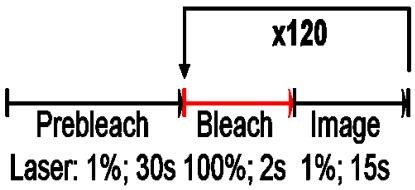

In the FRAP experiments, the entire nucleus was bleached at maximum laser output for 72 msec (EGFP-importin β; Dr Shotaro Otsuka) and 5 s (EGFP-labeled cargoes). Nuclear signal recovery images were acquired every 63 msec for 20 s (EGFP-importin β) and every 3 s for 20 min (EGFP-labeled cargoes). Fluorescence recovery was then expressed as nuclear fluorescence intensity relative to pre-bleach intensity.

2.2.3 *In vitro* nuclear transport assay

This was done based on the method first described by Adam et al., 1990. HeLa cells were washed twice with Transport Buffer (TB; 20 mM HEPES-KOH, pH 7.3, 5 mM

CH_3COONa, 2 mM ($(CH_3COO)_2Mg$, 110 mM CH_3COOK, 1 mM DTT and 0.5 mM EGTA), and incubated with 40 μg/ml digitonin at 0^oC for 5 min. Then the cells were washed twice, and incubated with TB containing 1 μM Rhodamine-linked 70 kDa Dextran and 2 mM dithiothrietol (DTT) at 37^oC for 15 min. Intact nuclei were selected and the time-lapse observation by fluorescence microscopy (Olympus FV 1200 IX83) was started just before the addition of purified EGFP-fused protein (1-5 μM). The integrity of the nuclear envelope was verified by the Rhodamine-linked 70 kDa.

2.2.4 Image analysis and kinetic analysis

Images were acquired using the Olympus FV1200 microscope and analysis was done by the in-built Fluoview FV software. Origin software (Light Stone) was used for curve-fitting and other kinetic analyses.

2.3 Results

2.3.1 Importin-facilitated cargo flux at steady state is bidirectional *in vivo*

Evidence abound to show that most members of the karyopherin β superfamily proteins are endogenously synthesized by HeLa cells in amounts that are physiologically relevant (Yaseen and Blobel, 1997; Mingot et al., 2001; Miyamoto et al., 2004; Van Der Watt et al., 2009). Therefore, the *in vivo* experiments in this study focused on well-known cargoes of some karyopherins. HeLa cells were transfected with EGFP-Snail (an importin β cargo). 24 h post-transfection, they were analyzed by continuously photobleaching of a portion of the cytoplasm (FLIP).

As shown in Figure 2.1, the fluorescence signal of the cargo in the nucleus reduced significantly compared with the non-bleached controls (sample size, n = 10 for the FLIP and control analyses). Similar results were obtained for eIF1A (a cargo for importin 13), rpL23A (a cargo for importin 5), as well as for cNLS-EGFP-eIF4A1 and three tandem EGFP fused with the cNLS of the large T-antigen of SV40 (EGFPx3-cNLS); the latter cargoes are both imported by the importin α/β pathway (Figures 2.1 and 2.3). These results indicate that import cargoes shuttle between the nucleoplasm and cytoplasm in living cells; the importin-cargo complex has other fates in addition to RanGTP-dependent dissociation in the nucleus.

Then the effect of leptomycin B (LMB), a well-established specific inhibitor of Crm1, on the nuclear efflux of the import cargo was examined. Earlier reports have established that exposure of HeLa cells to 5 ng/ml LMB for 4-24 h is sufficient to significantly block the Crm1-dependent export pathway (Kudo et al., 1998; Jang et al., 2003; Kumeta et al., 2010; Kuusisto et al., 2012). Prior treatment of the HeLa cells with 5 ng/ml LMB for 5-8 h before FLIP analysis did not significantly stop the nuclear fluorescence loss for all import cargoes tested (n = 10; Figure 2.2 and 2.3; Table 1), suggesting that Crm1 played a peripheral role, if any, in facilitating the export of the import cargoes out of the nucleus.

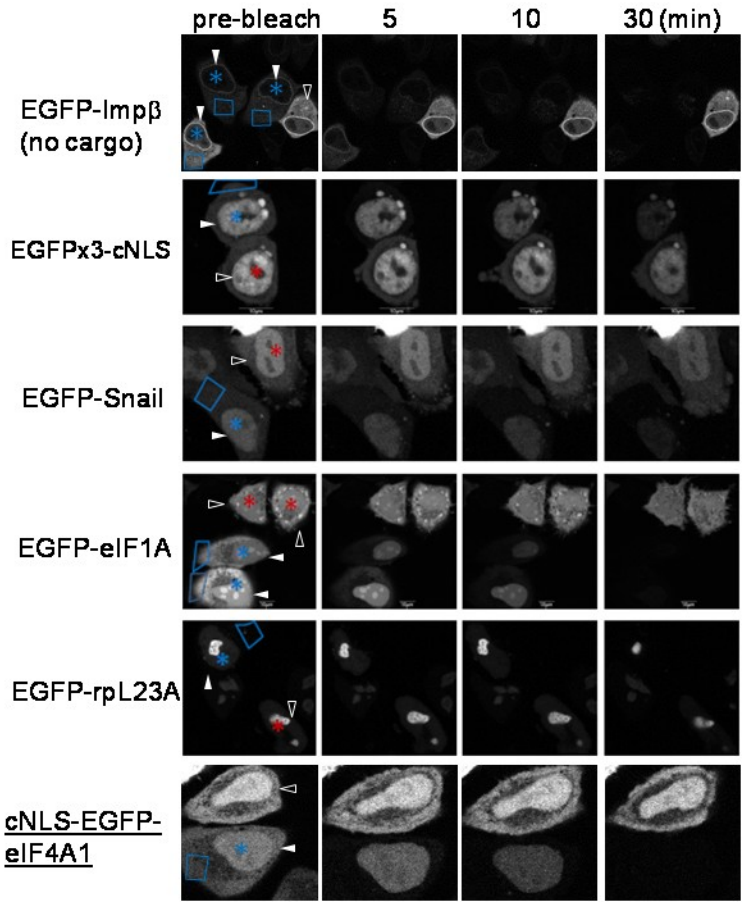

Figure 2.1 Flux dynamics of import cargoes *in vivo*. FLIP analysis of EGFP-labeled cargoes in HeLa cells. EGFP-importin β, three tandem EGFP fused with a cNLS (EGFPx3-cNLS), EGFP-labelled Snail, eIF1A, rpL23A and eIF4A1 were expressed in HeLa cells. Portions of the cytoplasm (blue regions) of cells (closed arrowheads) were continuous bleached in an alternating pattern with image capture for 30 min. The fluorescence signal intensities in the corresponding nuclei (blue asterisks, *) and the nuclei (red asterisks) of control, non-bleached cells (open arrowheads) were measured.

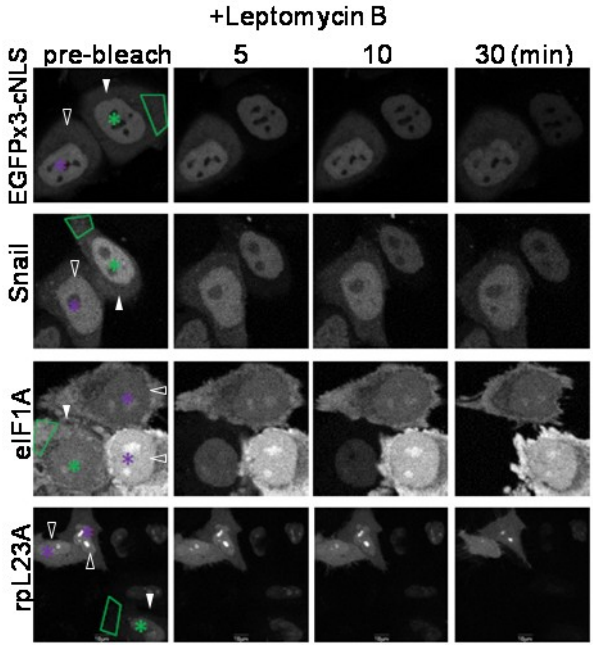

Figure 2.2 Efflux of import cargoes is Crm1-independent. FLIP analysis of EGFP-labeled cargoes in HeLa cells in the presence of leptomycin B (LMB). Three tandem EGFP fused with an NLS (EGFPx3-NLS), EGFP-tagged Snail, eIF1A and rpL23A were expressed in HeLa cells. 5 ng/ml LMB was added 5 - 8 h prior to continuous photobleaching, for 30 min, of portions of the cytoplasm (green regions) of cells (closed arrowheads). The signal intensities of the corresponding nuclei (green asterisks) and the nuclei (purple asterisks) of control, non-bleached cells (open arrowheads) were measured.

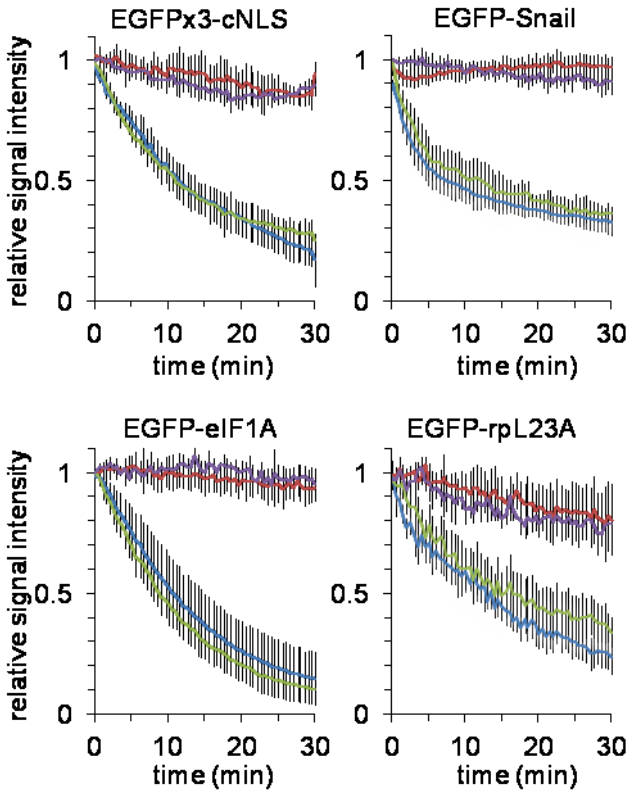

Figure 2.3 Quantification of nuclear fluorescence intensities in Figures 2.1 and 2.2. Relative fluorescence intensity of bleached and non-bleached nuclei are plotted (blue and red for bleached and non-bleached, respectively), together with LMB-treated cells (green and purple for bleached and non-bleached, respectively). Identical measurements were done in at least 10 different cells for statistical averaging. Error bars represent standard deviation (s.d.). The data were fit with a monoexponential decay equation (Y = a*exp(k_{out}*X)+c), and the kinetic constant, k_{out} was obtained from the mobile fraction. The immobile fraction, c, for EGFP-snail, EGFP-rpL23A, EGFP-eIF1A and EGFPx3-cNLS was estimated to be 35%, 34%, 18% and 11% respectively.

Table 2.1 Statistical evaluation (Student's t-test) of leptomycin B treatment on efflux constants (k_{out}).

	-LMB	**+LMB**
	$k_{out} \pm$ SD (x10^{-3} sec^{-1})	
EGFP-eIF1A	1.13 ± 0.52	1.38 ± 0.22
EGFP-rpL23A	0.98 ± 0.05	1.13 ± 0.67
EGFP-Snail	3.30 ± 0.96	2.60 ± 1.52
EGFPx3-cNLS	1.40 ± 0.82	1.26 ± 0.26

10 cells were used for the statistical evaluation of k_{out} values obtained from FLIP assays from three independent experiments. Values are expressed as Mean ± SD. For each cargo tested, there was no statistically significant difference ($P>0.05$). The Student's t-test confirmed that treatment with LMB did not cause a statistically significant difference between the k_{out} values (Figure 2.3)

2.3.2 Importin β can mediate the efflux of its cargo from the nucleus

The direct involvement of importin β in the efflux of the import cargo was then investigated. Digitonin-permeablized HeLa cells were pre-loaded with fluorescently-labeled import cargo (GST-cNLS-EGFP), and then the external medium was replaced with buffer alone or with buffer containing importin β. In the mock condition without any external proteins, the fluorescence signal of the cargo in the nucleus did not reduce after 20 min (n = 7; Figure 2.4A, top), whereas incubation with importin β significantly reduced the nuclear fluorescence signal (n = 6; Figures 2.4A: middle and bottom; and 2.4B). Furthermore, the addition of importin α together with importin β accelerated the efflux of GST-cNLS-EGFP (n = 4; Figure 2.4B). Taken together, the most credible interpretation is that free importin β introduced into the external medium spontaneously enters the nucleus, where it binds to the cargo. Then, it forms a complex with the cargo and exits the nucleus in a Ran-independent manner.

The *in vivo* flux dynamics revealed by the FLIP assays (Figures 2.1 - 2.3) is a general phenomenon for the two classes of karyopherin. Digitonin-permeabilized HeLa cell nuclei were incubated with either importin β-cargo complex (importin β-binding domain of importin α (IBB) and GFP-importin β; Figure 2.4C, top), or exportin-cargo complex (NES peptide and GFP-Crm1; Figure 2.4C, bottom). In both cases, the karyopherin-cargo complex rapidly entered the nuclei (10 min). When the external medium was replaced with buffer without any proteins, and observation was continued for another 20 min, both the importin- and exportin-cargo complexes were able to leak out of the nuclei (30 min). These

results strongly indicate that karyopherin-cargo complex shuttles across the NPC in both directions. Similar results were also obtained when karyopherins, in the absence of cargoes and RanGTP, were observed to rapidly accumulate in the nucleus of digitonin-treated cells to the same level as the extra-nuclear space (Figure 2.5).

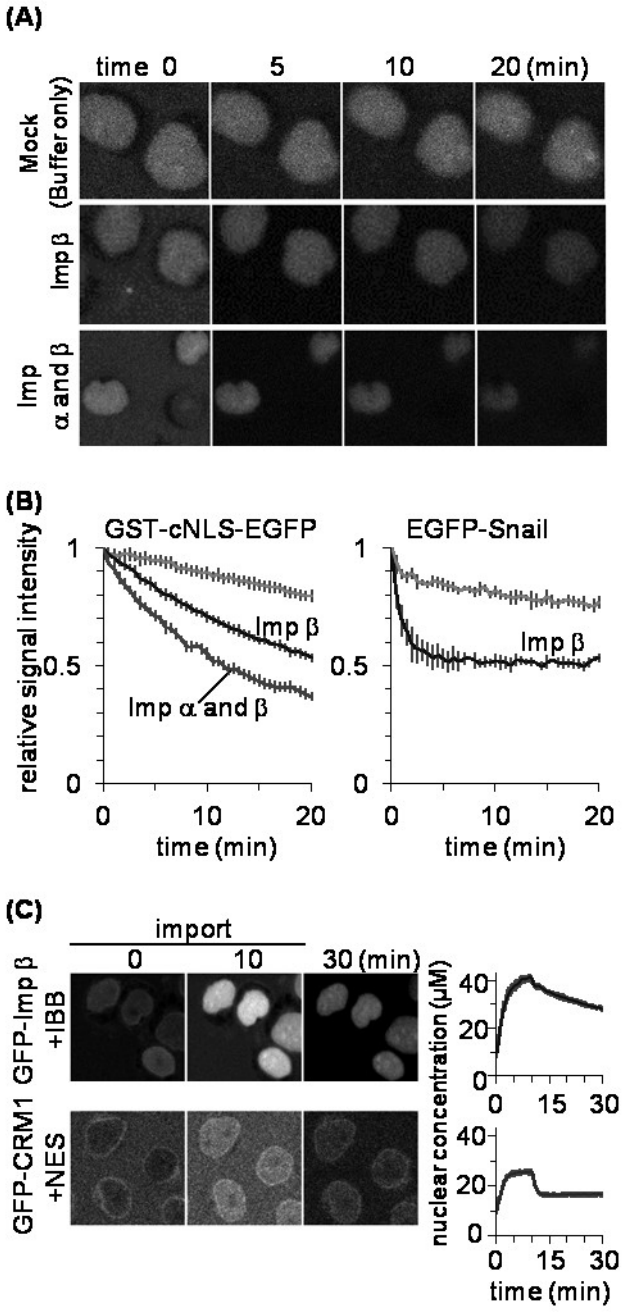
(A)
time 0
5
10
20 (min)
Mock (Buffer only)
Imp β
Imp α and β
(B)
GST-cNLS-EGFP
EGFP-Snail
relative signal intensity
Imp β
Imp α and β
time (min)
(C)
import
0
10
30 (min)
GFP-Imp β +IBB
GFP-CRM1 +NES
nuclear concentration (μM)
time (min)

Figure 2.4 (Experiment done by Dr S.H. Yoshimura). Importin β mediates the export of import cargoes in a Ran-independent manner. (A) Digitonin-permeabilized cells were pre-loaded with fluorescently labeled cargo (GST-cNLS-EGFP) by incubation in the presence of importin α, β, RanGDP and ATP regeneration system for 10 min. Afterwards, the external medium was replaced with one of the following: only buffer (top); buffer containing importin β (middle); or buffer with both importin α and β (bottom). Time-lapse microscope observation was performed for 20 min. Captured images at time 0, 5, 10, and 20 min are presented. **(B)** Signal intensity within each nucleus in (A) was quantified, averaged, and plotted against time; HeLa nuclei pre-loaded with GFP-cNLS-EGFP (left) and EGFP-snail (right). The same measurements were performed in a minimum of five different cells. The error bars represent standard deviation (s.d.). **(C)** 4 μM each of GFP-fused importin β, RanGDP and IBB, as well as an ATP regeneration system was added to the external medium of digitonin-treated HeLa cells (top). 1 μM GFP-fused Crm1, 4 μM RanGDP and 1 μM NES peptide were also added to semi-permeabilized cells (bottom). The observation was performed for 10 min, then the external medium was replaced with the buffer without any protein and observation was continued for another 20 min. The average fluorescence intensity of the nucleoplasm was measured, converted to concentration and plotted against time (right). The same measurements were performed in a minimum of five different cells. The error bars represent standard deviation (s.d.).

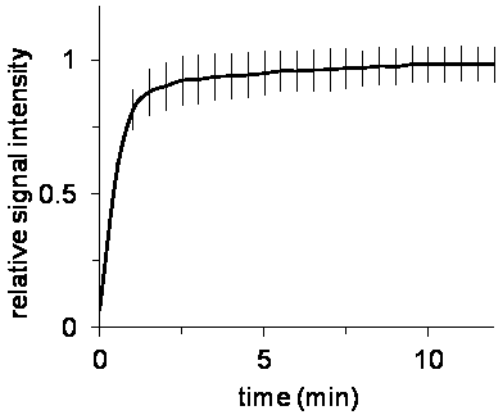

Figure 2.5 RanGTP is not required for nuclear karyopherin flux. Digitonin-permeabilized HeLa cells were incubated with importin β (1 μM) in the absence of RanGTP. The karyopherin swiftly entered the nucleus and reached the same level as that of the external medium (~1 μM).

2.3.3 karyopherin-cargo flux at steady state is affected by cargo properties

The next question was to understand how cargo properties might impact on the kinetics of importin β and cargo shuttling. To this end, HeLa cells were transfected with cargoes of different sizes and their flux rates across the NPC were examined by FRAP analysis (n = 5 for each cargo; Figure 2.6). The results revealed an inverse relationship between cargo size and influx rate: EGFPx3-cNLS, cNLS-EGFP-eIF4A1 and EGFP-snail have molecular weights of ~100, 73 and 60 kDa, respectively (Figure 2.6A-B). EGFP-eIF1A had a lower influx rate than EGFP-snail in spite of its relatively lesser molecular weight of ~50 kDa (Figure 2.6B). This may be due to the different importin pathway (importin 13) that ferries it across the NPCs.

Although all the substrates investigated are larger than the ~40 kDa canonical cut-off limit for passive (receptor-free) translocation, there is a likelihood that passive permeability might contribute to the observed flux. Indeed, there are reports of proteins such as β1-spectrin, actinin-4 and β-catenin (molecular weights >100 kDa) that are able to adapt their amphiphilic motifs to the microenvironment within the NPCs to spontaneously shuttle in a karyopherin-independent manner (Kumeta et al., 2012; Sharma et al., 2012). Therefore, additional experiments were performed to clarify the contribution of passive flux to the shuttling of karyopherin-dependent cargoes.

First, three tandem EGFP (EGFPx3; ~100 kDa) without an NLS was over-expressed in HeLa cells. The protein was predominantly distributed in the cytoplasm and did not

localize to the nucleus (Figure 2.7, top). Notwithstanding, FRAP experiments were performed on these cells. As shown, there was no detectable influx into the nucleus. In another approach, an *in vitro* transport assay using purified cNLS-EGFP-eIF4A1 (~73 kDa) was done in the absence of karyopherins that recognize the cNLS (Figure 2.7, bottom). As was the case with EGFPx3, there was no nuclear accumulation indicating that passive permeability may be negligible in the shuttling of karyopherin-dependent cargoes that are larger than the cut-off limit. Therefore, it was concluded that passive permeability of large cargoes made no significant input to the observed flux rates given that they did not show spontaneous passage through the NPC without the help of karyopherins.

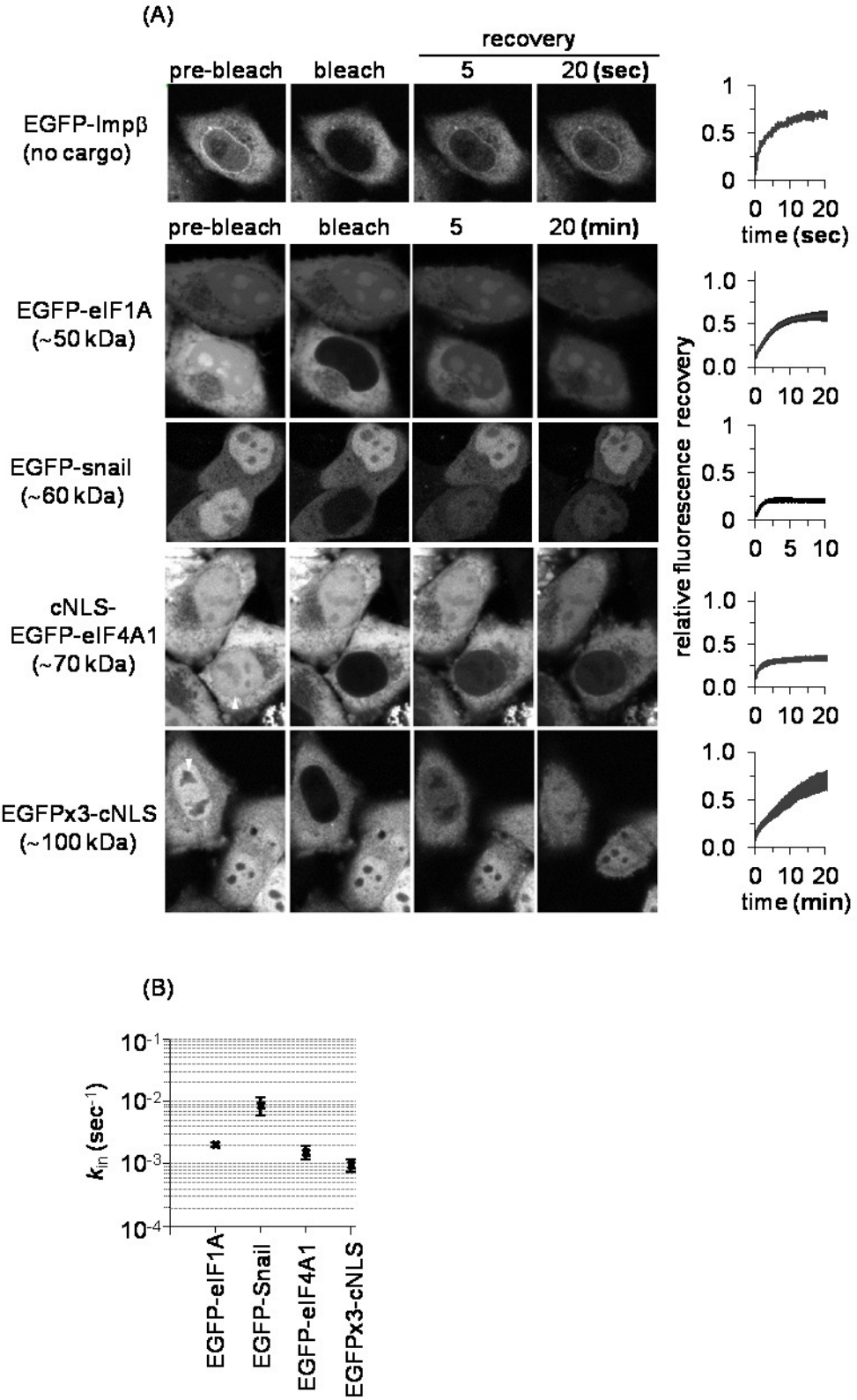
(A)
recovery
pre-bleach
bleach
5
20 (sec)
EGFP-Impβ
(no cargo)
time (sec)
pre-bleach
bleach
5
20 (min)
EGFP-eIF1A
(~50 kDa)
EGFP-snail
(~60 kDa)
cNLS-
EGFP-eIF4A1
(~70 kDa)
EGFPx3-cNLS
(~100 kDa)
relative fluorescence recovery
time (min)
(B)
k_{in} (sec^{-1})
EGFP-eIF1A
EGFP-Snail
EGFP-eIF4A1
EGFPx3-cNLS

Figure 2.6. Karyopherin-cargo flux is affected by cargo properties. FRAP analysis of nuclear influx of different cargoes. **(A)** EGFP-importin β and EGFP-labeled cargoes of importins ranging from ~50 to 100 kDa were transfected into HeLa cells for 24 h. Then the nucleus was photobleached at maximum output for 72 msec (EGFP-importin β; Dr Shotaro Otsuka) and 5 s (EGFP-labeled cargoes). Nuclear fluorescence recovery monitored every 63 msec for 20 s (EGFP-importin β) and every 3 s for 20 min (EGFP-labeled cargoes). Signal recovery intensities were measured and expressed relative to pre-bleach intensity (right). The same measurements were made in a minimum of five different cells. The error bars represent standard deviation (s.d.). **(B)** An exponential curve was fit to the FRAP data and the indicated k_{in} values obtained.

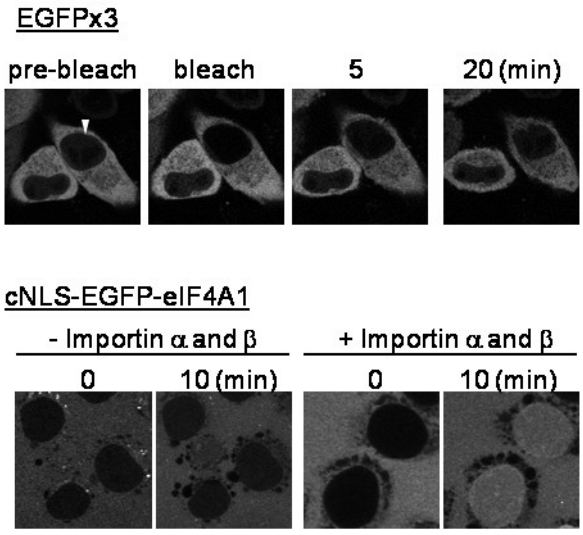

Figure 2.7 Cargoes larger than 40 kDa cannot passively diffuse into the nucleus; they require karyopherins for facilitated diffusion (Top) Three tandem EGFP (EGFPx3) was transfected into HeLa cells. 24 h post-transfection, nucleus (closed arrowhead) was bleached for 5 s and recovery was monitored for 20 min. (Bottom)) *In vitro* nuclear transport assay of cNLS-EGFP-eIF4A1. Purified cNLS-EGFP-eIF4A1 was added to the Transport Buffer with/without karyopherins prior to addition to digitonin-permeabilized HeLa nuclei that had been pre-incubated with Rhodamine-linked 70 kDa dextran. Time-lapse observation of nuclear accumulation (or the lack thereof) was done for 10 min.

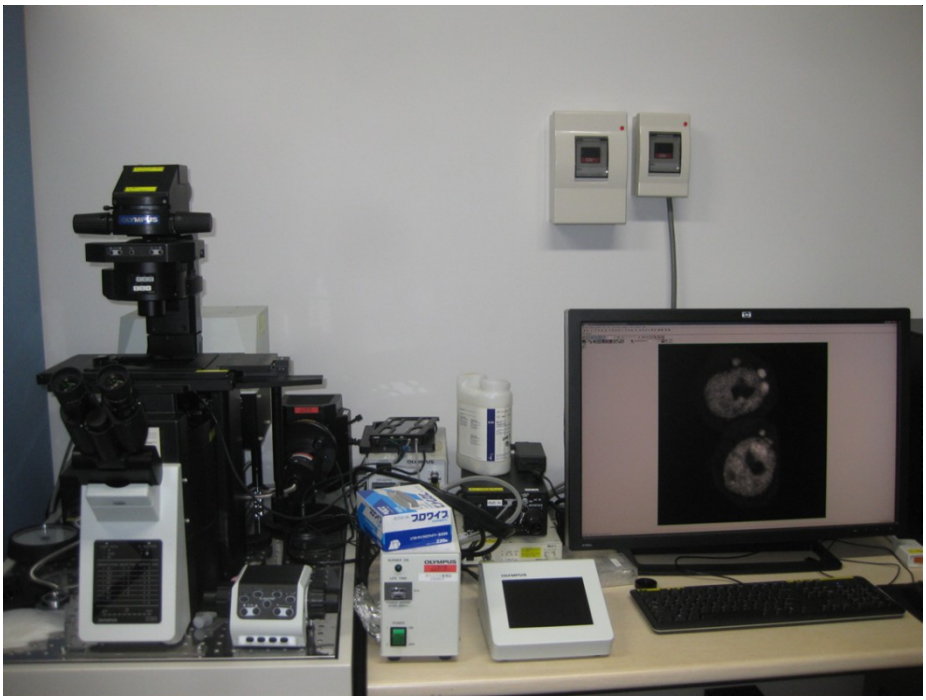

Figure 2.8 Olympus FV microscope used for the FLIP and FRAP analyses (the displayed image is from the FLIP analysis of EGFPx3-cNLS).

Chapter 3

Kinetic modeling of karyopherin-facilitated flux

3.1 Introduction

Kinetic approaches are integral to understanding the mechanism of many intracellular processes including nucleocytoplasmic transport, and they have been applied to elucidate several aspects of cargo translocation through the NPCs. In fact, thermal motion and entropic exclusion were proposed as the source of the driving force for cargo translocation through the NPC following the finding that there are no requirements for mechanoenzymes (like myosin) or ATP-/GTP-driven reactions for the transport process (Brownian Affinity model; Schwoebel et al., 1998; Englmeier et al., 1999; Rout et al., 2000). Kinetic studies further confirmed that the RanGTP gradient across the nuclear envelope (NE) does not necessarily drive transport (except for large cargoes), but mainly provides the energy for cargo accumulation in the appropriate side of the NE (Bischoff and Görlich, 1997; Lyman et al., 2002; Lowe et al., 2015)

Kinetic analyses also showed that the cargo translocation rate through the NPCs *in vitro* could be as high as ~1000 per sec, and cargoes are reported to pass through the central channel of the pores at relatively high speed (≥0.5 μm/s; Selective Phase model; Ribbeck and Görlich, 2001). Indeed, most of the models propounded to explain nuclear transport relied heavily on kinetic studies (please see Chapter 1, Section 1.2.2). In addition, transport receptor binding sites within the NPCs as well as residence times of various karyopherin-cargo complexes and nucleoporins have also been elucidated by kinetic investigations (Rabut et al., 2004; Yang et al., 2004; Kubitscheck et al., 2005; Timney et al., 2006)

Although tremendous amount of studies have been done to understand the dynamics of karyopherin-mediated cargo translocation through the NPCs, there is still not enough work in the literature about the kinetics and interactions that precede/succeed cargo translocation *in vivo*. Therefore, in order to understand the mechanistic details of the *in vivo* experimental observations described in Chapter 2, the flux of each free cargo as well as free and cargo-bound karyopherin was quantitatively estimated by a kinetic model.

3.2 Materials and Methods

3.2.1 *In vitro* nuclear transport assay to determine k_{in} and k_{out} for modeling

HeLa cells were digitonin-treated and time-lapse observation of bulk nuclear transport performed as described in Chapter 2, Materials and Methods, Section 2.2.3. An exponential curve ($Y = \exp(-tk_{out})Y_0 + (k_{in}/k_{out})(1- \exp(-tk_{out})$; where Y is nuclear signal intensity, Y_0 is Y at time, t=0) was fit to the data from which the kinetic constants, k_{in} and k_{out}, were obtained.

3.2.2 kinetic simulations

All molecular simulations were done by CellDesigner 4.4.

3.3 Results

3.3.1 Designing the kinetic model

A kinetic model of karyopherin-dependent nuclear import cycle is shown in Figure 3.1. In the model, the nucleoplasm and cytoplasm are delineated with the volume of the latter set to 5x that of the former. It is envisaged that karyopherins can shuttle between the two compartments with flux rate constants k_{in} and k_{out}, for inward and outward directions, respectively. These fluxes occur for free importin β (Figure 3.1, step 6), importin β-cargo complex (step 5), and importin β-RanGTP complex (step 7). In addition to the fluxes, there are interactions between karyopherin, cargo and Ran in each compartment (step 1, 3), with association and dissociation rate constants k_{on} and k_{off}, respectively. RanGTP-dependent dissociation of importin β from the cargo occurs in the nucleoplasm at an apparent rate constant of k_{on}[impβ-cargo-RanGTP] (step 2). RanGTP exists only in the nucleoplasm at a constant concentration due to the activity of chromatin-bound RCC1. RanGTP is hydrolyzed to RanGDP in the cytoplasm because RanGAP is localized therein (step 4).

RanBP1, as a co-activator of RanGAP, facilitates RanGTP hydrolysis due to its ability to form a RanGTP-RanBP1 complex, which is reported to be the optimal substrate for the enzymatic action of RanGAP (Bischoff and Görlich, 1997; Kuhlmann et al., 1997). Most of the factors that are necessary for active nuclear translocation are accommodated by this model; other co-factors and non-specific competing substrates that present in the

complex cellular environment were excluded to make computation and analysis less cumbersome.

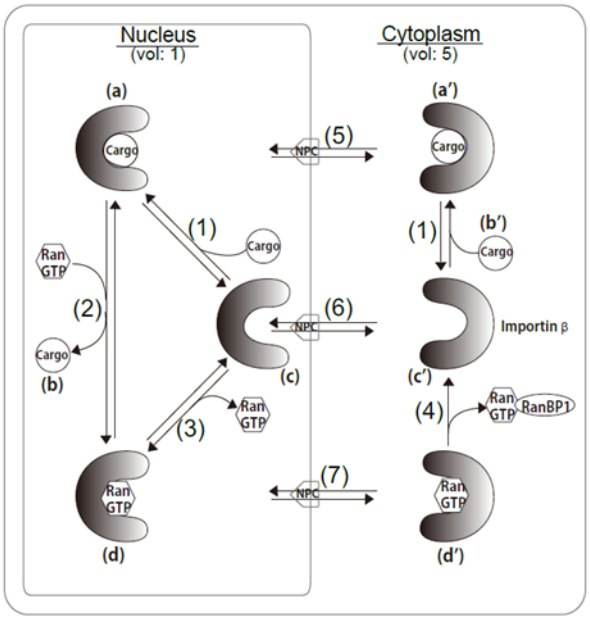

Figure 3.1 Kinetic model of importin β-dependent transport cycle. Rate constants (shown in Table 3.1 with corresponding numbers) from *in vitro* transport assay systems and surface plasmon resonance (SPR) were used to design this model. Free importin β, importin β-cargo complex and importin β-RanGTP complex pass through the NPC in both directions with the indicated flux rates. The steady-state concentration of the components (letters in parenthesis shown in Table 3.2) were obtained by simulation of *in vivo* dynamics under conditions where the cargo/importin β concentration ratio is 1:1; total cargo and importin β concentrations were each set to 3 μM. The nuclear concentration of free RanGTP and cytoplasmic concentration of RanBP1 were kept constant (1.23 μM and 3 μM respectively) throughout the entire duration of the simulation which was performed until equilibrium was attained.

Table 3.1: Kinetic parameters of bidirectional nuclear transport determined from surface plasmon resonance (SPR) and *in vitro* transport assays

	Reaction/cargo	Kinetic parameters			Reference
(1)	Impβ + IBB ⇌ Impβ-IBB	k_{on}	9.94×10^{4}	$M^{-1}sec^{-1}$	SPR
		k_{off}	1.32×10^{-3}	sec^{-1}	(by S.H.Y)
(2)	Impβ–IBB + RanGTP ⇌ Impβ-RanGTP +IBB	k_{on}	3.89×10^{4}	$M^{-1}sec^{-1}$	SPR
		k_{off}	n.d.		(by S.H.Y)
(3)	Impβ + RanGTP ⇌ Impβ-RanGTP	k_{on}	4.44×10^{4}	$M^{-1}sec^{-1}$	SPR
		k_{off}	1.07×10^{-3}	sec^{-1}	(by S.H.Y)
(4)	Impβ-RanGTP + RanBP1 ⇌ Impβ + RanGTP-RanBP1	k_{on}	3.00×10^{5}	$M^{-1}sec^{-1}$	Kuhlmann
		k_{off}	n.d.		*et al*., 1997.
(5)	$Impβ\text{-}IBB_{cyt}$ ⇌ $Impβ\text{-}IBB_{nuc}$	k_{in}	6.55×10^{-2}	sec^{-1}	*In vitro* transport
		k_{out}	1.68×10^{-2}	sec^{-1}	(this study)
(6)	$Impβ_{cyt}$ ⇌ $Impβ_{nuc}$	k_{in}	5.81×10^{-2}	sec^{-1}	*In vitro* transport
		k_{out}	1.07×10^{-2}	sec^{-1}	(this study)
(7)	$Impβ\text{-}RanGTP_{cyt}$ ⇌ $Impβ\text{-}GTP_{nuc}$	k_{in}	1.78×10^{-2}	sec^{-1}	*In vitro* transport
		k_{out}	2.04×10^{-2}	sec^{-1}	(this study)

S.H.Y = Dr Shige H. Yoshimura

n.d. = not determined

3.3.2 Obtaining kinetic parameters in the model

Free EGFP-importin β, as well as importin β bound to cargo (IBB) and RanGTP, shuttle through the NPC in both directions (inward and outward) with similar flux rate constants (k_{in} and k_{out}; Table 3.1). These constants, in addition to the association and dissociation rate constants (k_{on} and k_{off}) that were obtained and also summarized in Table 3.1, were used to design the kinetic model of karyopherin-dependent nuclear transport cycle (Figure 3.1). The k_{on} and k_{off} values obtained by my colleagues and other groups (Kuhlmann et al., 1997) were used to design the model.

3.3.3 Verification of the kinetic model

The fidelity of kinetic model was examined by simulation of different *in vivo* transport conditions. At the start of the simulation, the nucleus was assumed to be free of cargo and importin β. The initial concentration of cargo and importin β in the cytoplasm was each set at 3 μM, and a RanGTP gradient formed by maintaining the free RanGTP concentration in the nucleoplasm at a constant value of 1.23 μM throughout the simulation (Riddick and Macara, 2005). The entire system reached steady-state before 10 min (Figure 3.2). The steady-state concentrations and fluxes of each component are summarized in Tables 3.2 and 3.3. These simulations confirm that cargo accumulation in the nucleus is not irreversible and does not continue indefinitely given the saturation kinetics observed.

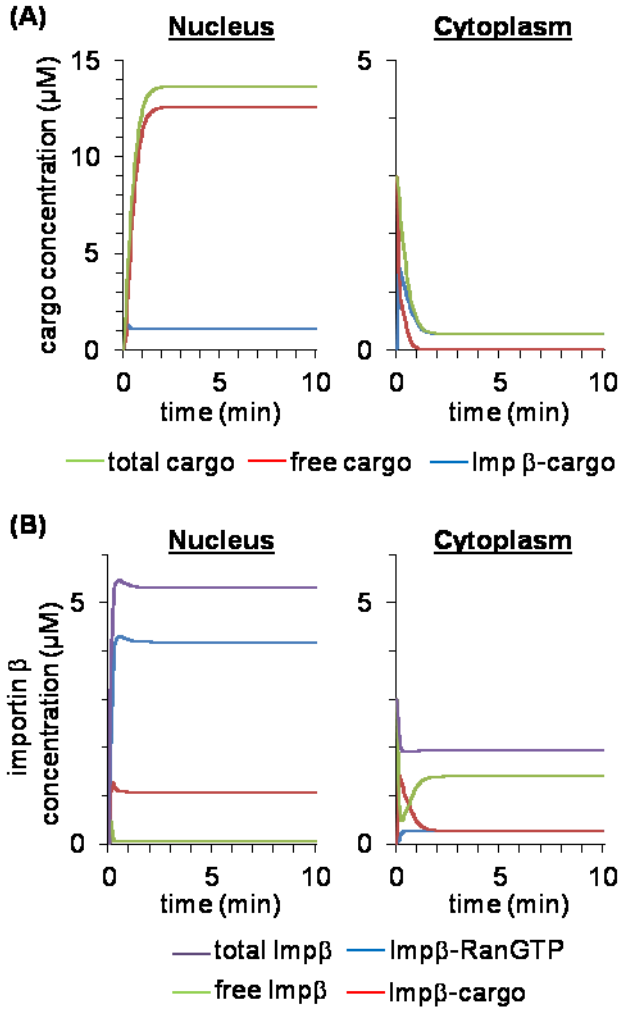

Figure 3.2 Simulation of *in vivo* steady state dynamics of the importin β-cargo transport cycle. At time 0, 3 μM each of importin β and the cargo (IBB) was present in the cytoplasm. **(A, B)** The nuclear concentration of free RanGTP and cytoplasmic concentration of RanBP1 were kept constant (1.23 μM and 3 μM respectively) and the simulation was performed until equilibrium was attained. Total cargo (free + bound with importin β) **(A)** and total importin β (free + bound with cargo + bound with RanGTP) **(B)** in the nucleus and in the cytoplasm are plotted against time (min).

Table 3.2: Steady-state concentrations of model components.

	Steady-state concentration (μM)			
	Importin β-cargo	Free cargo	Free importin β	Importin β-RanGTP
Nucleus	$1.54^{(a)}$	$11.46^{(b)}$	$0.07^{(c)}$	$3.81^{(d)}$
Cytoplasm	$0.40^{(a')}$	$0.004^{(b')}$	$1.28^{(c')}$	$0.24^{(d')}$

The letters in parenthesis— (a) – (d) and (a′) – (d′)—correspond to the same letters in the kinetic model (Figure 2.7). The concentration of total cargo and importin β were set at 3 μM each.

Table 3.3: Steady-state flux of karyopherins and cargoes in the kinetic model

		Influx μM/sec (Number of molecules/NPC/sec)	Efflux μM/sec
5	Importin β-IBB (8 kDa)	0.026 (29)	0.026 (6)
	Importin β-IBB-mCherry (~40 kDa)	0.0089 (10)	0.0089 (2)
	Importin β-GST-mCherry-IBB (~70 kDa)	0.0037 (4)	0.0037 (1)
6	Importin β	0.074 (83)	0.00071 (0.2)
7	Importin β-RanGTP	0.0044 (5)	0.078 (17)
	Total importin β (steps 5+6+7) (Number of molecules/NPC/sec)	(117)	(23.2)

Steps 5, 6 and 7 correspond to the same numbers in the kinetic model (Figure 3.1) and Table 3.2.

3.3.4 Simulating in vivo dynamics of karyopherins and cargoes

In the nuclear transport assays from which the kinetic parameters (k_{in} and k_{out}) were obtained to design the model, digitonin treatment and subsequent pre-incubation characteristically eliminate most of the endogenous proteins prior to addition of the transport substrate. Therefore, at the start of the experiment, the nuclei could be said to be hypothetically empty, which is certainly not the case at steady state *in vivo*. Consequently, it is conceivable that differences could exist between FRAP kinetics and the kinetics of cargo entry into hypothetically empty nuclei, such that the afore-mentioned predictions may not truly reflect the experimental observations. Indeed, the stark difference in the k_{in} of importin β in *in vivo* FRAP (0.138 sec^{-1}, Figure 2.6A) and the k_{in} of importin β entry into a hypothetical empty nucleus (0.0581 sec^{-1}, Table 3.1) buttresses this important point. Therefore, to address the possible effect of this difference on the *in vivo* steady-state dynamics, two experiments were done:

First, the simulation experiment described for Figure 3.2 was repeated using the kinetic parameters obtained from *in vivo* FRAP analysis of importin β. There was no significant difference in the steady-state distribution of cargo between the cytoplasm and the nucleus in spite of the different kinetics for FRAP and entry into a hypothetical empty nucleus (Figure 3.3). This demonstrates that steady-state dynamics can be approximated by the k_{in} obtained by the influx into the 'empty' nucleus. In the second experiment, the rate of influx into a hypothetically empty nucleus was compared with recovery kinetics of semi-permeabilized nuclei that were photobleached after attaining steady state *in vitro* (Figure

3.3). The k_{in} for accumulation was not significantly different from the k_{in} obtained from the FRAP analysis, further confirming that the kinetic parameters used for the modelling can reliably approximate the *in vivo* kinetics described.

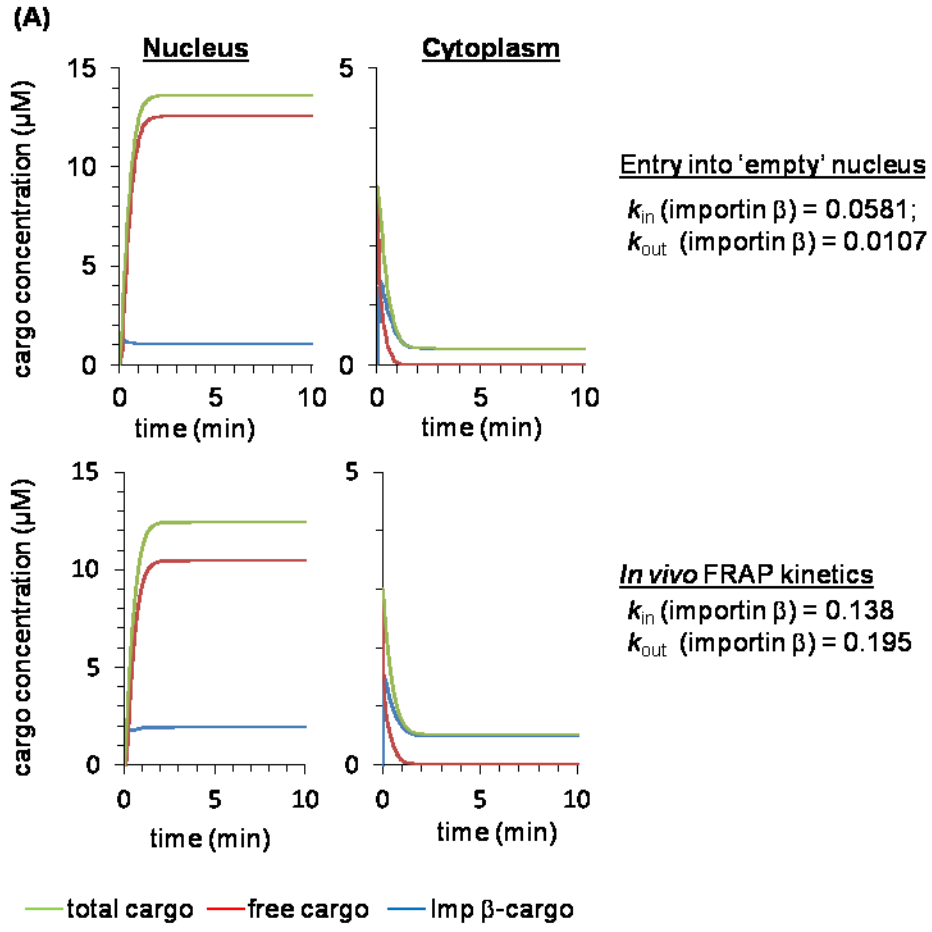

Figure 3.3: Simulation of cargo distribution using kinetic parameters of importin β obtained from *in vivo* FRAP kinetics and entry into hypothetical empty nucleus. Simulation experiments were repeated using k_{in} and k_{out} values of importin β obtained from entry into 'empty' nuclei (upper panels) and FRAP kinetics (lower panels). Simulations conditions: initial concentrations importin β and cargo in the cytoplasm were set at 3 μM each and all the other conditions maintained as described previously in the main text.

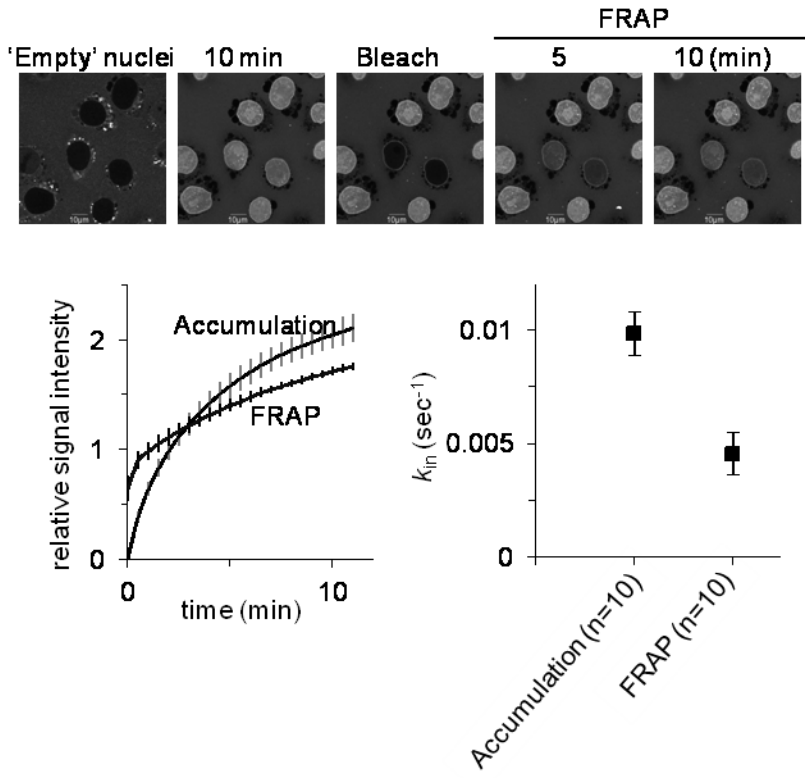

Figure 3.4: Comparison of FRAP kinetics and kinetics of entry into hypothetical empty nuclei. Hela cells were semi-permeabilized and resultant nuclei incubated with transport buffer to rid them of most soluble proteins. The 'empty' nuclei were then incubated with 1 μM importin β and time lapse observation done for 10 min. The nuclei were then photobleached for 5 s and FRAP observed for 10 min. A mono exponential curve was fit to the data and the respective k_{in} and k_{out} values were obtained as shown.

3.3.5 Analysis of steady-state fluxes *in vivo*

The simulation revealed that there are significant influx and efflux of importin β-cargo complex (~0.026 μM/sec for importin β-IBB complex, Table 3.3) as was observed in FLIP and FRAP analyses (Figures 2.1 and 2.6). The influx and efflux of importin β-IBB complex were estimated to be ~29 and ~6 molecules/NPC/sec, respectively, given that the volume of the cytoplasm and nucleoplasm are 5 and 1 pL respectively, and a single nucleus has ~2,700 NPCs (Ribbeck and Görlich, 2001). The total influx of importin β (free, IBB-bound and RanGTP-bound forms) was 117 molecules/NPC/sec (Table 3.3), much larger than that of the cargo (29 molecules/NPC/sec, Table 3.3). Indeed, FRAP analysis demonstrated the fast shuttling of EGFP-importin β *in vivo* (156 molecules/NPC/sec at an EGFP-importin β concentration of 1 μM; Table 3.4).

Mathematically, flux was computed as the product of steady-state concentration, rate constant, Avogadro's Number and volume of nucleus or cytoplasm divided by the estimated number of NPCs on a single nucleus. The fluxes of the importin-dependent cargoes in the *in vivo* FLIP and FRAP experiments were determined by applying the calculated rate constants (Table 3.4) and their steady-state nuclear or cytosolic concentrations which was assumed to be 1 μM given that simulation, in the presence of excess cargo, did not alter the steady-state concentration of importin β-cargo (Table 3.5).

Table 3.4: Flux of cargoes at steady-state *in vivo*.

Cargo	size	k_{in} ($x10^{-3}sec^{-1}$)	k_{out} ($x10^{-3}sec^{-1}$)	Influx (μM/sec) (Number of molecules/NPC/sec)	Efflux (μM/sec) (Number of molecules/NPC/sec)
No cargo (free importin β)	0	140	3.5	0.1400 (156)	0.0035 (3.9)
EGFP-eIF1A	~50 kDa	2.1	1.1	0.0021 (2.3)	0.0011 (1.3)
EGFP-rpL23A	~50 kDa		1.0	n.d	0.0010 (1.1)
EGFP-snail	~60 kDa	9.0	3.3	0.0090 (10)	0.0033 (3.7)
cNLS-EGFP-eIF4A1	~73 kDa	1.6		0.0016 (1.8)	n.d.
EGFPx3-cNLS	~100 kDa	1.0	1.4	0.0010 (1.1)	0.0014 (1.6)

Flux calculation was done using a steady-state concentration of 1 μM. n.d. = not determined.

Table 3.5: Concentrations of importin β-cargo complex at steady-state obtained from titrating cargo concentration in the kinetic model.

	Steady-state concentration (μM)							
Titrations	0.5 μM	1 μM	2 μM	3 μM	5 μM	10 μM	20 μM	50 μM
Nucleus	0.84	1.28	1.50	1.54	1.57	1.60	1.61	1.68
Cytoplasm	0.22	0.33	0.38	0.40	0.40	0.41	0.41	1.43

The range of titration of total cargo concentration was 0.5 – 50 μM. Total importin β concentration was fixed at 3 μM.

3.3.6 Factors affecting the in vivo transport dynamics: cargo size, Ran gradient and cargo/Kap ratio

At steady-state, the nuclear/cytoplasmic (nuc/cyt) ratio of total cargo (free and importin β-bound forms) was ~32, whereas that of total importin β (free, cargo-bound, and RanGTP-bound forms) was 2.7. The nuc/cyt ratio of cargo was not affected by influx and efflux rate constants of importin β-cargo complex (k_{in} (impβ-cargo)); they only affect the time required to reach equilibrium (Figure 3.5A). In contrast, the steady-state cargo fluxes largely depend on k_{in} and k_{out} values of importin β-cargo complex (Table 3.3), and, therefore, on the cargo size (Figure 2.6). Cargoes with ~40 and ~70 kDa showed steady-state influxes of ~10 and 4 molecules/NPC/sec, respectively. These values are in good agreement with flux of 1 – 10 molecules/NPC/sec determined in both the FLIP and FRAP analyses (Figures 2.1 and 2.6, Table 3.4).

Further confirmation of the fidelity of the model was obtained by simulating the effect of RanGTP on the steady-state flux. The nuclear concentration of RanGTP was titrated from 0.01 to 10 μM in the model. As the RanGTP concentration increased, the steady-state nuclear accumulation of the cargo also accelerated (Figure 3.5B).

Collectively, all of these results demonstrate that the kinetic model could explain the *in vivo* steady-state dynamics of karyopherin-dependent transport cycle.

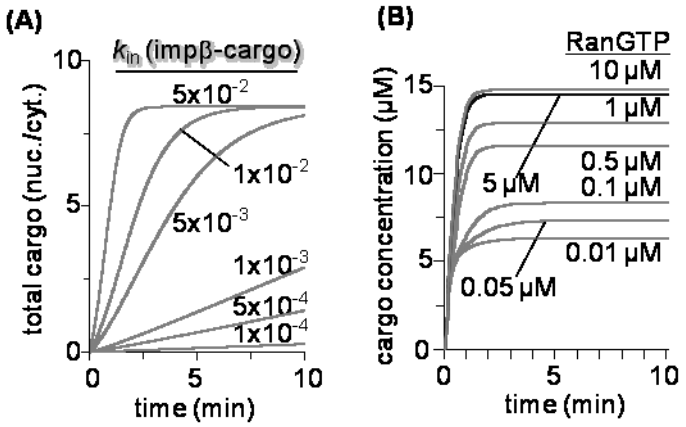

Figure 3.5 ***In vivo*** **simulation of the steady state dynamics of the importin β-cargo transport cycle**. **(A)** The effect of cargo size, represented by influx/efflux rate constants of importin β-cargo complex (k_{in} (importin β-cargo), on steady-state nuc/cyt cargo distribution *in vivo* was simulated. **(B)** *In vivo* simulation of steady-state nuclear distribution of cargo in the presence of different concentrations of RanGTP.

A single karyopherin molecule mediates the translocation of multiple and diverse cargoes. Therefore, it is pertinent to simulate how different cargo/karyopherin (cargo/kap) ratios affect the steady-state cargo distribution and flux. The kinetic simulation described above was performed at a fixed amount of importin β (3 μM) and varying amounts of initial cytoplasmic cargo (0.5 – 50 μM). As the cargo/kap concentration ratio increased, accumulation of the cargo in the nucleus (nuc/cyt ratio) increased (Figure 3.6A). However, in the presence of excess cargo (cargo/kap concentration ratios >1), there was no significant change in the steady-state concentration (Table 3.5) and flux of free importin β (Figure 3.6B) and importin β-cargo complex (Figure 3.6C). Conversely, in the presence of excess karyopherin (cargo/kap concentration ratios <1), fluxes of importin β-cargo are increased in a cargo/kap ratio-dependent manner, indicating that karyopherin availability might be a rate-limiting factor in the transport process.

3.3.7 Rate-determining step in the entire transport cycle

The steady-state fluxes were then compared with the binding/unbinding reaction rates (v_{on}, v_{off}) to ascertain the rate-determining step of cargo transport. Four steps of the import process were compared; i) importin β binding to the cargo (Figure 3.1, step (1) in the cytoplasm), ii) influx of importin β-cargo through the NPC (step (5)), iii) RanGTP-dependent cargo-release from importin β (step (2)); and iv) spontaneous dissociation of cargo from the importin β-cargo complex in the nucleus. At all cargo/kap ratio simulated, the rate of importin β-cargo binding (5.22×10^{-4} μM/sec) is much slower than the influx rate (2.59×10^{-2} μM/sec), as well as the cargo-release rates (RanGTP-dependent, $7.38 \times 10^{-}$

^{2} μM/sec; spontaneous, 2.04 x 10^{-3} μM/sec; Figure 3.6D), demonstrating that importin β-cargo binding in the cytoplasm is the rate-limiting step in the import process.

These results also highlight the fate of the importin β-cargo complex in the nucleus; whether it releases the cargo (step 2, on), or travels back to the cytoplasm (step 5, out). As shown in Figure 3.6D, at steady-state, these two different reaction steps have comparable rates (7.38 x 10^{-2} μM/sec for cargo-release and 2.59 x 10^{-2} μM/sec for efflux), although the cargo-release step is slightly faster than the efflux. Again, these results confirm that a significant portion of the imported cargo constantly shuttles across the NPCs at steady state.

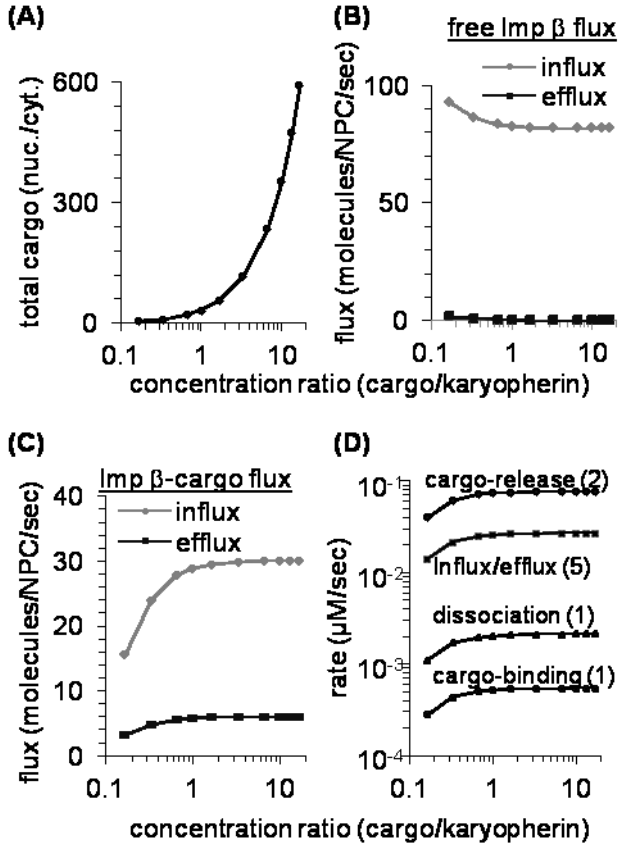

Figure 3.6. Kinetic simulation of conditions that affect steady-state cargo flux/distribution (A-D) Cargo concentration was varied from 0.5 – 50 μM and karyopherin concentration kept constant at 3 μM. Steady-state concentration ratio of total cargo (free + bound) in the nucleus and the cytoplasm **(A)**, free importin β influx/efflux **(B)** and importin β-cargo influx/efflux **(C)** were obtained and plotted against cargo/karyopherin (cargo/kap) concentration ratios. **(D)** The nuclear steady-state concentrations of importin β-cargo complex was integrated with k_{off} [importin β-cargo], k_{on} [importin β-RanGTP] and k_{out} [importin β-cargo] to obtain the rates of spontaneous dissociation (Figure 2.7, step 1), RanGTP-dependent cargo release (step 2) and efflux (step 5). In addition, rate of formation (v_{on}) of importin β-cargo complex was determined by combining the cytoplasmic steady-state concentrations of free importin β and free cargo with the k_{on} of step 1. These fluxes, as well as with the influx rates (step 5) of importin β-cargo, were plotted for the different cargo/kap concentration ratios as shown.

Chapter 4

Analysis of karyopherin flux in single NPCs

4.1 Introduction

4.1.1 NPC characterization: structural techniques and bulk experiments vs. single molecule imaging

The enormous size of each NPC—about 125 MDa in eukaryotes and 66 MDa in yeast—and high content of unstructured nucleoporins (Nups) have hampered their overall structure-function elucidation (Reichelt et al., 1990; Fahrenkrog et al., 2001; Frenkiel-Krispin et al., 2010). This has forced researchers to adopt a divide-and-conquer approach with X-ray crystallography (XC) and electron microscopy (EM) of portions of the NPC as well as bulk biochemical experiments providing much of the available information from which the extant models of orientation and probable mechanisms of nucleocytoplasmic transport were propounded (Hoelz et al., 2011).

Electron microscopy has contributed tremendously to both the structural and functional elucidation of the NPCs. Electron micrographs of the NPCs of yeast, *Dictyostelium* and mainly *Xenopus laevis* oocytes revealed the key structural units of NPCs: the central ring, cytoplasmic ring, nuclear ring, cytoplasmic filaments and nuclear basket (Fahrenkrog et al., 1998; Yang et al., 1998; Panté, 2007). In addition, cryo-electron microscopy also revealed more details that confirm that NPCs undergo structural deformations to allow translocation of large molecules (Hinshaw et al., 1992; Akey and Radermacher, 1993; Stoffler et al., 2003; Beck et al., 2004). Immuno-gold electron microscopy also provided early remarkable information about the localization of nucleoporins as well as the translocation size limit of the NPCs (Figure 4.1; Feldherr et al.,

1984; Dworetzky et al., 1988; Panté et al., 1994; Yokoyama et al., 1995; Fahrenkrog et al., 2002). In addition, available crystal structures of NPC components (Nups 43, 133, 120, 107/133 complex, and others) have also contributed immensely to our present understanding of nuclear translocation and sundry functions (Berke et al., 2004; Boehmer et al., 2008; Seo et al., 2009; Stuwe et al., 2015; Xu et al., 2015).

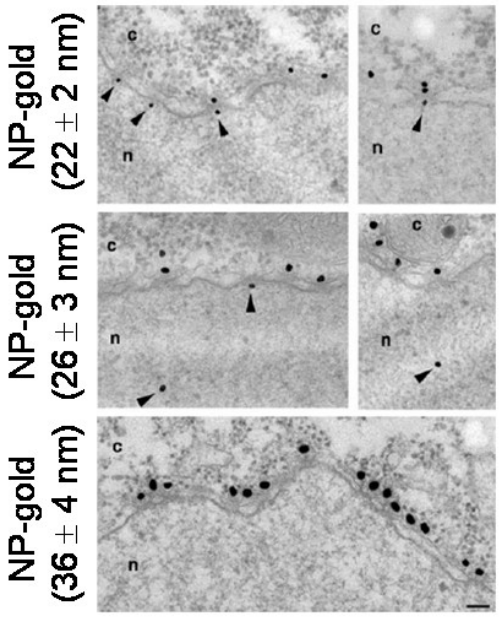

Figure 4.1 The translocation size limit of NPCs revealed by electron microscopy (adapted from Pante and Kann, 2002 with permission from The American Society for Cell Biology). Gold particles (black dots) of various diameters, 22 ± 2 nm (top), 26 ± 3 nm (middle), 36 ± 4 nm (bottom) were coated with nucleoplasmin (NP) and microinjected into the cytoplasm (c) of *Xenopus* oocyte nuclei. 1 h post-injection, nuclear import was monitored by electron microscopy. Arrowheads point to gold particles that were imported into the nucleus (n) or those that associated with the nucleoplasmic side of the NPCs. The micrographs clearly show that gold particles less than 36 nm could be imported from the cytoplasm into the nucleus.

Despite these huge efforts and accomplishments, the precise mechanism by which molecules are shuttled bi-directionally through the NPCs is still elusive. Whereas XC and EM involve sample preparation methods that lead to generation of data devoid of information about dynamic interactions within the pores, bulk experiments like those discussed in Chapter 2, characteristically, provide single averaged values for entire population of NPCs. Taken together, these approaches result in the loss of vital information from single nuclear pores that could fully elucidate the complex mechanisms involved in nucleocytoplasmic transport. In this regard, it would be most desirable to identify, monitor and analyze distinct, dynamic transport events in single NPC molecules—an approach aptly termed single molecule imaging (SMI).

4.1.2 Single Molecule Imaging (SMI) in NPC analysis

In principle, the rapid diffusion of free single molecules in an aqueous environment makes their detection difficult (Kusumi et al., 2010) . However, when their motion is slowed down by interacting with cellular components like Nups, then they become detectable (Yang et al., 2004). SMI measures the full distribution of an experimental parameter as opposed to the averaged value obtained from ensemble experiments (Ritchie et al., 2005). Common instrumentations for SMI include confocal microscopy, epifluorescence, Single-Point Edge Excitation Diffraction (SPEED) microscopy, 4Pi microscopy, Total Internal Reflection Fluorescence (TIRF) microscopy and quasi-TIRF (Figure 4.2; Lord et al., 2010; Luo et al., 2013).

SMI techniques that greatly reduce background intensity are most desirable because they guarantee an increase in the signal/noise ratio. TIRF microscopy meets this criterion as the evanescent wave it generates only illuminates a depth of ~100 nm into a sample (Axelrod, 1981; Tokunaga et al., 1997). It is routinely used to image diverse dynamics at cell surfaces, including membrane signaling and metabolite-induced oligomerization of receptors (Sako et al., 2000; Iino et al., 2001; Ueda et al., 2001; Matsuoka et al., 2006; Schaaf et al., 2009; Hern et al., 2010). However, a major drawback that limits the use of TIRF microscopy for SMI studies is that it cannot resolve intracellular structures that are far (>100 nm) from the cell surface and cover slip (Mattheyses et al., 2010). This technicality is overcome by the recently developed oblique epifluorescence technique, whereby the incident beam is positioned at an angle less than the critical angle such that the refracted beam emerges at an inclined angle (Figure 4.2; Tokunaga et al., 2008)). This modification of TIRF, known as quasi-TIRF, combines the high signal/noise ratio and better axial/temporal resolution of TIRF, with the high spatial resolution of confocal microscopy (Luo et al., 2013). It is also called *highly inclined and laminated optical sheet microscopy* (HILO), *pseudo-TIRF*, *oblique epi-illumination* and *variable angle epifluorescence* (Konopka and Bednarek, 2008; Tokunaga et al., 2008; Lord et al., 2010).

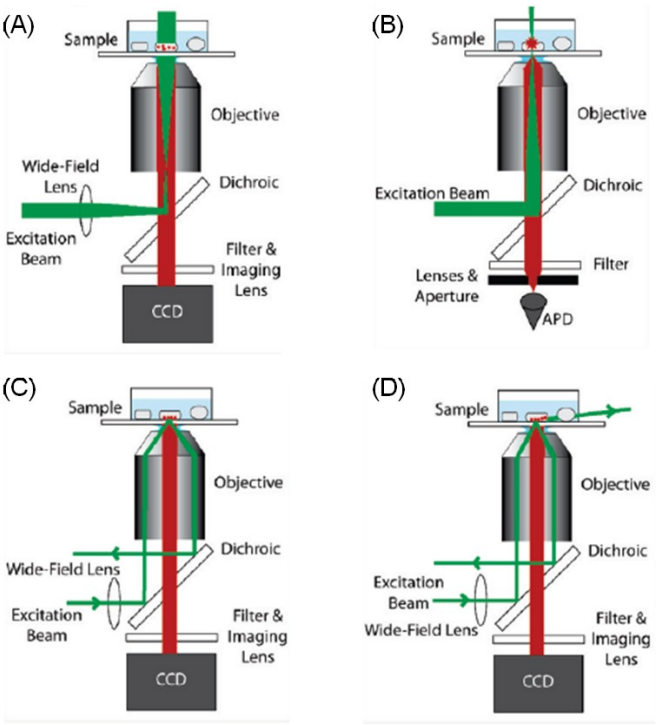

Figure 4.2 Instrumentations for single molecule imaging (culled from Lord et al., 2010 with permission from American Chemical Society). **(A) Epifluorescence:** a wide illumination volume is directed at the sample such that there out-of-focus emissions reduce the signal/background ratio; **(B) Confocal microscope:** the illumination volume passes through a pinhole and is converted into a diffraction-limited spot at the sample. The confocal spot is then scanned across the sample. This point detection significantly reduces out-of-focus fluorescence, but makes it difficult to image different parts of the sample simultaneously. **(C) TIRF:** Only a small fraction (~100 nm) of the sample is illuminated by the evanescent wave that results from positioning the excitation beam at an angle larger than the critical angle. **(D) Quasi-TIRF:** the excitation beam is positioned at an angle less than the critical angle such that the refracted beam emerges at an inclined angle, and only a narrow beam penetrates the sample.

In recent times, SMI investigations have led to an increase in the volume of information about the dynamic events in single NPCs. The residence time of free and cargo-bound importin β, NTF2, transportin as well as several nucleoporins have been unraveled by SMI studies (Görlich et al., 2003; Rabut et al., 2004; Kubitscheck et al., 2005; Riddick and Macara, 2005; Yang and Musser, 2006; Ma et al., 2012; Goryaynov and Yang, 2014). Other interesting revelations about nucleocytoplasmic transport that SMI studies have made possible include: large cargoes require multiple nuclear transport receptors for translocation (Tu et al., 2013); translocation involves several substeps with a high incidence of aborted transport events at the NPCs (Lowe et al., 2010); and spatial resolution of mRNA transport kinetics in mammalian NPCs (Grünwald and Singer, 2010).

Considering that the results presented in Chapters 2 and 3 are essentially averaged data, single molecule investigations were performed to further clarify the kinetic details observed. Specifically, the unique features of quasi-TIRF were used to identify and analyze single NPCs, which were visualized as fluorescent spots in the nuclear envelope as a result of the interactions between fluorescently-labelled protein molecules and Nups within each NPC (Figure 4.3).

4.2 Materials and Methods

4.2.1 DNA constructs, protein purification and labeling

cDNA encoding human importin β was amplified by PCR from HeLa single stranded (ss)DNA pool using the following primers: 5′-gccccgcgggccatggagctgatca-3′ (forward primer; *Sac*II site underlined); and 5′-cccaatggcgccgctcaagcttgg-3′ (reverse primer; *Not*I site underlined). The amplified fragment was then inserted into the *Sac*II and *Not*I sites of pH6HTN His_6HaloTag®T7 vector (Promega, Wisconsin USA) to produce hexahistindine (His_6)-tagged Halo-importin β DNA construct for expression in BL21-CondonPlus-RIL *Escherichia coli*. Protein expression was induced by 1 mM isopropyl thiogalactoside (IPTG) and elution from Nickel beads was by 30 – 250 mM imidazole. Purified recombinant Halo-importin β was then labeled with ~2.5 μM HaloTag Tetramethyl Rhodamine (TMR) ligand (Promega, Wisconsin USA). Excess dye was removed by Bio-Rad Bio-Spin® Bio-Gel P6 or P30 columns (100 μl labeled protein/column) and the labeling efficiency was checked by a fluorescence scanner (Typhoon Variable Mode Imager 9400, GE Healthcare, Little Chalfont, United Kingdom). Fluorescently-labeled protein was then aliquoted, snap-frozen in liquid nitrogen and stored at -80^{o}C until needed for single molecule experiments.

4.2.2 Analysis of single NPCs by narrow-field illumination

HeLa cells were permeabilized with 40 μg/ml digitonin and preincubated with transport buffer (TB; Chapter 2, Materials and Methods) with 2 mM or 100 mM DTT for 10 min

prior to observation by a quasi-TIRF microscope. Preincubation of HeLa cells with 2 mM H_2O_2 for 1 h at 37^oC, in the absence of DTT, was also done prior to digitonin permeabilization. 1 nM TMR-tagged Halo-importin β was then added, and 4000 images were acquired at an exposure rate of 15 msec/frame for 60 s. Incident beam was at an angle of 55.17^o. The Photostability of the TMR fluorophore in the tagged protein was initially determined by imaging 1 nM fluorescently-labeled Halo-importin β non-specifically bound to poly-L-lysine (PLL)-coated glass-bottom dish.

4.2.3. Data Analysis

Particle tracking and analysis were executed by the custom-built software (WinATRv2r7a_64) designed by Dr. Takahiro Fujiwara.

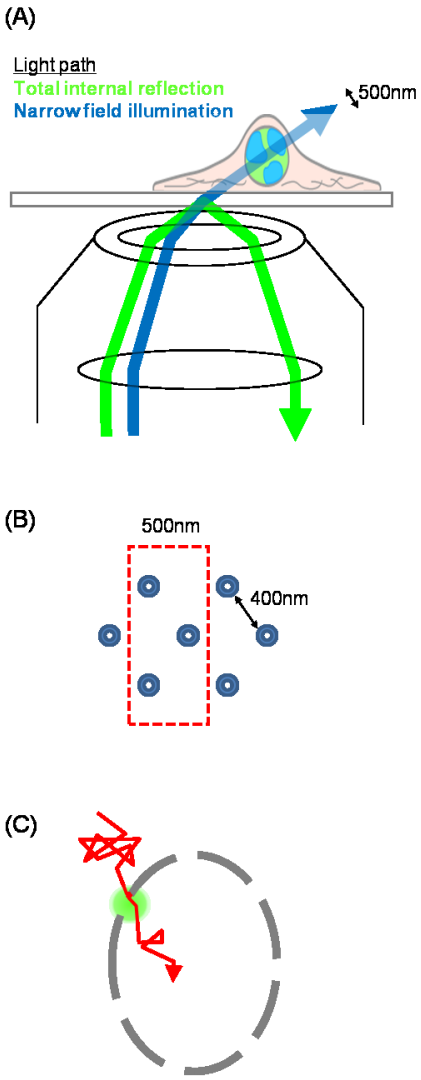

Figure 4.3 Detection of single NPCs by narrow-field illumination. (A). Light path for narrow-field illumination. **(B).** Illustration of how the ~500 nm refracted beam in (A) illuminates single NPCs, which are reportedly spaced by (~400 nm). **(C).** Illustration of how the motion of a diffusing molecule (red trajectory) is slowed down by interaction (green spot) in the NPC (slits) to enable its detection.

4.3 Results

4.3.1 Lifetime of single TMR fluorescence used to label Halo-importin β

Common limitations of many fluorophores used in single molecule imaging include blinking, poor resistance to photobleaching, and large size that may interfere with the intracellular dynamics of the labeled protein (Dickson et al., 1997; Yang et al., 2004; Xia et al., 2013). Therefore, it was important to validate the property of the fluorescent dye under the intended experimental condition prior to the actual measurements. The TMR-conjugated Halo-importin β was attached to a cover glass and illuminated with the quasi-TIRF excitation laser, followed by the 15 ms/frame time-lapse recording of the fluorescent signals. The average lifetime of TMR-labeled Halo-importin β before loss of signal (measure of photostability) was estimated to be ~1.5 ± 0.5 s (n =13; Figure 4.4). This is longer than the reported residence time of free and cargo-bound importin β in the NPCs during transport (950 ms, Görlich et al., 2003; 400 ms, Riddick and Macara, 2005). The bleaching is clearly distinguishable from the signal fluctuation and there was no restoration of fluorescence after bleaching, which makes the dye suitable for the single fluorescence imaging.

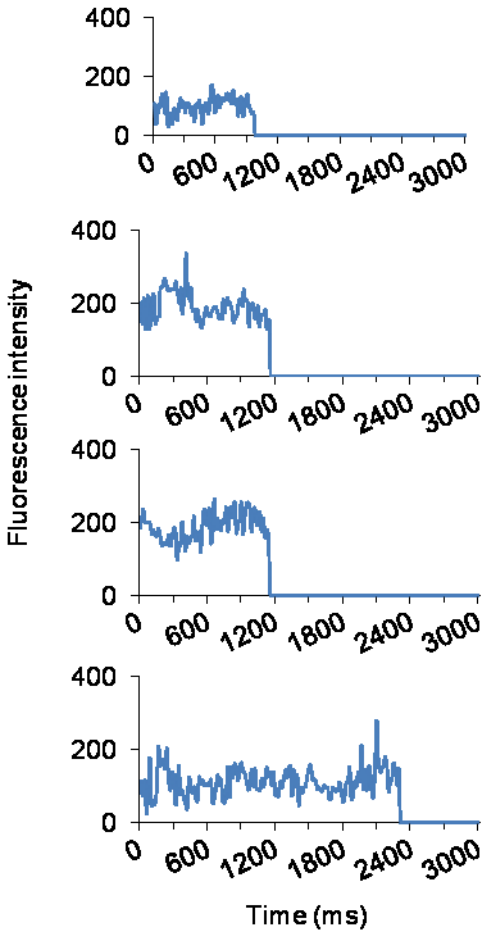

Figure 4.4 Fluorescence lifetime of four TMR®–tagged Halo-importinβ molecules non-specifically bound to poly-L-lysine coated glass surface. 1 nM TMR-labeled Halo-importin β in transport buffer (TB; Chapter 2, Materials and Methods) containing 2 mM DTT was added to poly-L-lysine coated glass-bottom dish. Images of single TMR-tagged Halo-importin β molecules bound to the bottom of the dish were collected at a rate of 15 ms/frame for 3 s. Background intensity was subtracted and lifetime of each single molecule presented as fluorescence intensity against time. TMR is photobleached in a single step and does not blink.

4.3.2 Transport dynamics within single NPCs

The kinetic events in single NPCs were investigated. Digitonin-treated HeLa cells were preincubated with transport buffer containing 2 mM DTT for 10 min. Then 1 nM TMR-tagged Halo-importin β was added, and single NPC observation was done by quasi-TIRF microscope. 4000 images were captured at an exposure rate of 15 ms/frame for 60 s. A low concentration (1 nM) of importin β was used for the observations so as to fully distinguish the transport events in each NPC. (Figure 4.5, left). The interaction of labeled importin β molecules with nucleoporins within the NPCs slows the Brownian motion of the molecules so that they become detectable as fluorescent spots on the nuclear envelope (Figure 4.5, left; Tokunaga et al., 2008).

80 NPCs were analyzed. The number and residence time of labeled importin β molecules that interacted with each NPC were analyzed and expressed as histograms (representative histograms of 4 NPCs are shown in Figure 4.6 A-D). Two populations of importin β were observed: one population interacted with the NPCs for <100 ms. These events with short residence time are most likely transient interactions, considering that the reported transport time of importin β is about 400 ms (Riddick and Macara, 2005).

The second population of importin β molecules had residence times longer than 100 ms which could represent actual transport events (Figure 4.6 A-D; Appendix 1). The NPCs (n=22) that had these longer events were then analyzed further. A threshold of 100 ms was set and the average residence time in each of the NPCs was estimated. The data show that the average residence time in the NPCs ranged from 150 to 500 ms (Figure 4.6 A-D; E).

One-way ANOVA confirmed that there are statistically significant differences among the average residence times for the different NPCs. This suggests that there may be different populations of NPCs that differ from one another in their interaction with importin β.

4.3.3 Effect of disulfide bonds on NPC variations

To understand the basis of the observed differential interaction among the NPCs, the relationship between the disulfide bond content of each NPC and interaction with importin β was investigated, considering that an earlier study had shown that disulphide bonds within the NPCs contribute to selectivity of the pores (Yoshimura et al., 2013). Digitonin-treated HeLa cells were exposed to 2 mM hydrogen peroxide (H_2O_2; to induce uniform oxidation in the 52 NPCs analyzed) or 100 mM DTT (to reduce of most disulfide bonds in the 68 NPCs analyzed). Both conditions resulted in NPCs with different average residence times similar to treatment with 2 mM DTT (Appendix 2).

Collectively, these results suggest that there might be different populations of NPCs with different abilities to interact with cargo. The results further show that disulfide bonds within the NPCs may alter their permeability to cargoes, but the functional heterogeneity may not be affected.

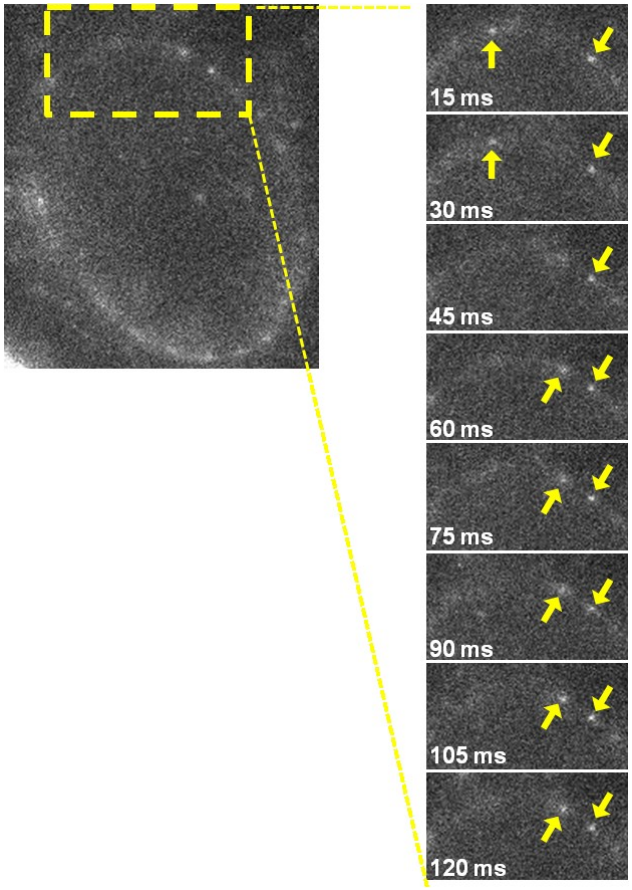

Figure 4.5 Identification of single transport event. Permeabilized HeLa cells were incubated with transport buffer containing 2 mM DTT. 1 nM TMR-tagged Halo-importin β was added, and single molecule observation was done by quasi-TIRF microscope. 4000 images were acquired at a rate of 15 ms/frame for 60 s. Freely diffusing importin β molecules are not detectable because of their rapid Brownian motion. However, when they interact with the nucleoporins in the NPCs, their motion is slowed down and they become detectable as bright fluorescent spots, which correspond with single NPCs on the nuclear envelope. The clear outline of the nuclear envelope (NE; left panel) is shown. The time-lapse images (right panel) show single NPCs (yellow arrows) interacting with importin β molecules in a portion of the NE (inset).

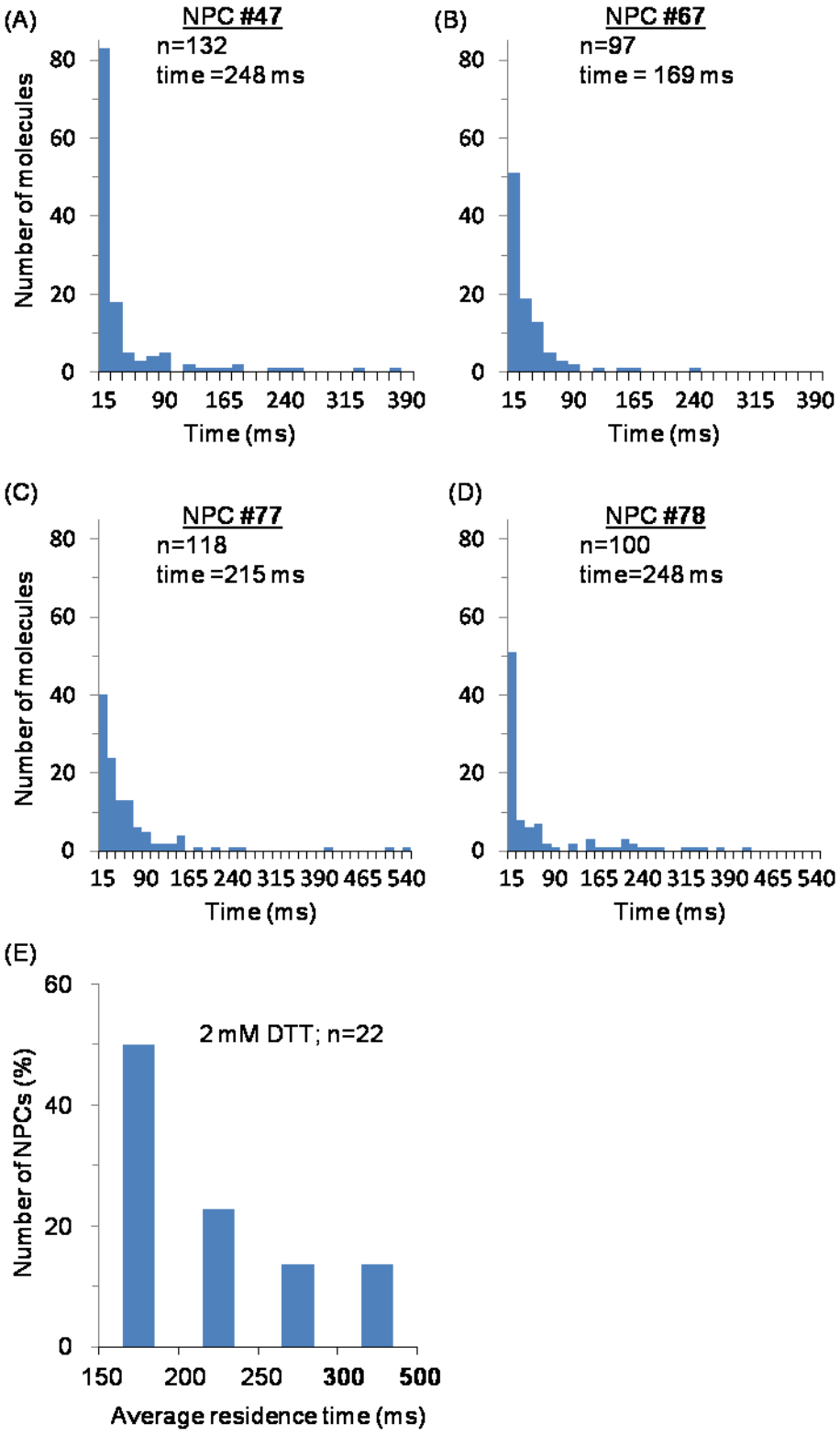
(A)
NPC #47
n=132
time =248 ms
Number of molecules
Time (ms)
(B)
NPC #67
n=97
time = 169 ms
Time (ms)
(C)
NPC #77
n=118
time =215 ms
Number of molecules
Time (ms)
(D)
NPC #78
n=100
time=248 ms
Time (ms)
(E)
2 mM DTT; n=22
Number of NPCs (%)
Average residence time (ms)

Figure 4.6 Analysis of residence time of importin β in 22 NPCs reveal that different populations of NPCs exist in the nuclear envelope. (A-E) The number and residence times of importin β molecules that interacted with 4 representative NPCs are shown (A-D). The average residence time of molecules in NPCs (n=22) that had interactions longer than a threshold of 100 ms was then calculated and plotted against the number of NPCs (expressed in frequency %; E). The results suggest that there may be different populations of NPCs with different residence times and binding affinities.

CHAPTER 5

Discussion and Conclusion

5.1 Discussion

The starting point for the nuclear import narrative is usually the binding of cargoes, in the low RanGTP environment of the cytoplasm, by an appropriate importin, with or without the aid of an adaptor molecule such as importin α or snurportin. Thereafter, the complex docks at the NPC, interacts with nucleoporins as it translocates through the NPC and finally, cargo dissociation in the high RanGTP environment of the nucleus (Ribbeck et al., 1998; Fahrenkrog and Aebi, 2003). The kinetic analysis of these various transport reactions/steps *in vitro* revealed the important roles played by the concentration, size and properties of the transport components. The intracellular dynamics of these components have also been dissected by a number of *in vivo* studies involving time-lapse fluorescence observation. However, there is little information about the detailed molecular state of the labeled protein *in vivo*. Therefore, in this study, *in vivo* and *in vitro* experimental systems were combined to explain the detailed dynamics of nuclear transport components in a living cell.

5.2 Karyopherin-cargo complex has other fates in addition to dissociation

In vivo FLIP analysis of all the fluorescently-labeled NLS cargoes expressed in HeLa cells proved that they were all exported from the nucleus in a Crm1-independent manner following continuous photobleaching of the cytoplasm (Figures 2.1-2.3; Table 1). This is a strong indication that the respective importins serve as export mediators for their cognate cargoes. A similar conclusion was arrived at by Kopito and Elbaum (2007) using *in vitro* experiments, where reconstituted nuclei that had accumulated GFP-nucleoplasmin were

subjected to FRAP. One of their inferences was that the fluorescence recovery in the nuclei was proof of the reversibility of nuclear transport. They argued that an influx of fluorescent cargo could only have been at the instance of the efflux of bleached molecules. FLIP data presented in this study provide *in vivo* evidence that nuclear transport is indeed reversible for either importins or exportins.

These findings are in agreement with an early work that first linked nuclear import and shuttling of nucleolin after transient transfection and microinjection into HeLa cells (Schmidt-Zachmann et al., 1993). The results are also in consonance with subsequent microinjection studies that revealed that pyruvate kinase and β-galactosidase, which are predominantly cytosolic, could shuttle bidirectionally when they are fused with a classical or M9 NLS(Guiochon-Mantel et al., 1994; Michael et al., 1995). Indeed, the bidirectional karyopherin-cargo translocation could be the explanation for the conclusion by Michael *et al*. that the M9 sequence of hnRNPA1 serves as both an NLS and NES (Michael et al., 1995). Furthermore, the FLIP data confirm the *in vitro* observation that importin 13 is able to export eIF1A from permeabilized HeLa nuclei, even in the absence of a RanGTP gradient (Mingot et al., 2001; Grünwald et al., 2013). The *in vitro* experiments using purified components and semi-permeabilized HeLa cells, give direct proof that NLS-cargoes, complexed with importins, do shuttle the NPCs in both directions (Figure 2.4).

5.3 Kinetic flux rates in single NPCs and *in vivo*

The *in vivo* flux rates of the different cargoes examined in this study ranged from 1 – 10 molecules/NPC/sec (Table 3.4) at a 1 μM steady-state nuclear concentration of karyopherin-cargo complex. These values are similar to the kinetic predictions (Table 3.3) as well as values obtained by other researchers using cell extracts and micro-injection approaches (Keminer et al., 1999; Nemergut and Macara, 2000). However, they are significantly lower than the ~1000 molecules/NPC/sec calculated in an earlier study of nonsteady-state kinetics involving higher initial concentrations of cargoes (Ribbeck and Görlich, 2001).

The average retention times (150 -500 ms) estimated for the interaction of importin β with the nucleoporins in each of the single NPCs (Figure 4.6) are in agreement with earlier studies (<2000 ms, Rabut et al., 2004; 400 ms, Riddick and Macara, 2005). These values correspond to dissociation constants (k_{off}; inverse of residence time) of 2 – 7 s^{-1} which is within the range of previous estimates for importin β interaction with NPCs (0.1 – 20 s^{-1}; Chaillan-Huntington et al., 2000; Ben-Efraim and Gerace, 2001). The off-rate variations make it plausible to speculate that NPCs that have low affinity (high k_{off}) may have a high incident of aborted transport events, and consequently reduced flux through them (Lowe et al., 2010). Indeed, preliminary results suggest that cargo flux in single NPCs is as low as was reported in the bulk experiments and kinetic simulations (Figure 5.1; Tables 3.3-3.4). At 1 nM experimental condition in the presence of 2 mM DTT, it was revealed that ~85% of the NPCs studied had flux rates less than 1 importin β molecule per

sec, and only ~15% of the NPCs had rates from 1 – 2.5 importin β molecule per sec (Figure 5.1, blue bars). These results are in good agreement with earlier studies (Tokunaga et al., 2008). Similar results were obtained regardless of the redox condition (Figure 5.1, red and green bars).

5.4 The rate-limiting step in nuclear transport is karyopherin-cargo interactions

The observed low cargo flux in both the *in vivo* and single molecule experiments brings to the fore the question about what step might be rate-limiting in the entire transport cycle. Simulation experiments showed that karyopherin availability and its rate of complex formation with cargo in the cytoplasm (Figure 3.1, step 1) is slower than the rate of influx of the complex into the nucleus (step 5) at all cargo/kap concentration ratios (Figure 3.6D). This suggests that importin β-cargo interaction may be slower than cargo translocation through the NPCs at steady state. Collectively, these findings are in perfect agreement with previous studies that suggest that the determining factors for nuclear transport are receptor-cargo affinity and the ease of locating specific cargoes within the complex cellular environment of numerous non-specific substrates (Smith et al., 2002; Timney et al., 2006; Kim and Elbaum, 2013).

Although the findings of this study indicate that nuclear pore permeability is not rate-limiting, it is still a key factor in the transport process. As a matter of fact, it has been argued that free karyopherins constantly occupy the NPCs to exclude interaction of non-specific molecules thereby enhancing the selectivity of the pores (Zilman et al., 2007). This

view is supported by the results of the kinetic simulations reported in this thesis which revealed that, at cargo/kap ratio of 1:1, free importin β had a high steady-state influx of ~83 molecules/NPC/sec compared with either importin β-RanGTP and importin β-cargo which were 20x and 3x lesser, respectively (Table 3.3). Moreover, this study reveals that bidirectional flux is not limited to unbound karyopherins alone, but also includes karyopherin-cargo complexes.

Bidirectional flux could also be a cellular mechanism to optimally conserve energy given the energetic cost of the the recycling step in a unidirectional model. Another significance of bidirectionality is that it could contribute to the cell's ability to maintain proper distribution of cargoes in both the nucleus and the cytoplasm. This is plausible given that previous studies reported that cells have many strategies to export proteins that are predominantly cytosolic but which still enter the nucleus by diffusion or facilitated transport if they possess cryptic NLSs (Bohnsack et al., 2002).

5.5 Thermodynamics drives bidirectional nuclear transport

The laws of thermodynamics, especially the Second Law, stipulate that equilibrium (or steady state) is established between two inter-linked systems by a constant bidirectional flux of molecules between them. The data presented so far agrees with this assertion. Specifically, it was interesting to note that bidirectional flux was largely driven by the unique properties (size, hydrophobicity, charge, etc) of the cargoes themselves considering their effects on the influx and efflux rates of karyopherin-cargo complex (Figures 2.6 and

3.5A). These data strongly suggest that thermodynamic factors, rather than the RanGTP gradient, provide the driving force for nuclear transport. In fact, it is firmly established that the RanGTP gradient is dispensable for nuclear transport considering that incubation of digitonin-permeabilized cells with karyopherins, in the absence of Ran, still leads to nuclear accumulation to the same level as the extranuclear space (Figure 2.5). These lines of argument agree with previous findings that thermodynamic factors have a dominant influence on nuclear transport (Kopito and Elbaum, 2009).

These findings are also in agreement with published reports that strongly suggest that neither transport directionality nor flux rates of small cargoes (~50 – 120 kDa) are significantly dependent on availability of Ran (Lyman et al., 2002; Lowe et al., 2015). Instead, their data show that RanGTP may be needed for the translocation of very large cargoes (~200 kDa and above). They showed that in the absence of RanGTP, a portion of the pool of importin β binds stably to Nup153 on the nucleoplasmic face of the NPC, thereby reducing the number of free karyopherin molecules needed for cargo accumulation. Addition of RanGTP reduces the interaction of importin β with Nup153 such that the pool of available karyopherin is increased to effect dramatic accumulation of cargo. It seems the RanGTP gradient mainly functions to ensure that steady-state concentrations of the cargo are attained in the appropriate destination.

5.6 Conclusion and future perspectives

Taken together, all the data from this study clearly show that bidirectional flux of free and bound karyopherins is a mechanism that the cell employs to ensure that the concentration and quality of transport cargoes are optimal in the appropriate compartments at steady state. The quantitative flux details also reveal that availability of karyopherins and their affinity for cargoes are the limiting conditions for nucleocytoplasmic translocation.

An interesting perspective from this study is the observation that there may be more than one population of NPCs that differ in terms of flux and residence times (Figures 5.1). Indeed, there are few reports about functional variations within/among NPCs. Different interaction affinities between importin β and several nucleoporins have been reported (Isgro and Schulten, 2005; Otsuka et al., 2008). In addition, yeast NPCs adjacent to the nucleolus have been reported not to have the Mlp proteins whereas those situated at a distance from the nucleolus still have the proteins (Niepel et al., 2005; Raices and D'Angelo, 2012).

The idea of a functional heterogeneity among the NPCs raises some germane questions: are there NPCs exclusively specialized for import or export? Are there NPCs dedicated to the transport of specific molecules? The answer to these questions will provide further clarity on the elusive transport mechanism through the nuclear pores. One approach to resolve the question about the mutual exclusivity, or otherwise, of import and export

through the same NPC is to do simultaneous single molecule analysis of import and export cargoes labeled with different dye colours.

Another perspective that would be worth exploring in the future is the application of the high predictive capacity of the kinetic model developed and extensively simulated in this study to understand the kinetics and mechanisms involved in the nuclear export pathway. The paucity of experimental model systems for the investigation of nuclear export has been a main limitation against our knowledge of the process in comparison with the nuclear import cycle.

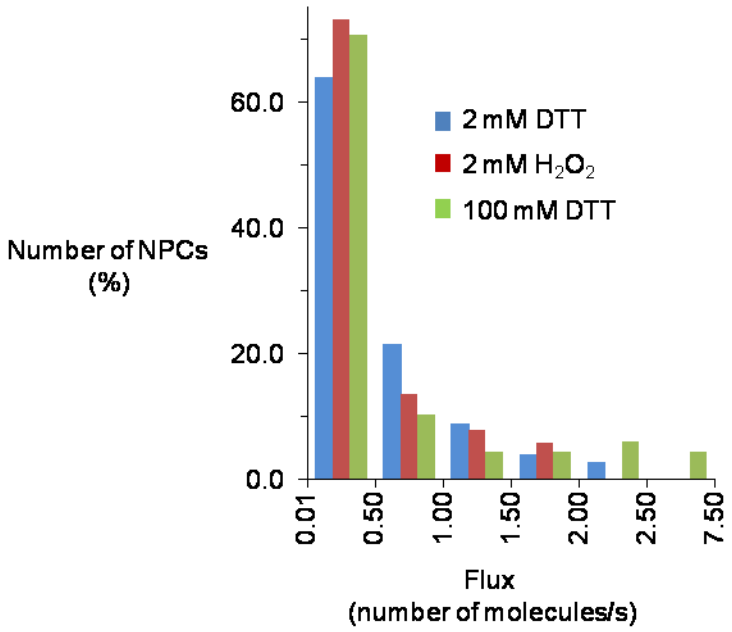

Figure 5.1 The flux of importin β molecules through single NPCs. 1 nM TMR-lableled Halo-importin β was added to digitonin-permeabilized HeLa cells, in the presence of 2 mM DTT [blue bars], 2 mM H_2O_2 (red bars) and 100 mM DTT (green bars). 4,000 images were collected at 15msec/frame for 60s. The flux of Halo-importinβ molecules that interacted with the NPCs in the different redox conditions is shown: 2 mM DTT (~2400 molecules interacted with 80 NPCs); 2 mM H_2O_2 (~1400 molecules interacted with 52 NPCs); and 100 mM DTT (~3100 molecules interacted with 68 NPCs). NPCs differ in the number of importin β molecules they can accommodate. Flux is expressed as number of importin β molecule observed per NPC for the duration of the experiment (60 s). The number of NPCs investigated was converted to percentages for comparison.

REFERENCES

Adam, S. A., Marr, R. S. and Gerace, L. (1990). Nuclear protein import in permeabilized mammalian cells requires cytoplasmic factors. *J Cell Biol* **111**, 807–816.

Akey, C. W. and Radermacher, M. (1993). Architecture of the Xenopus Nuclear Pore Complex Revealed by Three-Dimensional Cryo-Electron Microscopy. *J Cell Biol* **122**, 1–19.

Andrade, M. A. and Bork, P. (1995). HEAT repeats in the Huntington's disease protein. *Nat Genet* **11**, 115–116.

Axelrod, D. (1981). Cell-substrate contacts illuminated by total internal reflection fluorescence. *J Cell Biol* **89**, 141–145.

Bayliss, R., Littlewood, T. and Stewart, M. (2000). Structural basis for the interaction between FxFG nucleoporin repeats and importin-beta in nuclear trafficking. *Cell* **102**, 99–108.

Beck, M., Förster, F., Ecke, M., Plitzko, J. M., Melchior, F., Gerisch, G., Baumeister, W. and Medalia, O. (2004). Nuclear pore complex structure and dynamics revealed by cryoelectron tomography. *Science* **306**, 1387–1390.

Ben-Efraim, I. and Gerace, L. (2001). Gradient of Increasing Affinity of Importin beta for Nucleoporins along the Pathway of Nuclear Import. *J Cell Biol* **152**, 411–417.

Berke, I. C., Boehmer, T., Blobel, G. and Schwartz, T. U. (2004). Structural and functional analysis of Nup133 domains reveals modular building blocks of the nuclear pore complex. *J Cell Biol* **167**, 591–597.

Bischoff, F. R. and Görlich, D. (1997). RanBP1 is crucial for the release of RanGTP from importin β-related nuclear transport factors. *FEBS Lett* **419**, 249–254.

Boehmer, T., Jeudy, S., Berke, I. C. and Schwartz, T. U. (2008). Structural and functional studies of Nup107/Nup133 interaction and its implications for the architecture of the nuclear pore complex. *Mol Cell* **30**, 721–31.

Bogerd, H. P., Fridell, R. A., Benson, R. E., Hua, J. and Cullen, B. R. (1996). Protein sequence requirements for function of the human T-cell leukemia virus type 1 Rex nuclear export signal delineated by a novel in vivo randomization-selection assay. *Mol Cell Biol* **16**, 4207–14.

Bohnsack, M. T., Regener, K., Schwappach, B., Saffrich, R., Paraskeva, E., Hartmann, E. and Görlich, D. (2002). Exp5 exports eEF1A via tRNA from nuclei and synergizes with other transport pathways to confine translation to the cytoplasm. *EMBO J* **21**, 6205–6215.

Bupp, J. M., Martin, A. E., Stensrud, E. S. and Jaspersen, S. L. (2007). Telomere anchoring at the nuclear periphery requires the budding yeast Sad1-UNC-84 domain protein Mps3. *J Cell Biol* **179**, 845–854.

Callan H.G, and T. S. G. (1950). Experimental Studies on Amphibian Oocyte Nuclei. I. Investigation of the Structure of the Nuclear Membrane by Means of the Electron Microscope. *Proc R Soc L B Biol Sci* **137**, 367–378.

Cansizoglu, A. E., Lee, B. J., Zhang, Z. C., Fontoura, B. M. A. and Chook, Y. M. (2007). Structure-based design of a pathway-specific nuclear import inhibitor. *Nat Struct & Mol Biol* **14**, 452–454.

Chaillan-Huntington, C., Braslavsky, V. C., Kuhlmann Jurgen and Stewart, M. (2000). Dissecting the Interactions between NTF2 , RanGDP , and the Nucleoporin X F X FG Repeats *. *J Biol Chem* **275**, 5874–5879.

Chang, W., Worman, H. J. and Gundersen, G. G. (2015). Accessorizing and anchoring the LINC complex for multifunctionality. *J Cell Biol* **208**, 11–22.

Chook, Y. M. and Blobel, G. (1999). Structure of the nuclear transport complex karyopherin-beta2-Ran x GppNHp. *Nature* **399**, 230–7.

Chook, Y. M. and Blobel, G. (2001). Karyopherins and nuclear import. *Curr Opin Struct Biol* **11**, 703–715.

Chook, Y. M. and Süel, K. E. (2011). Nuclear import by karyopherin-βs: Recognition and inhibition. *Biochim Biophys Acta - Mol Cell Res* **1813**, 1593–1606.

Cingolani, G., Petosa, C., Weis, K. and Müller, C. W. (1999). Structure of importin-beta bound to the IBB domain of importin-alpha. *Nature* **399**, 221–229.

Cingolani, G., Bednenko, J., Gillespie, M. T. and Gerace, L. (2002). Molecular basis for the recognition of a nonclassical nuclear localization signal by importin beta. *Mol Cell* **10**, 1345–1353.

Conti, E. and Izaurralde, E. (2001). Nucleocytoplasmic transport enters the atomic age. *Curr Opin Cell Biol* **13**, 310–319.

Conti, E., Uy, M., Leighton, L., Blobel, G. and Kuriyan, J. (1998). Crystallographic analysis of the recognition of a nuclear localization signal by the nuclear import factor karyopherin α. *Cell* **94**, 193–204.

Conti, E., Müller, C. W. and Stewart, M. (2006). Karyopherin flexibility in nucleocytoplasmic transport. *Curr Opin Struct Biol* **16**, 237–244.

Denning, D. P., Patel, S. S., Uversky, V., Fink, A. L. and Rexach, M. (2003). Disorder in the nuclear pore complex: the FG repeat regions of nucleoporins are natively unfolded. *Proc Natl Acad Sci U S A* **100**, 2450–2455.

Dickson, R. M., Cubitt, A. B., Tsien, R. Y. and Moerner, W. E. (1997). On/off blinking and switching behaviour of single molecules of green fluorescent protein. *Nature* **388**, 355–358.

Dong, X., Biswas, A. and Chook, Y. M. (2009). Structural basis for assembly and disassembly of the CRM1 nuclear export complex. *Nat Struct Mol Biol* **16**, 558–560.

Dworetzky, S. I., Lanford, R. E. and Feldherr, C. M. (1988). The effects of variations in the number and sequence of targeting signals on nuclear uptake. *J Cell Biol* **107**, 1279–87.

Engelsma, D., Bernad, R., Calafat, J. and Fornerod, M. (2004). Supraphysiological nuclear export signals bind CRM1 independently of RanGTP and arrest at Nup358. *EMBO J* **23**, 3643–52.

Englmeier, L., Olivo, J. and Mattaj, I. (1999). Receptor-mediated substrate translocation through the nuclear pore complex without nucleotide triphosphate hydrolysis Ludwig. *Curr Biol* **8**, 30–41.

Fabre, E. and Hurt, E. (1997). Yeast genetics to dissect the nuclear pore complex and nucleocytoplasmic trafficking. *Annu Rev Genet* **31**, 277–313.

Fahrenkrog, B. and Aebi, U. (2003). The nuclear pore complex: nucleocytoplasmic transport and beyond. *Nat Rev Mol Cell Biol* **4**, 757–766.

Fahrenkrog, B., Hurt, E. C., Aebi, U. and Panté, N. (1998). Molecular Architecture of the Yeast Nuclear Pore Complex: Localization of Nsp1p Subcomplexes. *J Cell Biol* **143**, 577–588.

Fahrenkrog, B., Stoffler, D. and Aebi, U. (2001). Nuclear Pore Complex Architecture and Functional Dynamics. *Curr Top Microbiol Immunol* **259**, 95–117.

Fahrenkrog, B., Maco, B., Fager, A. M., Köser, J., Sauder, U., Ullman, K. S. and Aebi, U. (2002). Domain-specific antibodies reveal multiple-site topology of Nup153 within the nuclear pore complex. *J Struct Biol* **140**, 254–267.

Feldherr, C. M., Kallenbach, E. and Schultz, N. (1984). Movement of a Karyophilic Protein through the Nuclear Pores of Oocytes. *J Cell Biol* **99**, 2216–2222.

Fischer, U., Huber, J., Boelens, W. C., Mattaj, I. W. and Lührmann, R. (1995). The HIV-1 Rev activation domain is a nuclear export signal that accesses an export pathway used by specific cellular RNAs. *Cell* **82**, 475–483.

Floer, M. and Blobel, G. (1999). Putative reaction intermediates in Crm1-mediated nuclear protein export. *J Biol Chem* **274**, 16279–86.

Fornerod, M., Ohno, M., Yoshida, M. and Mattaj, I. W. (1997). CRM1 Is an Export Receptor for Leucine-Rich Nuclear Export Signals. *Cell* **90**, 1051–1060.

Forwood, J. K. and Jans, D. A. (2002). Nuclear import pathway of the telomere elongation suppressor TRF1: inhibition by importin alpha. *Biochemistry* **41**, 9333–9340.

Forwood, J. K., Lam, M. H. and Jans, D. A. (2001a). Nuclear import of Creb and AP-1 transcription factors requires importin-beta 1 and Ran but is independent of importin-alpha. *Biochemistry* **40**, 5208–17.

Forwood, J. K., Harley, V. and Jans, D. A. (2001b). The C-terminal Nuclear Localization Signal of the Sex-determining Region Y (SRY) High Mobility Group Domain Mediates Nuclear Import through Importin ??1. *J Biol Chem* **276**, 46575–46582.

Frenkiel-Krispin, D., Maco, B., Aebi, U. and Medalia, O. (2010). Structural Analysis of a Metazoan Nuclear Pore Complex Reveals a Fused Concentric Ring Architecture. *J*

Mol Biol **395**, 578–586.

Frey, S., Richter, R. P. and Görlich, D. (2006). FG-rich repeats of nuclear pore proteins form a three-dimensional meshwork with hydrogel-like properties. *Science* **314**, 815–817.

Fukuda, M., Asano, S., Nakamura, T., Adachi, M., Yoshida, M., Yanagida, M. and Nishida, E. (1997). CRM1 is responsible for intracellular transport mediated by the nuclear export signal. *Nature* **390**, 308–311.

Gall, J. G. (1967). Octagonal nuclear pores. *J Cell Biol* **32**, 391–399.

Gorlich, D. and Kutay, U. (1999). Transport Between the Cell Nucleus and the Cytoplasm. *Annu Rev Cell Dev Biol* **15**, 607–660.

Görlich, D., Kostka, S., Kraft, R., Dingwall, C., Laskey, R. a, Hartmann, E. and Prehn, S. (1995). Two different subunits of importin cooperate to recognize nuclear localization signals and bind them to the nuclear envelope. *Curr Biol* **5**, 383–392.

Görlich, D., Panté, N., Kutay, U., Aebi, U. and Bischoff, F. R. (1996). Identification of different roles for RanGDP and RanGTP in nuclear protein import. *EMBO J* **15**, 5584–94.

Görlich, D., Seewald, M. J. and Ribbeck, K. (2003). Characterization of Ran-driven cargo transport and the RanGTPase system by kinetic measurements and computer simulation. *EMBO J* **22**, 1088–1100.

Goryaynov, A. and Yang, W. (2014). Role of Molecular Charge in Nucleocytoplasmic Transport. *PLoS One* **9**, e88792.

Grossman, E., Medalia, O. and Zwerger, M. (2012). Functional Architecture of the Nuclear Pore Complex. *Annu Rev Biophys* **41**, 557–584.

Grünwald, D. and Singer, R. H. (2010). In vivo imaging of labelled endogenous β-actin mRNA during nucleocytoplasmic transport. *Nature* **467**, 604–607.

Grünwald, M., Lazzaretti, D. and Bono, F. (2013). Structural basis for the nuclear export activity of Importin13. *EMBO J* **32**, 899–913.

Guiochon-Mantel, A., Delabre, K., Lescop, P. and Milgrom, E. (1994). Nuclear localization signals also mediate the outward movement of proteins from the nucleus. *Proc Natl Acad Sci U S A* **91**, 7179–83.

Harel, A. and Forbes, D. J. (2004). Importin beta: Conducting a much larger cellular symphony. *Mol Cell* **16**, 319–330.

Harley, V. R., Layfield, S., Mitchell, C. L., Forwood, J. K., John, A. P., Briggs, L. J., McDowall, S. G. and Jans, D. A. (2003). Defective importin beta recognition and nuclear import of the sex-determining factor SRY are associated with XY sex-reversing mutations. *Proc Natl Acad Sci U S A* **100**, 7045–7050.

Hern, J. A., Baig, A. H., Mashanov, G. I., Birdsall, B., Corrie, J. E. T., Lazareno, S., Molloy, J. E. and Birdsall, N. J. M. (2010). Formation and dissociation of M1 muscarinic receptor dimers seen by total internal reflection fluorescence imaging of single molecules. *Proc Natl Acad Sci U S A* **107**, 2693–2698.

Herold, A., Truant, R., Wiegand, H. and Cullen, B. R. (1998). Determination of the functional domain organization of the importin alpha nuclear import factor. *J Cell Biol* **143**, 309–18.

Hinshaw, J. E. and Milligan, R. A. (2003). Nuclear pore complexes exceeding eightfold rotational symmetry. *J Struct Biol* **141**, 259–268.

Hinshaw, J. E., Carragher, B. O. and Milligan, R. a (1992). Architecture and design of

the nuclear pore complex. *Cell* **69**, 1133–1141.

Hoelz, A., Debler, E. W. and Blobel, G. (2011). The Structure of the Nuclear Pore Complex. *Annu Rev Biochem* **80**, 613–643.

Huber, J., Cronshagen, U., Kadokura, M., Wada, T., Sekine, M. and Lu, R. (1998). Snurportin1 , an m 3 G-cap-specific nuclear import receptor with a novel domain structure. **17**, 4114–4126.

Hutten, S., Flotho, A., Melchior, F. and Kehlenbach, R. H. (2008). The Nup358-RanGAP Complex Is Required for Efficient Importin alpha/beta-dependent Nuclear Import. *Mol Biol Cell* **19**, 308–317.

Iino, R., Koyama, I. and Kusumi, a (2001). Single molecule imaging of green fluorescent proteins in living cells: E-cadherin forms oligomers on the free cell surface. *Biophys J* **80**, 2667–2677.

Isgro, T. a. and Schulten, K. (2005). Binding dynamics of isolated nucleoporin repeat regions to importin-beta. *Structure* **13**, 1869–1879.

Jakel, S. and Gorlich, D. (1998). Importin β, transportin, RanBP5 and RanBP7 mediate nuclear import of ribosomal proteins in mammalian cells. *EMBO J* **17**, 4491–4502.

Jang, B.-C., Munoz-Najar, U., Paik, J.-H., Claffey, K., Yoshida, M. and Hla, T. (2003). Leptomycin B, an Inhibitor of the Nuclear Export Receptor CRM1, Inhibits COX-2 Expression. *J Biol Chem* **278**, 2773–2776.

Kalderon, D., Roberts, B. L., Richardson, W. D. and Smith, A. E. (1984). A short amino acid sequence able to specify nuclear location. *Cell* **39**, 499–509.

Keminer, O. and Peters, R. (1999). Permeability of Single Nuclear Pores. *Biophys J* **77**, 217–228.

Keminer, O., Siebrasse, J. P., Zerf, K. and Peters, R. (1999). Optical recording of signal-mediated protein transport through single nuclear pore complexes. *Proc Natl Acad Sci U S A* **96**, 11842–11847.

Kim, S. and Elbaum, M. (2013). A Simple Kinetic Model with Explicit Predictions for Nuclear Transport. *Biophys J* **105**, 565–569.

Konopka, C. A. and Bednarek, S. Y. (2008). Variable-angle epifluorescence microscopy: A new way to look at protein dynamics in the plant cell cortex. *Plant J* **53**, 186–196.

Kopito, R. B. and Elbaum, M. (2007). Reversibility in nucleocytoplasmic transport. *Proc Natl Acad Sci U S A* **104**, 12743–8.

Kopito, R. B. and Elbaum, M. (2009). Nucleocytoplasmic transport: a thermodynamic mechanism. *HFSP J* **3**, 130–141.

Koyama, M. and Matsuura, Y. (2010). An allosteric mechanism to displace nuclear export cargo from CRM1 and RanGTP by RanBP1. *EMBO J* **29**, 2002–2013.

Kubitscheck, U., Grunwald, D., Hoekstra, A., Rohleder, D., Kues, T., Siebrasse, J. P. and Peters, R. (2005). Nuclear transport of single molecules: dwell times at the nuclear pore complex. *J Cell Biol* **168**, 233–243.

Kudo, N., Wolff, B., Sekimoto, T., Schreiner, E. P., Yoneda, Y., Yanagida, M., Horinouchi, S. and Yoshida, M. (1998). Leptomycin B inhibition of signal-mediated nuclear export by direct binding to CRM1. *Exp Cell Res* **242**, 540–547.

Kuhlmann, J., Macara, I. and Wittinghofer, A. (1997). Dynamic and equilibrium studies on the interaction of Ran with its effector, RanBP1. *Biochemistry* **36**, 12027–35.

Kumeta, M., Yoshimura, S. H., Harata, M. and Takeyasu, K. (2010). Molecular mechanisms underlying nucleocytoplasmic shuttling of actinin-4. *J Cell Sci* **123**,

1020–1030.

Kumeta, M., Yamaguchi, H., Yoshimura, S. H. and Takeyasu, K. (2012). Karyopherin-independent spontaneous transport of amphiphilic proteins through the nuclear pore. *J Cell Sci* 4979–4984.

Kurisaki, A., Kose, S., Yoneda, Y., Heldin, C. H. and Moustakas, A. (2001). Transforming growth factor-beta induces nuclear import of Smad3 in an importin-beta1 and Ran-dependent manner. *Mol Biol Cell* **12**, 1079–1091.

Kusumi, A., Shirai, Y. M., Koyama-Honda, I., Suzuki, K. G. N. and Fujiwara, T. K. (2010). Hierarchical organization of the plasma membrane: Investigations by single-molecule tracking vs. fluorescence correlation spectroscopy. *FEBS Lett* **584**, 1814–1823.

Kutay, U. and Güttinger, S. (2005). Leucine-rich nuclear-export signals: Born to be weak. *Trends Cell Biol* **15**, 121–124.

Kuusisto, H. V., Wagstaff, K. M., Alvisi, G., Roth, D. M. and Jans, D. a. (2012). Global enhancement of nuclear localization-dependent nuclear transport in transformed cells. *FASEB J* **26**, 1181–1193.

la Cour, T., Gupta, R., Rapacki, K., Skriver, K., Poulsen, F. M. and Brunak, S. (2003). NESbase version 1.0: A database of nuclear export signals. *Nucleic Acids Res* **31**, 393–396.

Lam, M. H. C., Briggs, L. J., Hu, W., Martin, T. J., Gillespie, M. T. and Jans, D. A. (1999). Importin b recognizes parathyroid hormone-related protein (PTHrP) with high affinity and mediates its nuclear import in the absence of importine a. *J Biol Chem* **274**, 7391–7398.

Lee, S. J., Sekimoto, T., Yamashita, E., Nagoshi, E., Nakagawa, A., Imamoto, N., Yoshimura, M., Sakai, H., Chong, K. T., Tsukihara, T., et al. (2003). The structure of importin beta bound to SREBP 2: nuclear import of a transcription factor. *Science (80-)* **302**, 1571–1575.

Lee, B. J., Cansizoglu, A. E., Süel, K. E., Louis, T. H., Zhang, Z. and Chook, Y. M. (2006). Rules for Nuclear Localization Sequence Recognition by Karyopherinβ2. *Cell* **126**, 543–558.

Lim, R. Y. H., Huang, N.-P. P., Köser, J., Deng, J., Lau, K. H. A., Schwarz-Herion, K., Fahrenkrog, B. and Aebi, U. (2006). Flexible phenylalanine-glycine nucleoporins as entropic barriers to nucleocytoplasmic transport. *Proc Natl Acad Sci* **103**, 9512–9517.

Liu, Q., Pante, N., Misteli, T., Elsagga, M., Crisp, M., Hodzic, D., Burke, B. and Roux, K. J. (2007). Functional association of Sun1 with nuclear pore complexes. *J Cell Biol* **178**, 785–798.

Lord, S. J., Lee, H. D. and Moerner, W. E. (2010). Single-molecule spectroscopy and imaging of biomolecules in living cells. *Anal Chem* **82**, 2192–2203.

Lowe, A. R., Siegel, J. J., Kalab, P., Siu, M., Weis, K. and Liphardt, J. T. (2010). Selectivity mechanism of the nuclear pore complex characterized by single cargo tracking. *Nature* **467**, 600–3.

Lowe, A. R., Tang, J. H., Yassif, J., Graf, M., Huang, W. Y. C., Groves, J. T., Weis, K. and Liphardt, J. T. (2015). Importin-β modulates the permeability of the nuclear pore complex in a Ran-dependent manner. *Elife* **17**, 151–152.

Luo, W., He, K., Xia, T. and Fang, X. (2013). Single-molecule monitoring in living cells by use of fluorescence microscopy. *Anal Bioanal Chem* **405**, 43–49.

Lyman, S. K., Guan, T., Bednenko, J., Wodrich, H. and Gerace, L. (2002). Influence of cargo size on Ran and energy requirements for nuclear protein import. *J Cell Biol* **159**, 55–67.

Ma, J., Goryaynov, A., Sarma, A. and Yang, W. (2012). Self-regulated viscous channel in the nuclear pore complex. *Proc Natl Acad Sci U S A* **109**, 7326–7331.

Macara, I. G. (2001). Transport into and out of the Nucleus. *Microbiol Mol Biol Rev* **65**, 570–594.

Marfori, M., Mynott, A., Ellis, J. J., Mehdi, A. M., Saunders, N. F. W., Curmi, P. M., Forwood, J. K., Bodén, M. and Kobe, B. (2011). Molecular basis for specificity of nuclear import and prediction of nuclear localization. *Biochim Biophys Acta - Mol Cell Res* **1813**, 1562–1577.

Matsuoka, S., Iijima, M., Watanabe, T. M., Kuwayama, H., Yanagida, T., Devreotes, P. N. and Ueda, M. (2006). Single-molecule analysis of chemoattractant-stimulated membrane recruitment of a PH-domain-containing protein. *J Cell Sci* **119**, 1071–9.

Mattheyses, A. L., Simon, S. M. and Rappoport, J. Z. (2010). Imaging with total internal reflection fluorescence microscopy for the cell biologist. *J Cell Sci* **123**, 3621–3628.

Mckenna, T., Baek, J. and Eriksson, M. (2013). Laminopathies. In *Genetic Disorders* (ed. Puiu, M.), pp. 27–63.

Michael, W. M., Choi, M. and Dreyfuss, G. (1995). A nuclear export signal in hnRNP A1: a signal-mediated, temperature- dependent nuclear protein export pathway. *Cell* **83**, 415–422.

Mingot, J. M., Kostka, S., Kraft, R., Hartmann, E. and Görlich, D. (2001). Importin 13: A novel mediator of nuclear import and export. *EMBO J* **20**, 3685–3694.

Miyamoto, Y., Saiwaki, T., Yamashita, J., Yasuda, Y., Kotera, I., Shibata, S., Shigeta, M., Hiraoka, Y., Haraguchi, T. and Yoneda, Y. (2004). Cellular stresses induce the nuclear accumulation of importin alpha and cause a conventional nuclear import block. *J Cell Biol* **165**, 617–23.

Monecke, T., Dickmanns, A. and Ficner, R. (2014). Allosteric control of the exportin CRM1 unraveled by crystal structure analysis. *FEBS J* **281**, 4179–4194.

Moore, J. D., Yang, J., Truant, R. and Kornbluth, S. (1999). Nuclear import of Cdk/cyclin complexes: Identification of distinct mechanisms for import of Cdk2/cyclin E and Cdc2/cyclin B1. *J Cell Biol* **144**, 213–224.

Nachury, M. V and Weis, K. (1999). The direction of transport through the nuclear pore can be inverted. *Proc Natl Acad Sci U S A* **96**, 9622–9627.

Nagoshi, E., Imamoto, N., Sato, R. and Yoneda, Y. (1999). Nuclear import of sterol regulatory element-binding protein-2, a basic helix-loop-helix-leucine zipper (bHLH-Zip)-containing transcription factor, occurs through the direct interaction of importin beta with HLH- Zip. *Mol Biol Cell* **10**, 2221–2233.

Nair, R., Carter, P. and Rost, B. (2003). NLSdb: Database of nuclear localization signals. *Nucleic Acids Res* **31**, 397–399.

Nemergut, M. E. and Macara, I. G. (2000). Nuclear import of the ran exchange factor, RCC1, is mediated by at least two distinct mechanisms. *J Cell Biol* **149**, 835–50.

Neville, M., Stutz, F., Lee, L., Davis, L. I. and Rosbash, M. (1997). The importin-beta family member Crm1p bridges the interaction between Rev and the nuclear pore complex during nuclear export. *Curr Biol* **7**, 767–775.

Niepel, M., Strambio-De-Castillia, C., Fasolo, J., Chait, B. T. and Rout, M. P. (2005).

The nuclear pore complex-associated protein, Mlp2p, binds to the yeast spindle pole body and promotes its efficient assembly. *J Cell Biol* **170**, 225–235.

Otsuka, S., Iwasaka, S., Yoneda, Y., Takeyasu, K. and Yoshimura, S. H. (2008). Individual binding pockets of importin-beta for FG-nucleoporins have different binding properties and different sensitivities to RanGTP. *Proc Natl Acad Sci U S A* **105**, 16101–16106.

Paine, P. L., Moore, L. C. and Horowitz, S. B. (1975). Nuclear envelope permeability. *Nature* **254**, 109–14.

Palmeri, D. and Malim, M. H. (1999). Importin beta can mediate the nuclear import of an arginine-rich nuclear localization signal in the absence of importin alpha. *Mol Cell Biol* **19**, 1218–1225.

Pante, N. and Kann, M. (2002). Nuclear Pore Complex Is Able to Transport Macromolecules with Diameters of 39 nm. *Mol Biol Cell* **13**, 425–434.

Panté, N. (2007). Contribution of Electron Microscopy to the Study of the Nuclear Pore Complex Structure , Composition , and Function. In *Modern Research and Educational Topics in Microscopy* (ed. Mendez-Vilas, A.) and Diaz, J.), pp. 144–153. FORMATEX.

Panté, N., Bastos, R., McMorrow, I., Burke, B. and Aebi, U. (1994). Interactions and three-dimensional localization of a group of nuclear pore complex proteins. *J Cell Biol* **126**, 603–617.

Paschal, B. (2002). Translocation through the nuclear pore complex. *Trends Biochem Sci* **27**, 593–596.

Patel, S. S., Belmont, B. J., Sante, J. M. and Rexach, M. F. (2007). Natively Unfolded

Nucleoporins Gate Protein Diffusion across the Nuclear Pore Complex. *Cell* **129**, 83–96.

Pemberton, L. F., Blobel, G. and Rosenblum, J. S. (1998). Transport routes through the nuclear pore complex. *Curr Opin Cell Biol* **10**, 392–399.

Peters, R. (2005). Translocation Through the Nuclear Pore Complex: Selectivity and Speed by Reduction-of-Dimensionality. *Traffic* **6**, 421–427.

Peters, R. (2009). Translocation through the nuclear pore: Kaps pave the way. *BioEssays* **31**, 466–477.

Quan, Y., Ji, Z.-L., Wang, X., Tartakoff, A. M. and Tao, T. (2008). Evolutionary and transcriptional analysis of karyopherin beta superfamily proteins. *Mol Cell Proteomics* **7**, 1254–1269.

Rabut, G., Doye, V. and Ellenberg, J. (2004). Mapping the dynamic organization of the nuclear pore complex inside single living cells. *Nat Cell Biol* **6**, 1114–1121.

Raices, M. and D'Angelo, M. A. (2012). Nuclear pore complex composition: a new regulator of tissue-specific and developmental functions. *Nat Rev Mol Cell Biol* **13**, 687–699.

Reichelt, R., Holzenburg, a, Buhle, E. L., Jarnik, M., Engel, a and Aebi, U. (1990). Correlation between Structure and Mass-Distribution of the Nuclear-Pore Complex and of Distinct Pore Complex Components. *J Cell Biol* **110**, 883–894.

Ribbeck, K. and Görlich, D. (2001). Kinetic analysis of translocation through nuclear pore complexes. *EMBO J* **20**, 1320–30.

Ribbeck, K. and Görlich, D. (2002). The permeability barrier of nuclear pore complexes appears to operate via hydrophobic exclusion. *EMBO J* **21**, 2664–2671.

Ribbeck, K., Lipowsky, G., Kent, H. M., Stewart, M. and Görlich, D. (1998). NTF2 mediates nuclear import of Ran. *EMBO J* **17**, 6587–98.

Ribbeck, K., Kutay, U., Paraskeva, E. and Görlich, D. (1999). The translocation of transportin--cargo complexes through nuclear pores is independent of both Ran and energy. *Curr Biol* **9**, 47–S1.

Riddick, G. and Macara, I. G. (2005). A systems analysis of importin-alpha-beta mediated nuclear protein import. *J Cell Biol* **168**, 1027–1038.

Riddick, G. and Macara, I. G. (2007). The adapter importin-alpha provides flexible control of nuclear import at the expense of efficiency. *Mol Syst Biol* **3**, 118.

Ritchie, K., Shan, X.-Y., Kondo, J., Iwasawa, K., Fujiwara, T. and Kusumi, A. (2005). Detection of non-Brownian diffusion in the cell membrane in single molecule tracking. *Biophys J* **88**, 2266–2277.

Robbins, J., Dilworth, S. M., Laskey, R. A. and Dingwall, C. (1991). Two interdependent basic domains in nucleoplasmin nuclear targeting sequence: Identification of a class of bipartite nuclear targeting sequence. *Cell* **64**, 615–623.

Rout, M. P. and Aitchison, J. D. (2001). The Nuclear Pore Complex as a Transport Machine. *J Biol Chem* **276**, 16593–16596.

Rout, M. P. and Blobel, G. (1993). Isolation of the yeast nuclear pore complex. *J Cell Biol* **123**, 771–783.

Rout, M. P., Aitchison, J. D., Suprapto, A., Hjertaas, K., Zhao, Y. and Chait, B. T. (2000). The Yeast Nuclear Pore Complex: Composition, Architecture, and Transport Mechanism. *J Cell Biol* **148**, 635–652.

Rout, M. P., Aitchison, J. D., Magnasco, M. O. and Chait, B. T. (2003). Virtual gating

and nuclear transport: The hole picture. *Trends Cell Biol* **13**, 622–628.

Sako, Y., Minoghchi, S. and Yanagida, T. (2000). Single-molecule imaging of EGFR signalling on the surface of living cells. *Nat Cell Biol* **2**, 168–172.

Schaaf, M. J. M., Koopmans, W. J. A., Meckel, T., Van Noort, J., Snaar-Jagalska, B. E., Schmidt, T. S. and Spaink, H. P. (2009). Single-molecule microscopy reveals membrane microdomain organization of cells in a living vertebrate. *Biophys J* **97**, 1206–1214.

Schmidt-Zachmann, M. S., Dargemont, C., Kühn, L. C. and Nigg, E. a (1993). Nuclear export of proteins: the role of nuclear retention. *Cell* **74**, 493–504.

Schwoebel, E. D., Talcott, B., Cushman, I. and Moore, M. S. (1998). Ran-dependent signal-mediated nuclear import does not require GTP hydrolysis by Ran. *J Biol Chem* **273**, 35170–35175.

Seo, H.-S., Ma, Y., Debler, E. W., Wacker, D., Kutik, S., Blobel, G. and Hoelz, A. (2009). Structural and functional analysis of Nup120 suggests ring formation of the Nup84 complex. *Proc Natl Acad Sci U S A* **106**, 14281–6.

Shah, S. and Forbes, D. J. (1998). Separate nuclear import pathways converge on the nucleoporin Nup153 and can be dissected with dominant-negative inhibitors. *Curr Biol* **8**, 1376–86.

Sharma, M., Jamieson, C., Johnson, M., Molloy, M. P. and Henderson, B. R. (2012). Specific Armadillo repeat sequences facilitate beta-catenin nuclear transport in live cells via direct binding to nucleoporins Nup62, Nup153, and RanBP2/Nup358. *J Biol Chem* **287**, 819–831.

Siomi, H. and Dreyfuss, G. (1995). A nuclear localization domain in the hnRNP A1

protein. *J Cell Biol* **129**, 551–560.

Smith, A. E., Slepchenko, B. M., Schaff, J. C., Loew, L. M. and Macara, I. G. (2002). Systems analysis of Ran transport. *Science (80-)* **295**, 488–491.

Solmaz, S. R., Blobel, G. and Melcak, I. (2013). Ring cycle for dilating and constricting the nuclear pore. *Proc Natl Acad Sci* **110**, 5858–5863.

Stade, K., Ford, C. S., Guthrie, C. and Weis, K. (1997). Exportin 1 (Crm1p) is an essential nuclear export factor. *Cell* **90**, 1041–1050.

Starr, D. a (2009). A nuclear-envelope bridge positions nuclei and moves chromosomes. *J Cell Sci* **122**, 577–586.

Starr, D. A. and Fridolfsson, H. N. (2010). Interactions Between Nuclei and the Cytoskeleton Are Mediated by SUN-KASH Nuclear-Envelope Bridges. *Annu Rev Cell Dev Biol* **26**, 421–444.

Stewart, M. (2006). Structural basis for the nuclear protein import cycle. *Biochem Soc Trans* **34**, 701–704.

Stewart, M. (2007). Molecular mechanism of the nuclear protein import cycle. *Nat Rev Mol Cell Biol* **8**, 195–208.

Stoffler, D., Feja, B., Fahrenkrog, B., Walz, J., Typke, D. and Aebi, U. (2003). Cryo-electron Tomography Provides Novel Insights into Nuclear Pore Architecture: Implications for Nucleocytoplasmic Transport. *J Mol Biol* **328**, 119–130.

Strawn, L. a, Shen, T., Shulga, N., Goldfarb, D. S. and Wente, S. R. (2004). Minimal nuclear pore complexes define FG repeat domains essential for transport. *Nat Cell Biol* **6**, 197–206.

Ström, A. and Weis, K. (2001). Importin beta-like nuclear transport receptors. *Genome*

Biol **2**, 1–9.

Stuwe, T., Correia, A. R., Lin, D. H., Paduch, M., Lu, V. T. and Kossiakoff, A. a (2015). Architecture of the nuclear pore complex coat. *Science (80-)* **347**,.

Sun, C., Fu, G., Ciziene, D., Stewart, M. and Musser, S. M. (2013). Choreography of importin-α/CAS complex assembly and disassembly at nuclear pores. *Proc Natl Acad Sci U S A* **110**, E1584–93.

Suntharalingam, M. and Wente, S. R. (2003). Peering through the Pore: Nuclear Pore Complex Structure, Assembly, and Function. *Dev Cell* **4**, 775–789.

Tapley, E. C. and Starr, D. A. (2013). Connecting the nucleus to the cytoskeleton by SUN–KASH bridges across the nuclear envelope. *Curr Opin Cell Biol* **25**, 57–62.

Tetenbaum-Novatt, J., Hough, L. E., Mironska, R., McKenney, a. S. and Rout, M. P. (2012). Nucleocytoplasmic Transport: A Role for Nonspecific Competition in Karyopherin-Nucleoporin Interactions. *Mol Cell Proteomics* **11**, 31–46.

Timney, B. L., Tetenbaum-Novatt, J., Agate, D. S., Williams, R., Zhang, W., Chait, B. T. and Rout, M. P. (2006). Simple kinetic relationships and nonspecific competition govern nuclear import rates in vivo. *J Cell Biol* **175**, 579–593.

Tokunaga, M., Kitamura, K., Saito, K., Iwane, A. H. and Yanagida, T. (1997). Single molecule imaging of fluorophores and enzymatic reactions achieved by objective-type total internal reflection fluorescence microscopy. *Biochem Biophys Res Commun* **235**, 47–53.

Tokunaga, M., Imamoto, N. and Sakata-Sogawa, K. (2008). Highly inclined thin illumination enables clear single-molecule imaging in cells. *Nat Methods* **5**, 159–161.

Tran, P. T., Marsh, L., Doye, V., Inoue, S. and Chang, F. (2001). A Mechanism for

Nuclear Positioning in Fission Yeast Based on Microtubule Pushing. *J Cell Biol* **153**, 397–412.

Truant, R. and Cullen, B. R. (1999). The arginine-rich domains present in human immunodeficiency virus type 1 Tat and Rev function as direct importin beta-dependent nuclear localization signals. *Mol Cell Biol* **19**, 1210–7.

Tu, L.-C., Fu, G., Zilman, A. and Musser, S. M. (2013). Large cargo transport by nuclear pores: implications for the spatial organization of FG-nucleoporins. *EMBO J* **32**, 3220–30.

Ueda, M., Sako, Y., Tanaka, T., Devreotes, P. and Yanagida, T. (2001). Single-Molecule Analysis of Chemotactic Signaling in Dictyostelium Cells. *Science (80-)* **294**, 864–867.

Van Der Watt, P. J., Maske, C. P., Hendricks, D. T., Parker, M. I., Denny, L., Govender, D., Birrer, M. J. and Leaner, V. D. (2009). The karyopherin proteins, Crm1 and Karyopherin beta 1, are overexpressed in cervical cancer and are critical for cancer cell survival and proliferation. *Int J Cancer* **124**, 1829–1840.

Wälde, S. and Kehlenbach, R. H. (2010). The Part and the Whole: functions of nucleoporins in nucleocytoplasmic transport. *Trends Cell Biol* **20**, 461–469.

Watson, M. L. (1959). Further observations on the nuclear envelope of the animal cell. *J Biophys Biochem Cytol* **6**, 147–156.

Weis, K. (2002). Nucleocytoplasmic transport: Cargo trafficking across the border. *Curr Opin Cell Biol* **14**, 328–335.

Weis, K. (2003). Regulating Access to the Genome. *Cell* **112**, 441–451.

Wen, W., Meinkoth, J. L., Tsien, R. Y. and Taylor, S. S. (1995). Identification of a

signal for rapid export of proteins from the nucleus. *Cell* **82**, 463–473.

Wente, S. R. (2000). Gatekeepers of the nucleus. *Science (80-)* **288**, 1374–7.

Wente, S. R. and Rout, M. P. (2010). The Nuclear Pore Complex and Nuclear Transport. *Cold Spring Harb Perspect Biol* **2**, 1–19.

Winey, M., Yarar, D., Giddings, T. H. and Mastronarde, D. N. (1997). Nuclear pore complex number and distribution throughout the Saccharomyces cerevisiae cell cycle by three-dimensional reconstruction from electron micrographs of nuclear envelopes. *Mol Biol Cell* **8**, 2119–2132.

Xia, T., Li, N. and Fang, X. (2013). Single-Molecule Fluorescence Imaging in Living Cells. *Annu Rev Phys Chem* **64**, 459–480.

Xu, S. and Powers, M. (2013). In vivo analysis of human nucleoporin repeat domain interactions. *Mol Biol Cell* **24**, 1222–1231.

Xu, D., Farmer, A., Collett, G., Grishin, N. V. and Chook, Y. M. (2012). Sequence and structural analyses of nuclear export signals in the NESdb database. *Mol Biol Cell* **23**, 3677–3693.

Xu, C., Li, Z., He, H., Wernimont, A., Li, Y., Loppnau, P. and Min, J. (2015). Crystal structure of human nuclear pore complex component NUP43. *FEBS Lett* **589**, 3247–3253.

Yang, W. (2011). "Natively unfolded" nucleoporins in nucleocytoplasmic transport: Clustered or evenly distributed? *Nucleus* **2**, 10–16.

Yang, W. and Musser, S. M. (2006). Nuclear import time and transport efficiency depend on importin beta concentration. *J Cell Biol* **174**, 951–61.

Yang, Q., Rout, M. P. and Akey, C. W. (1998). Three-Dimensional Architecture of the

Isolated Yeast Nuclear Pore Complex: Functional and Evolutionary Implications. *Mol Cell* **1**, 223–234.

Yang, W., Gelles, J. and Musser, S. M. (2004). Imaging of single-molecule translocation through nuclear pore complexes. *Proc Natl Acad Sci U S A* **101**, 12887–92.

Yaseen, N. R. and Blobel, G. (1997). Cloning and characterization of human karyopherin beta3. *Proc Natl Acad Sci U S A* **94**, 4451–6.

Yokoyama, N., Hayashi, N., Seki, T., Panté, N., Ohba, T., Nishii, K., Kuma, K., Hayashida, T., Miyata, T. and Aebi, U. (1995). A giant nucleopore protein that binds Ran/TC4. *Nature* **376**, 184–188.

Yoshimura, S. H., Otsuka, S., Kumeta, M., Taga, M. and Takeyasu, K. (2013). Intermolecular disulfide bonds between nucleoporins regulate karyopherin-dependent nuclear transport. *J Cell Sci* **126**, 3141–50.

Yoshimura, S. H., Kumeta, M. and Takeyasu, K. (2014). Structural Mechanism of Nuclear Transport Mediated by Importin β and Flexible Amphiphilic Proteins. *Structure* **22**, 1699–1710.

Zilman, A., Di Talia, S., Chait, B. T., Rout, M. P. and Magnasco, M. O. (2007). Efficiency, Selectivity, and Robustness of Nucleocytoplasmic Transport. *PLoS Comput Biol* **3**, e125.

APPENDIX 1

Residence time profile of 80 NPCs exposed to 2 mM DTT in the single molecule study

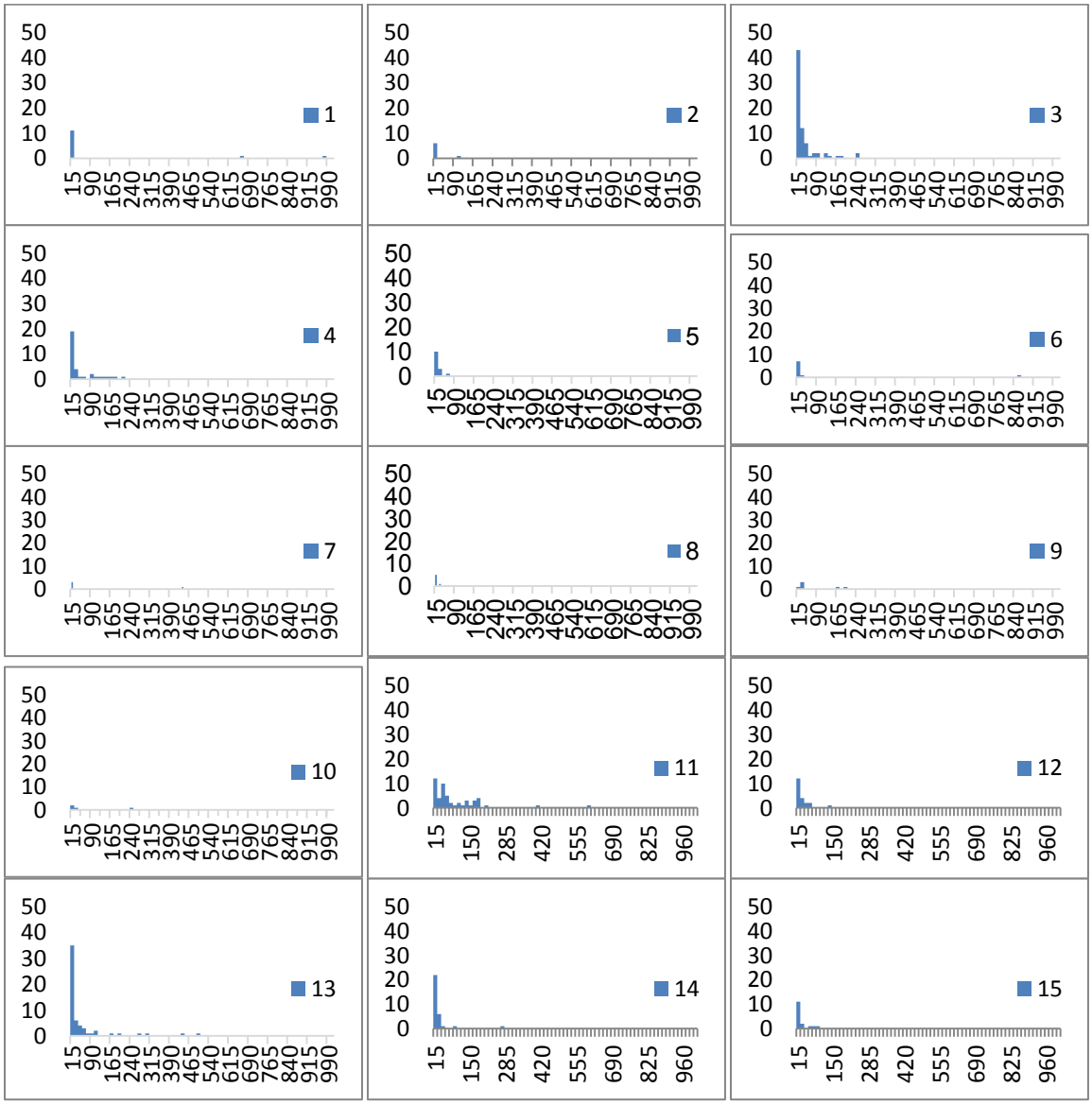

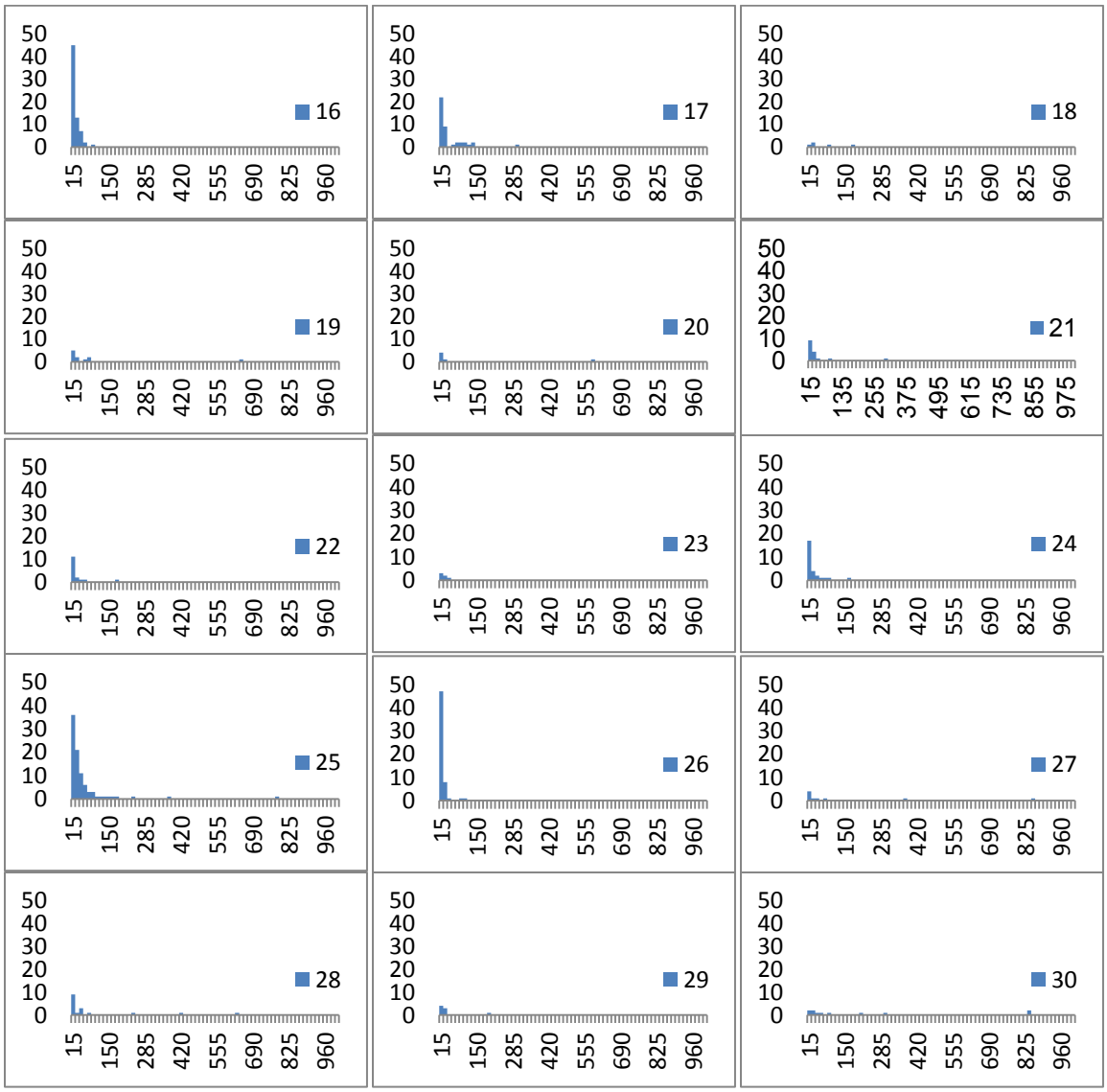
50
40
30
20
10
0
16
17
18
19
20
21
22
23
24
25
26
27
28
29
30
15
150
285
420
555
690
825
960
135
255
375
495
615
735
855
975
Time (ms)

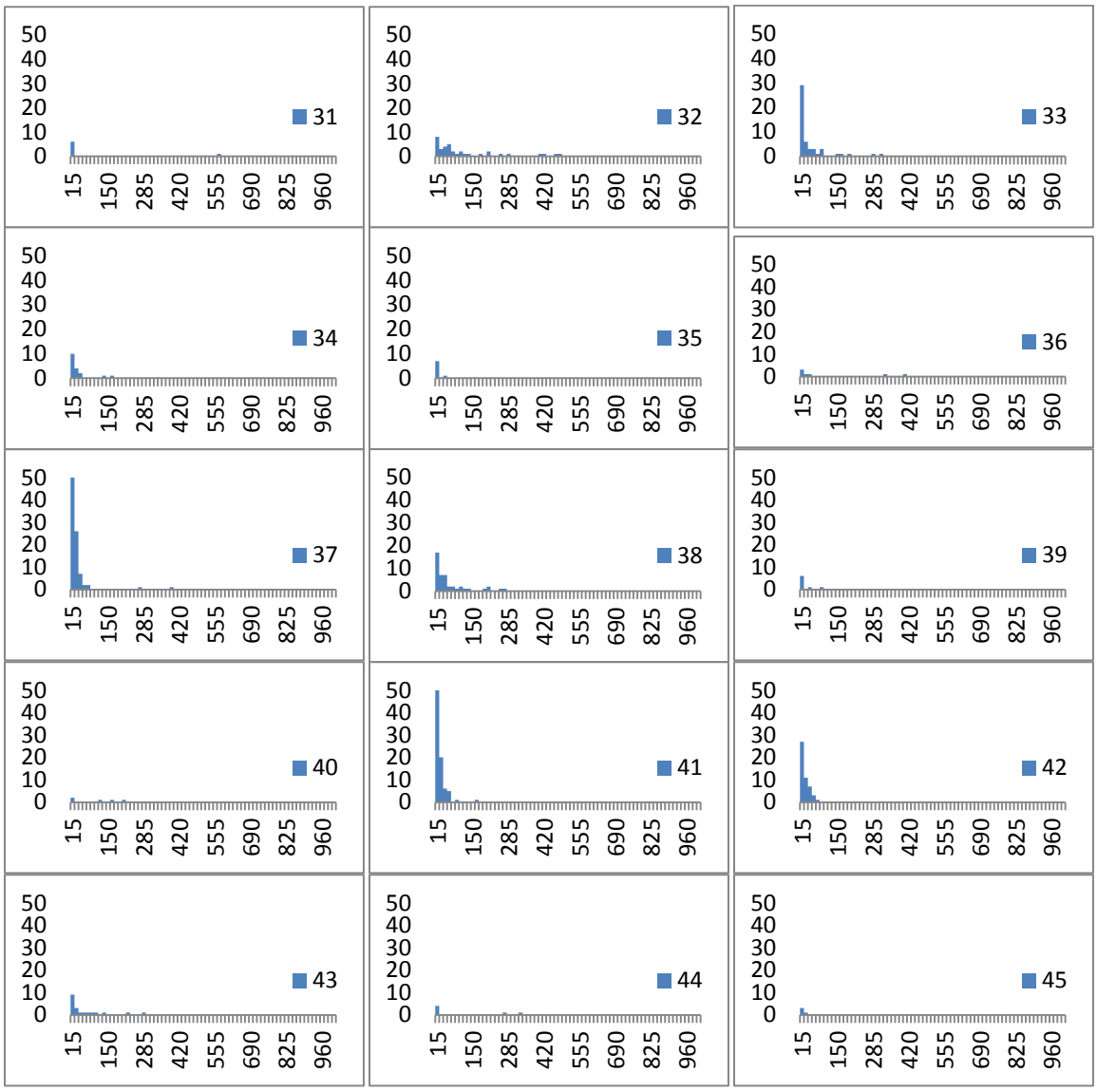
50
40
30
20
10
0
15
150
285
420
555
690
825
960
31
32
33
34
35
36
37
38
39
40
41
42
43
44
45
Time (ms)

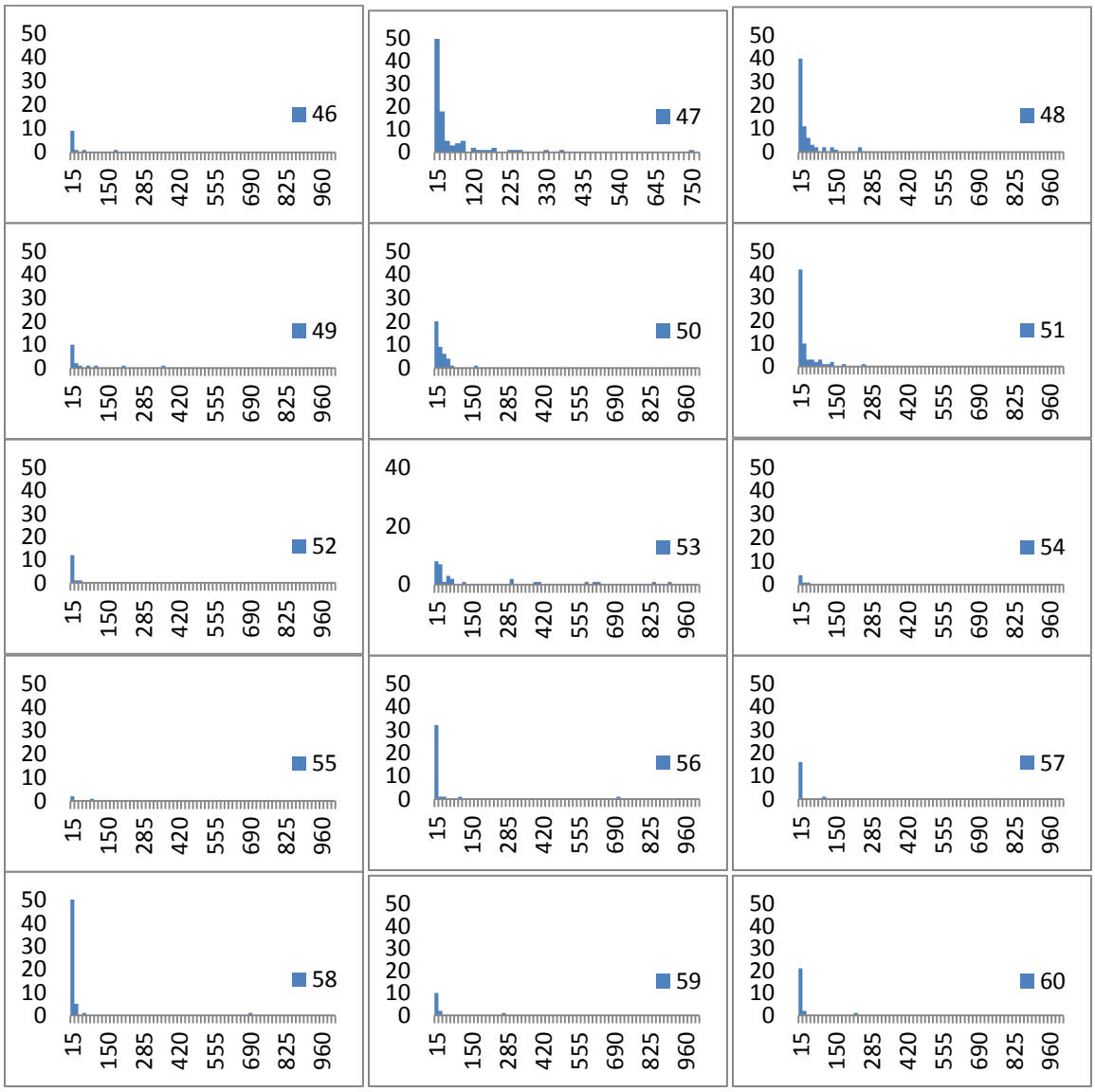
46
47
48
49
50
51
52
53
54
55
56
57
58
59
60
Time (ms)

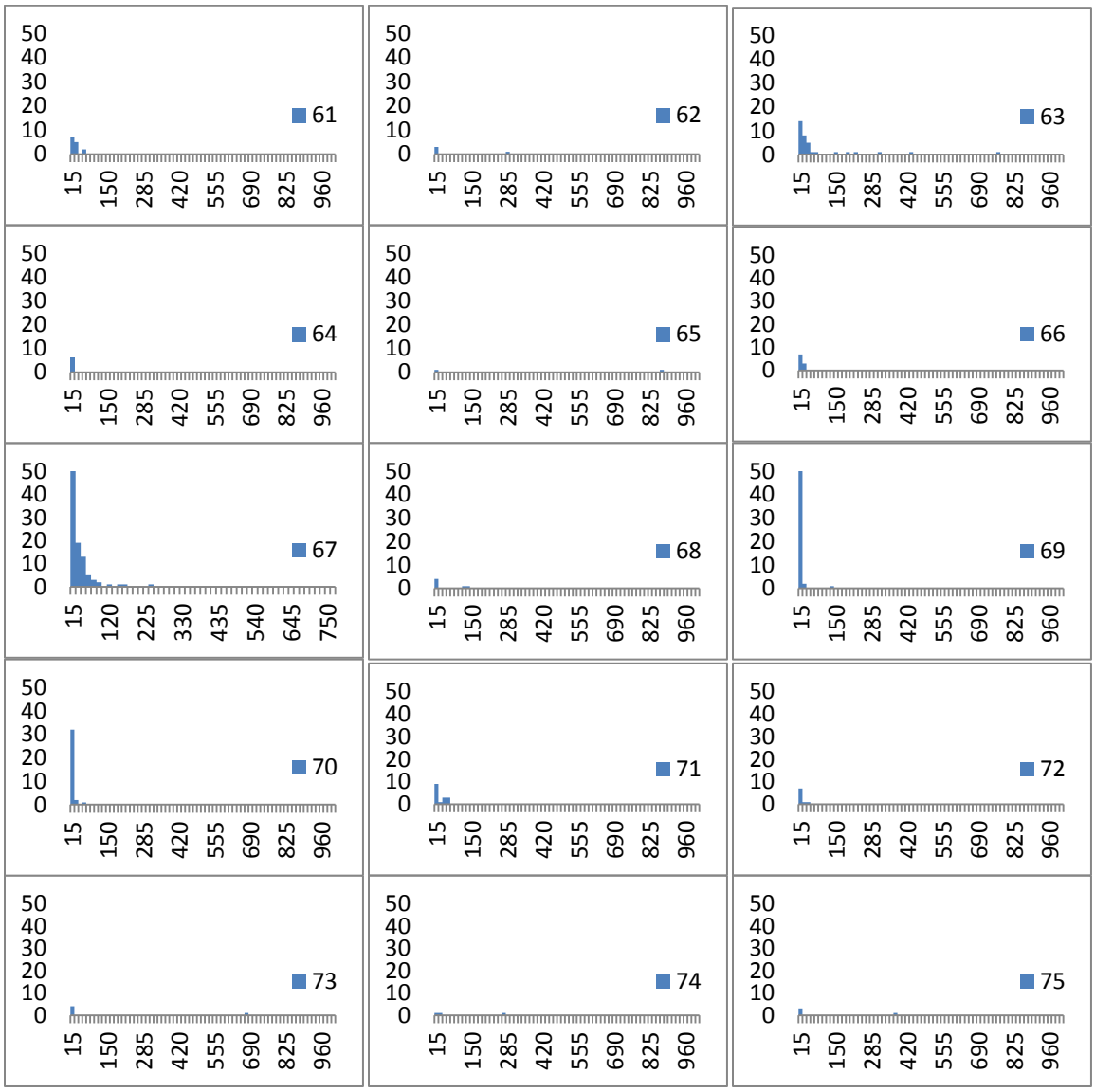
50
40
30
20
10
0
61
62
63
64
65
66
67
68
69
70
71
72
73
74
75
15
150
285
420
555
690
825
960
120
225
330
435
540
645
750
Time (ms)

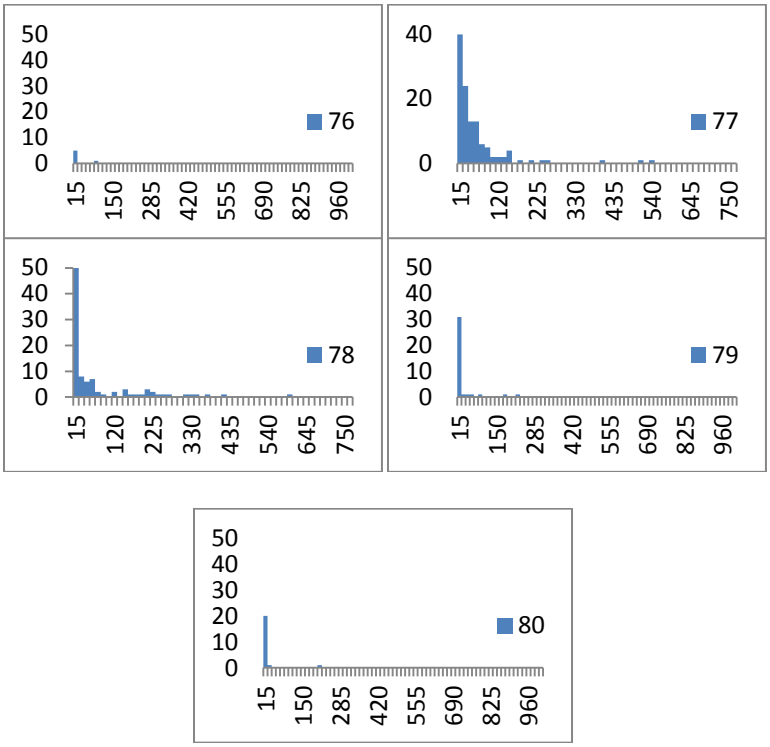
50
40
30
20
10
0
15
150
285
420
555
690
825
960
76
40
20
0
15
120
225
330
435
540
645
750
77
50
40
30
20
10
0
15
120
225
330
435
540
645
750
78
50
40
30
20
10
0
15
150
285
420
555
690
825
960
79
50
40
30
20
10
0
15
150
285
420
555
690
825
960
80
Time (ms)

APPENDIX 2

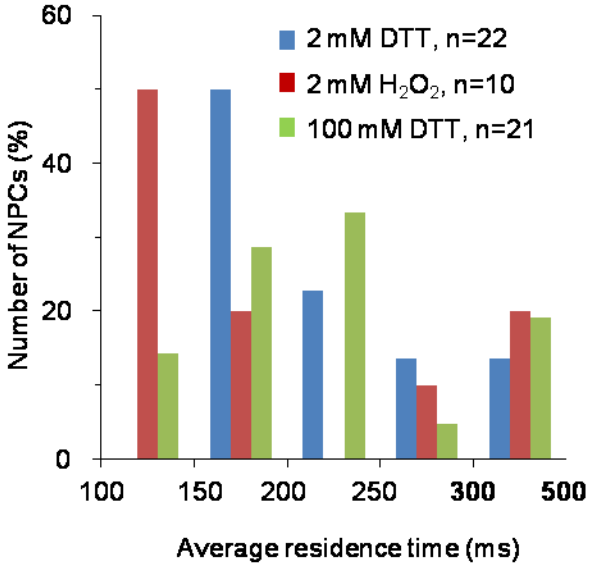

Residence time of importin β molecules in NPCs exposed to different redox conditions (related to Figure 4.6E). The average residence time of molecules in NPCs that had interactions longer than a threshold of 100 ms in different redox environments was calculated and plotted against the number of NPCs (expressed in frequency %; 2 mM DTT, n= 22; 2 mM H_2O_2, n=10; 100 mMDTT, n=21). Similar to the 2 mM DTT condition, the results suggest that the different populations of NPCs are also maintained in different redox conditions.